HYDROCRACKING OF SHORT RESIDUE OVER UNSUPPORTED AND SUPPORTED MAGNETITE NANOCATALYSTS

By

Shaheel Maharaj

Supervised by:

Dr David Lokhat

A thesis submitted in the fulfillment for the degree

of Master of Science in Engineering

in the

Discipline of Chemical Engineering,

College of Agriculture, Engineering and Science,

University of KwaZulu–Natal, Durban, South Africa

December 2017

Examiner's Copy

Statement of Authorship

I, SHAHEEL MAHARAJ declare that:

(i) The information reported in this report, except where otherwise indicated, is my original work.

(ii) This report has not been submitted for any degree or examination at any other university.

(iii) This report does not contain other persons' data, pictures, graphs or other information, unless specifically acknowledged as being sourced from other persons.

(iv) This report does not contain other persons' writing, unless specifically acknowledged as being sourced from other researchers. Where other written sources have been quoted, then:

a. Their words have been re-written but the general information attributed to them has been referenced;

b. Where their exact words have been used, their writing has been placed inside quotation marks, and referenced.

(v) This report does not contain text, graphics or tables copied and pasted from the internet, unless specifically acknowledged, and the source being detailed in the thesis and in the references sections.

_____ Date: 15/12/2017

STUDENT'S SIGNATURE

Executive Summary

With the rapid depletion of crude oil and current cracking methods of heavy petroleum residue all resulting in the production of undesirable coke formation, a better solution must be found. This project investigated the use of an unsupported molybdenum-doped magnetite nano-catalyst, as well as a magnetite nanocatalyst on a mesoporous silica support, to determine if the use of these catalysts can be successful in cracking petroleum residue. Short residue from the vacuum distillation column supplied by SAPREF, was used throughout the experimental work.

A lot of effort went into the preparation of the feedstock due to the high viscosity of short residue. The solvent used during experimental work was toluene, which was used to dilute the short residue. A temperature range between 350˚C and 400˚C was used in order to determine temperature effects on product distribution from the cracking reaction. The feedstock to catalyst ratio was also varied, using the unsupported catalyst, in order to determine the effects of the amount of catalyst on the reaction. Kerosene and gas oil are the desired products due to their higher heating value and use as liquid fuels compared to the heavier residue. There is a strong interaction between temperature and catalyst to feedstock ratio. The high temperature-high catalyst combination gave improved gas oil yields over the low temperature-high catalyst combination. Results carried out at 400˚C with a high catalyst amount showed the most favourable results with a yield of 49.3% and 6% of gas oil and kerosene respectively. Aquaprocessing (catalytic splitting of water that occurs on the surface complexes of the iron-based catalyst, at a relatively low pressure) was simulated at the experimental conditions using kinetics from literature for a nickel-based catalyst. The simulated composition profiles proved that the unsupported magnetite nanocatalyst was much more efficient in upgrading residue than the nickel based catalyst, due to the presence of greater amounts of lighter components. Analysis of the catalyst after the cracking reaction shows that no major phase changes had taken place and that the catalyst could be regenerated to be used again.

The supported magnetite nanocatlyst was compared to conventional nickel-molybdenum and cobalt-molybdenum catalyst, in a fixed bed reactor set up. The supported catalyst proved to be the most consistent, and was able to shift the residue into the lighter fractions more effectively than the conventional catalysts. The supported catalyst was the most effective in cracking the vacuum residue, mostly into vacuum gas oil. The yields using the catalyst compared quite favourably with the unsupported catalyst, with the unsupported catalyst yielding more lighter

components. The most favourable results implementing a supported catalyst were also at 400˚C, due to the extensive decrease in vacuum residue and a corresponding increase in lighter components.

Ultimately this investigation proved that hydrocracking can take place with the use of a supported and unsupported magnetite nanocatalyst, at lower temperatures than that of conventional methods and aquaprocessing. It was also proven that the process can be upscaled to industry level, as shown with the performance of the supported catalyst. A larger temperature range could give better clarity in the performance of the catalyst for future petroleum residue cracking.

Table of Contents

List of Figures

Chapter 2

Chapter 4

Appendix A

Appendix B

Appendix E

Appendix F

Appendix G

Appendix H

List of Tables

Chapter 2

Chapter 3

Appendix C

Appendix D

Appendix E

Appendix G

Appendix H

Nomenclature

E_a	Activation Energy	kJ/mol
A	Pre-exponential Factor	1/min
k_i	Reaction constant	
˚C	Degrees Celsius	
2θ	Diffraction Angle	degrees
I	Intensity	counts
λ	Incident x-ray wavelength	
β	The full-width--at-half-maximum of the highest intensity powder diffraction reflection	radians
θ	half diffraction angle	degrees
K	Shape Factor	

CHAPTER 1

1.1 Introduction

Crude oil is the altered remains of prehistoric organic material. By definition it is a naturally occurring, unrefined petroleum product composed of hydrocarbon deposits and other organic materials (Biasca, et al., 2003). It is used to produce usable products such as gasoline, diesel and other forms of petrochemicals. Two important stages of the refining process of crude oil are, vacuum distillation and atmospheric distillation, as these stages are where most of the useful products are separated out from. Due to the heavy reliance on crude oil over the last few decades, its extensive use has resulted in the world's crude oil reserves to deplete at a rapid rate therefore it is classified as a non-renewable resource. Analysts have estimated that the crude reserves will run out in the next forty years (Gary, 2004), hence alternate solutions must be found.

In recent times research into treating and cracking heavy and residual oils into more desirable lighter fuels has gained a lot of interest due to the extensive world-wide need for light petroleum products, from diminishing reserves of sweet crude oils. After the process of crude distillation, there is large amounts of heavy oils namely atmospheric and vacuum residue. These are by-products of crude oil distillation. It is however not easy to convert these residual oils into the useful hydrocarbons. (Enkhsaruul, 1992).

The heavy residue that is produced after crude distillation could be upgraded posing a decent viable solution. The residue produced from an atmospheric distillation unit is often referred to as long residue, whilst that produced from a vacuum distillation unit is often referred to as short residue. Throughout this investigation short residue supplied by SAPREF was experimented with.

Methods used today to upgrade petroleum residue include catalytic cracking, thermal cracking as well as hydrocracking. However, all of these methods result in excessive amounts of coke being formed. This coke formation results in the catalyst used becoming deactivated and could also cause blockages within the reactor (Sadeghbeigi, 2000).

Due to the high demand of crude oil, the consumption of fuels and various other petrochemical products has increased, the situation can be regarded as a real-life crisis. The upgrading of

crude oil has been done over a vast number of years to get as much desirable components as possible from the crude oil. The goal of upgrading heavy oils and vacuum residue are to decrease boiling point and viscosity, desulphurisation, demetallation and the level of impurities (Sahu et al., 2015). Due to the negative factors associated with current cracking methods, advancement in catalyst technology is a necessity to provide a long term sustainable solution to obtaining the valuable materials from the heavy residue.

Short residue produced from the vacuum distillation column in crude oil refining is one of the lowest grades of crude oil due to the presence of impurities such as asphaltenes, sulphur, nitrogen and other heavy metals (Enkhsaruul, 1992). Its use could provide a solution of being able to extract as much valuable materials as possible from crude oil, ultimately prolonging the 'lifespan' of crude oil in the world today to fulfil the requirements of modern civilisation.

Studies have shown that the use of a molybdenum magnetite nanocatalyst will provide more resistance to the undesirable coke being formed (Gary,2004), which will be beneficial for future refining processes.

1.2 Project Aims & Objectives

The main aim of this project was to investigate the performance of supported and unsupported magnetite nano-particle catalysts for the hydrocracking of heavy petroleum residue, in terms of the yield of upgraded products. The results obtained were compared to conventional hydrocracking.

Objectives

- Preparation and characterization of the magnetite nanoparticle catalyst and the short residue is also a vital component for the experiment. X-ray diffraction techniques was used for this.
- Preparation of the feedstock. Short residue is extremely difficult process, hence a suitable method had to be devised in order to get measurable quantities of the short residue.
- Performing the hydrocracking reaction of the short residue in a batch reactor, using an unsupported catalyst, in order to see if the heavy residue could be shifted into its lighter fractions.

- Performing the hydrocracking of the short residue in a fixed bed reactor set up, using a supported catalyst. The result will be compared to that of the unsupported catalyst.
- Hydrocracking of short residue using conventional catalyst namely nickel molybdenum and cobalt molybdenum, which will be compared to the performance of the magnetite nanocatalyst.
- Analysis of whether the supported and unsupported magnetite nano-catalyst could be re-used or not.
- A macroscale simulation based on the general material balances of the reactor for the hydrocracking procedure, on MATLAB^{TM}, using available kinetic data and comparing the simulation results to experimental results.

1.3 Scope of Dissertation

- Chapter 1 covers the introduction and motivation of the topic of hydrocracking of short residue using supported and unsupported magnetite nanocatalysts. Also, included are the aims and objectives of this investigation.
- Chapter 2 is an in-depth literature review of the topic, taking a look at the process of crude oil distillation, current petroleum cracking methods, types of reactors, catalysts used in the cracking procedure, characterisation of the short residue and the process of aquaprocessing.
- Chapter 3 is an explanation of the methods and materials implemented to achieve the objectives of the investigation. This includes the experimental work involving both unsupported and supported catalysts.
- Chapter 4 includes an in-depth analysis of the results achieved for the supported and unsupported catalysts and comparisons are drawn from the analysis.
- Chapter 5 discusses the conclusions drawn from the investigation and whether the aim and objectives could be achieved. Any recommendations to improve the design are also discussed in this section.
- All Appendices needed to support the results of the investigation are included after Chapter 5. These include all the raw data, sample calculations, schematics of experimental set ups, HAZOP Analysis and simulation results.

CHAPTER 2

2.0 Literature Survey

2.1 Crude Oil Refining

Crude oil is made up of a complex mixture of hydrocarbons and other chemicals. Refining processes are put in place to separate these hydrocarbons into more valuable products such as petroleum and diesel. The following flow diagram represents the crude oil refining process:

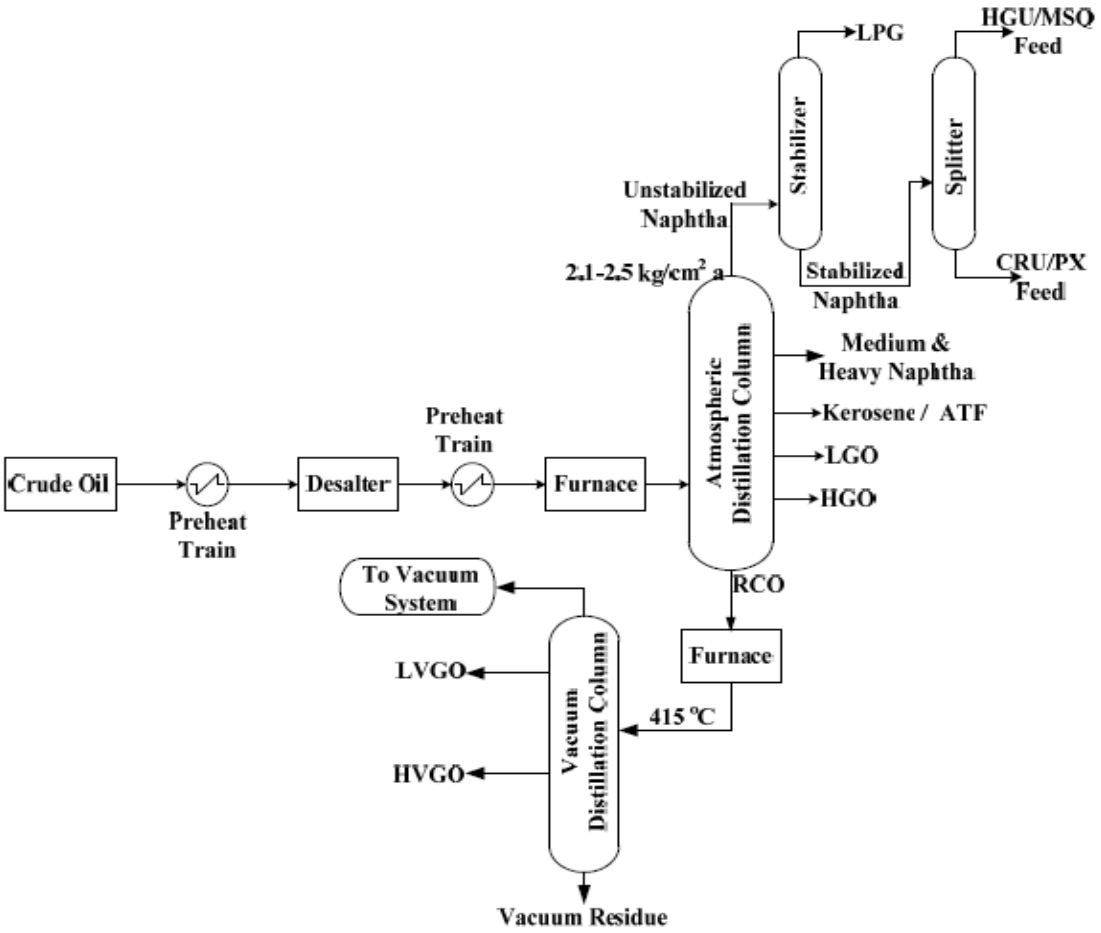

Figure 2.1-Flow diagram of the crude oil refining process (NPTEL, 2012.)

Crude oil storage: Crude oil is generally harnessed from natural sources and then stored in the 'crude' form until it can be transported to be processed at a refining facility and then in turn, can be converted to a more valuable product (Rana el al., 2007). The storage tanks used, also utilise the mechanism of gravitational settling to separate the bituminous sediment from the water. The separation depends on the amount of time the crude oil is stored in the tanks. In most cases crude oil contains sulphur, hence the storage tanks are specially designed using advanced technology and materials to prevent corrosion caused by any sulphur present.

Crude oil desalters: Contained within the crude oil is a variety of salts, mainly chlorides (Sadeghbeigi, 2000). It is possible that water and the chloride salts can combine to form hydrochloric acid within the atmospheric distillation column. This can cause severe damage to equipment and result in poor distillation. Crude oil is heated to about 80˚C before entering the desalter unit (Kister, 1992). The desalters are cleaned by spraying the salts with fresh water to wash away salts from the crude oil, usually forming an emulsion. High voltage electrostatic fields are then used to remove the water.

Crude oil heater: After the crude oil passes the desalter it is heated further by exchanging heat with distillation products, liquid from the tower bottoms and internal cycle streams . A fuel-fired furnace is then used to heat the crude oil further to a temperature of 400˚C, after which the oil is sent to the atmospheric distillation column (Sadeghbeigi, 2000).

Atmospheric Distillation Column: The atmospheric distillation column separates the various components of the crude oil by exploiting the differences between boiling points of each of the components (Sadeghbeigi, 2000). In the column, there is a high concentration of lower boiling, high volatile components at the top of the column, while the higher boiling and less volatile components are separated from the bottom of the column. The temperature gradient along the height of the column is responsible for this separation. The atmospheric distillation column operates as any conventional distillation column, with a reboiler heating up the bottoms of the column while an overhead condenser provides cooling at the top. At each stage of the column, hydrocarbons approach vapour-liquid equilibrium, which ultimately allows the lighter hydrocarbons to escape the top of the column while the heavier components fall to the bottom (Pujado et al., 2006). From the top stage to the bottom, the operating pressure also decreases. This pressure range is close to atmospheric pressure. Ultimately this results in high concentrations of specific hydrocarbons at different stages that can be easily extracted.

Crude oil contains various fractions such as kerosene, naphtha, gas oil, vacuum gas oil and other heavier components (Biasca et al., 2003). Once most of the lighter components are removed by atmospheric distillation, the heavy residue remaining is sent the vacuum distillation column where it is refined further under reduced pressure.

Vacuum distillation: A typical flow diagram of a vacuum distillation column is shown in the figure 2.2:

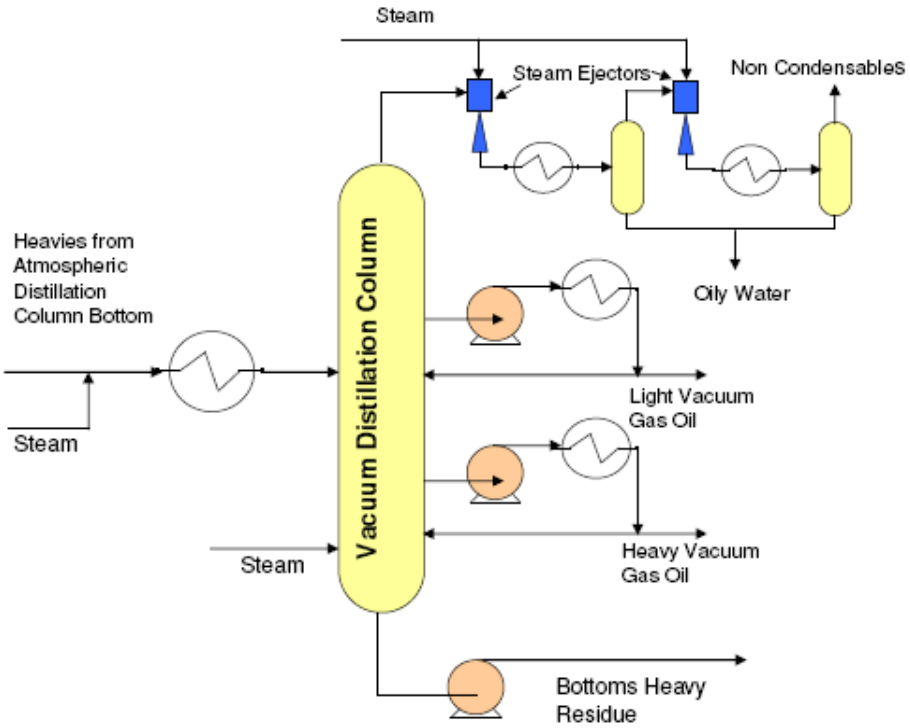

Figure 2.2 - Typical flow diagram of a vacuum distillation unit (Cherzer & Gruia, 1996)

From the above figure, the steam ejectors are used to remove the lighter hydrocarbon vapours by steam ejectors which operate at low pressures from the top of the column. The vapours are then cooled to condense the steam which entered with the feed to the column. The condensed mixture of oil and water is removed and recycled back to the column after boiling it (Hildebrand, 1972).

There are two different hydrocarbons cuts produced in the column; light vacuum gas oil and heavy vacuum gas oil. These oils are separated in the column by the difference between their boiling point ranges. The liquid that is drawn out at a low pressure has to be pumped, after which it is heated and then sent back to the column (Furimsky, 1998). A small amount of this liquid is taken out as light or heavy vacuum gas oil. The light vacuum gas oil is sent to a hydrotreater and then to a catalytic cracking unit to be broken down into smaller chain hydrocarbons. The heavy gas oil is sent to a hydrocracking unit to achieve lighter components.

The heavy hydrocarbons that cannot be boiled remain at the bottom of the column, which is then pumped out as vacuum residue.

2.1.1 Long & Short residue

Short residue is the heavy oil that is removed from the bottoms of the vacuum distillation column. This heavy oil is a highly viscous fluid that is made up of asphaltenes, waxes, resins and polycyclic heteroaromatic hydrocarbons containing sulphur and nitrogen (Pujado et al., 2006). It also has a high molecular weight, low H/C ratio and is a highly complex material.

Long residue on the other hand is removed from the bottoms of the atmospheric distillation column. Long residue is less viscous than short residue but shares the same processing routes to convert the residue into lighter components.

2.2 Cracking of petroleum residues and heavy oils

Due to the high demand for lighter, short chained feedstocks the heavy long chained hydrocarbons have to be broken down. Technologies used today to upgrade heavy petroleum residues can be vastly categorised into two processes, namely carbon rejection and hydrogen addition processes. Carbon rejection rearranges the hydrogen atoms amongst the different components, which then results in an increase in the H/C ratios for certain components and lower H/C ratios for the other components (Gupta & Gera, 2015). This process results in more carbon coke being formed. Hydrogen addition processes encompass reactions between the petroleum residue and an external source of hydrogen, ultimately resulting in an increase of the overall H/C ratio. Hydrogen-carbon atomic ratio (H/C) of feedstock is an important factor in determining the operation conditions for the system. High ratios mean that the feedstock has a high hydrogen saturation and can be processed at relatively severe operation conditions (Gang Yang & Eser, 2002). The change in H/C atomic ratio during the upgrading process can be used to measure the hydrogenation activity of a catalyst. These upgrading methods can be classified further below.

2.2.1 Carbon Rejection Methods

Carbon rejection technologies have been used in industry for more than a decade. In the process, the feed is heated under inert atmosphere and atmospheric pressure to break it into their smaller and lighter components. The hydrogen within the system attaches to the carbon molecule and is redistributed among the different components so that some components have

increased H/C atomic ratios while other components show a decrease in the H/C ratio. This process leads to coke being formed, which can be further processed to produce valuable materials. The types of carbon rejection technologies are discussed below.

Thermal cracking

Thermal processes are vital to the upgrading of heavy petroleum residue. Thermal cracking occurs at high temperature and moderate pressure (Pujado, et al., 2006). Here the hydrogen is transferred from the heavier, larger molecules to the lighter molecules, resulting in a decrease in the C/H ratio. It is used to upgrade heavy oil into lighter fractions, distillates or petroleum coke.

The reactions that take place can be summarised as follows:

- Dehydrogenation of naphthenes which lead to the formation of aromatics.
- Condensation of aliphatic components which result in the formation of aromatics.
- Condensation of aromatics to form better quality aromatics.
- Dimerisation

The critical process variables involved in thermal cracking are the feed stock properties, cracking temperature and residence time (Gupta & Gera, 2015).

Gasification

Gasification involves preheating the feed to extremely high temperatures (>1000˚C) in the absence of air (Biasca, et al., 2003). During this process, the feed is heated to form products such as, carbon black, gas and ash. This technology can be seen as an alternative for power generation and other sectors. However due to poor selectivity and product separation, means that this method is not implemented on a large scale compared to other technologies.

Delayed Coking

Delayed coking is a popular carbon rejection process used for vacuum residue upgradation, due to the advantage of feed variation. The liquid product is partially converted which forms metal and carbon free products (Furimsky, 1998). For this process, experimental conditions determine the product selectivity. Delayed coking results in the formation of large amounts of coke as well as a low liquid product yield, hence the process is seen as unfeasible to many (Gupta & Gera, 2015).

The desired temperature for the reaction to occur is reached by preheating the feed in a furnace, and then it is fed to the coking drums where the cracking reaction takes place. Any coke formed during the reaction is deposited at the bottom of the reactor (Sathya, 2013). The overhead vapours formed in the coke drums flow into the fractionating column. The vapours are then separated into overhead streams containing low pressure gas, naphtha and two side streams containing gas oil. On the fractionating column, there is a recycle stream which mixes with the fresh feed in the bottom of the column which is then further preheated in coke heaters and flows to the coke drums (Sathya, 2013). Partial cracking and partial vaporisation are the two main reactions involved in this process. These reactions crack the two vapour phases in the coke drum, which leads to polymerisation of the liquid phase resulting in the formation of coke in the drum.

The feed for the delayed coking process include vacuum residue, FCC residual, or cracked residue. The products from a delayed coking unit are Gases, Naphtha, Fuel oil, Gas oil and Coke.

Fluid coking

This process is non- catalytic fluidised bed process where coking of the fluidised bed is achieved by spraying the internal surface with fine, heated coke particles (Sadeghbeigi, 2000). This process also achieves formation of light hydrocarbons with a decrease in coke formation by implementing higher temperatures with shorter contact time than delayed coking. The importance of a shorter residence time is that greater yield quantities of liquid less coke, but this leads to a product lower in value.

Flexi Coking

It is a continuous process that involves thermal cracking in a bed fluidized coke and gasification of the coke produced at 870^{o}C (Rana et al., 2007). This process contains an additional step of gasification. It can be applied to a wide variety of feed stocks.

Visbreaking

Visbreaking, one of the oldest and cost-effective methods for upgrading heavy petroleum residues, results in a product composed mainly of gasoline and a small amount of gas (Shen, et al., 1997). The asphaltene content does not vary much in the product during this process, hence stable fuel is produced. This process can be regarded as a mild thermal cracking procedure, where long chain molecules within the heavy residue are broken down into shorter and lighter

molecules leading to a reduction in viscosity of the feed (Sathya, 2013). Visbreaking is a non-catalytic thermal process. It reduces the viscosity and pour point of heavy petroleum fractions so that product can be sold as fuel oil. The process is a viable option if there is a low demand for motor fuel. If the demand had to increase, delayed coking is a better option (Shen et al., 1997). A given conversion in a visbreaker can be achieved by two ways:

1. In-coil visbreaking implementing low residence times and high temperatures.
2. In-soaker visbreaking implementing high residence times and low temperatures.

The following represents the visbreaking reaction:

$$CH_3\text{-}CH_2\text{-}CH_2\text{-}CH_2\text{-}CH_2\text{-}CH_2\text{-}CH_3 \rightarrow CH_3\text{-}CH_2\text{-}CH{=}CH_2 + CH_3\text{-}CH_2\text{-}CH_3$$

Soaker visbreaking Process

For this technology, operation of the furnace at a decreased outlet temperature and a soaker drum is provided at the outlet of the furnace to allow sufficient residence time to obtain the required conversion while at the same time allowing for a stable residue product. This in turn increases the heater run and lowers the frequency of unit shut down for heater decoking (Shen, et al., 1997). The products that exit the drum is quenched and distilled in the downstream fractionator.

The feed to a soaker visbreaker may consist of atmospheric residue to achieve gasoline and diesel oil or vacuum residue to achieve a reduction in viscosity.

The typical reactions that take place in a soaker vibreaking unit can be summarised as follows:

- Separation of the Carbon-Carbon bond.
- Cyclisation of olefinic compounds to naphthenes.
- Condensation of the cyclic molecules to polyaromatics.
- Side reactions: Formation of H_2S, thiophenes, mercaptans, phenol

The products may contain gas, naphtha, gas oil and furnace oil, the composition of which will depend upon the type of feedstock processed. Generally, a potential product yield may be gas in the range of 1-2%, naphtha 2-3%, gas oil 5-7%, furnace oil 90-92% (NPTEL, 2012).

The soaking drum increases the residence time so that the furnace operates at lower temperatures. It also results in lower operating costs due to lower temperature with less coke formation and larger gas oil yield.

Coil Visbreaker Process

In this process, a furnace operates at high temperatures to achieve the desirable amount of cracking. Quenching of the cracked components takes place, which are then distilled in a downstream fractionator. There have been improvements in the visbreaker coil heater design which isolates one or more heater passes for decoking. This in turn eliminates the need to shut the entire visbreaker down to decoke the furnace. The integration of vacuum distillation units with the coil visbreaking process is gaining popularity all over the world. (Sieli, 1998).

Thermal processes and technologies based on coking show a disadvantage due to the amount of low value by-products that are formed and will require further processing. Further processing these by-products will result in higher costs and use of resources (Atkins, et al., 2010). Therefore, thermal processes are not vital as compared to catalytic upgrading techniques, in the processing of heavy petroleum residues.

Fluid Catalytic Cracking

In comparison to thermal cracking, fluid catalytic cracking (FCC) occurs at lower temperatures and pressures. It is also more selective, flexible and is carried out using a catalyst. This method requires a vapour phase for the cracking reaction and results in a better selectivity for the gasoline and low yields of gas than thermal processes (Gupta & Gera, 2015). Both Vacuum residue and Atmospheric residue have high boiling points as well as a large amount of impurities which causes difficulty in vaporising the feed (Cherzer & Gruia, 1996). This process often leads to metal and coke depositing on the catalyst which would lead the catalyst to deactivate. Fluidised catalytic cracking is therefore limited in industry because it requires feeds of good quality and low amounts of impurities.

Solvent De-asphalting

This method involves the physical separation of imprities in the feed, namely metals and asphaltenes, based on their molecular weight and not the boiling point (Biasca, et al., 2003). Light paraffinic solvents such as propane, butane and n-heptane are added to the feed mixture. The paraffinic oil prevents asphalt and other impurities from dissolving in it, this allows for the impurities to be removed from the mixture (Billon, et al., 1997). Some of the limitations to this process are high energy costs, low motor fuel demand and the limited use of de-asphalted products. This technology is not being used on a large scale currently, but the interest in the technology is increasing (Billon, et al., 1997)

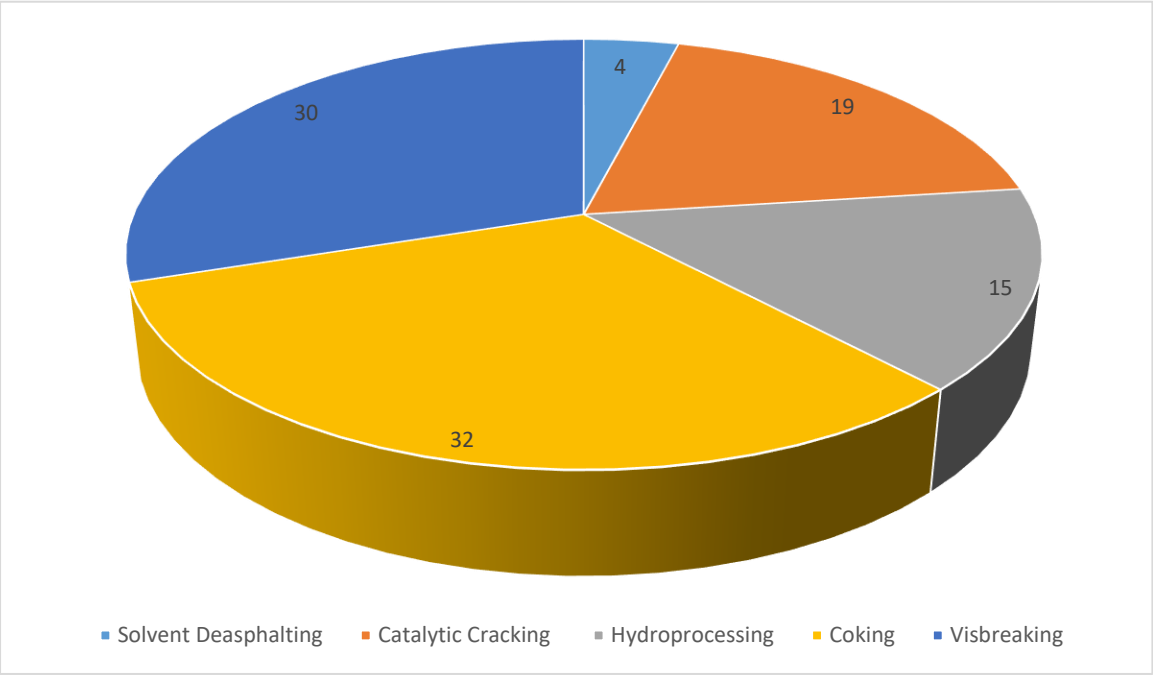

Figure 2.3 - Historical Worldwide Residue Conversion Selection (Billon et al., 1997)

2.2.2 Hydrogen Addition Processes

Hydrocracking

Hydrocracking by definition, is a form of catalytic cracking carried out in petroleum refining processes where heavy oil passes through a vessel under high temperature and pressure in the presence of a catalyst and steam (Ramon, 2016).

Hydrocracking technology has gained popularity over the last few decades in light petroleum refining (Rana, 2007). After full industrialisation of light petroleum oil, hydrocracking processes were then implemented for heavy oil and vacuum residue upgradation (Sadeghbeigi, 2000). The technologies used today to upgrade heavy residues are fixed-bed, ebullated-bed, moving-bed or slurry phase reactors. The operating principles for these reactors share some similarities but differ in some technical aspects as well as impurity tolerance.

Product selectivity is directly dependent on the catalyst properties such as shape, chemical composition, size, active sites and experimental conditions for the reaction (Cherzer & Gruia, 1996). For each of the reactor technologies, the operating conditions differ extensively, hence the nature of the feed, use of proper reactor system and catalyst are vital for the hydrocracking of the vacuum residue (Sahu et al., 2015).

In a fixed bed reactor, there is a continuous requirement for the withdrawal of deactivated catalyst, and immediate addition of fresh catalyst. A fixed bed reactor is basically a cylindrical tube, filled with a solid catalyst and reactants moving through the bed while being cracked into lighter products. Numerous configurations exist for the catalyst bed; these include multiple configurations such as one large bed, several parallel packed tubes, or catalyst packed on a tube support (Hildebrand, 1972). These configurations can be modified to meet reaction conditions and to maintain temperature control within the reaction system.

Advantages of a fixed bed reactor include ideal plug flow behaviour, decrease cost in maintenance and a decrease in loss due to attrition and wear. Another important aspect for the design of such a reactor is heat management. If the heat management is poor, heat distribution could lead to non-uniform rates of reaction which ultimately may lead to low reactant conversion. (Trambouze & Euzen, 2004).

For moving bed reactors, the fresh catalyst enters at the top while the deactivated catalyst exits the bottom of the reactor (Gupta & Gera, 2015). There is a fluid phase present within the unit that flows up through a packed bed. The feed is solid and is fed at the top of the reactor, and subsequently flows down. It is then removed from the bottom. Special control valves are required in the reactor, to maintain close control of the solids. For this reason, moving bed reactors are less frequently used than fixed bed reactors.

There are advantages to using a moving bed reactor which includes continuous removal of the spent catalyst when the active life has been depleted. These reactors can be used to obtain high conversion rates under decent conditions for selectivity. However, this technology does suffer from the problems associated with the manipulation of large quantities of granular solids. (Trambouze & Euzen, 2004). In most cases, hydrocracking of heavy residual oil requires multiple beds of catalyst, for fixed bed reactors. If the feed is of low quality for fixed bed reactors, a combination of ebullated-bed with fixed bed reactors can be more effective than using an individual system. (Gang Yang & Eser, 2002).

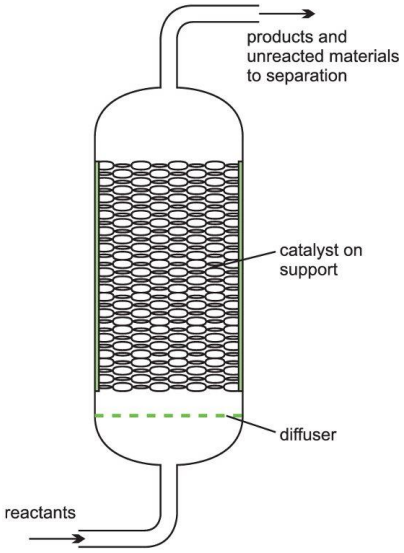

Figure 2.5 - Schematic of a fixed bed reactor (Alarcon-Gaete, 2016)

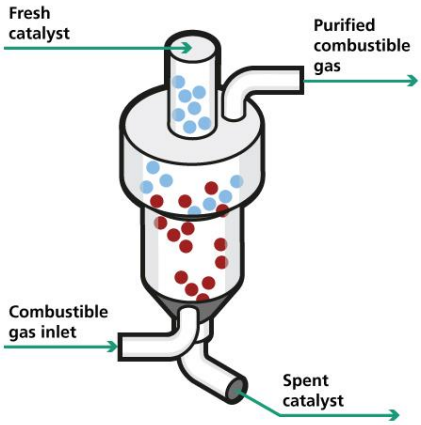

Figure 2.4 - Schematic of a moving bed reactor (www.iff.fraunhofer.de)

The feed to a hydrocracking unit may consist of cracked naphtha, straight run gas oil, thermally cracked stocks, solvent deasphalted residual oils, vacuum gas oils, cycle oils, coker gas oils and straight run naphtha (Furimsky, 1998).

The products produced include diesel fuels, heating oils, solvent, thinners, liquefied petroleum gas (LPG), motor gasoline, reformer feeds, aviation turbine fuel, lube oil and FCC feed.

Improvements in hydrocracking technology and catalyst technology have been the forefront of reactor technology research. In hydrocracking technology vital developments in mild hydrocracking and residual hydrocracking, have proven to be necessary. Mild hydrocracking (MHC) is categorized by comparatively low conversion (20-40%) as compared to conventional hydrocracking which can give conversions between the range of 70-100% of heavy distillate at excessive pressures (NPTEL, 2012).. Recent mild hydrocracking processes are able to produce as low as 10 ppm sulphur diesel. This is done by hydro-cracking under mild pressure (Sathya, 2012). The yield of lighter fractions obtained from the hydro cracker is greater than that obtained from other similar processes. Due to the increase in the demand of environmentally acceptable products, processes are put in place to meet specifications for gasoline and diesel, allowing for the use of hydrocracking technology to limit sulphur and aromatics in petroleum products. Post treatment is deemed unnecessary for the hydrocracked products (Sathya, 2012).

Hydrocracking technology involves two types of catalyst, namely hydro pre-treatment catalyst and hydrocracking catalyst (Cherzer & Gruia, 1996). For the pre-treatment catalyst, the main aim is to remove the nitrogen from the feed which allows for improved performance of the second stage hydrocracking catalyst, as well as the initiation of the sequence of reactions by saturation of aromatic compounds (Rana, 2007). The hydrocracking catalyst on the other hand is a bi-functional catalyst and serves the function to upgrade components by cracking and hydrogenation-dehydrogenation function. The acid sites provide cracking activity. Metals sulphides such as Wo, Mo, Co or Ni provide the necessary hydrogenation and dehydrogenation activity. These metals catalyse the hydrogenation of heavy feeds causing them to be more reactive for the cracking process and hetero-atom removal, which in turn leads to a reduction in the formation of coke (Gang Yang & Eser, 2002).

An example of a typical reaction that takes place is:

$$C_{22}H_{46} + H_2 \longrightarrow C_{16}H_{34} + C_6H_{14}$$

Hydrocracking reactions also involve the splitting of carbon-carbon bonds and or carbon-carbon rearrangement reactions.

The process variables that are critical in hydrocracking are hydrogen partial pressure, reaction temperature, hourly feed velocity of feedstock and hydrogen recycle ratio (Gary, 2004).

An increase in temperature causes accelerated cracking on acid sites, which then leads to displacement of the equilibrium of hydrogenation reactions, towards dehydrogenation. If the temperature is too high, the cracking of the aromatic structure is limited (Raseev, 2003).

Pressure on the other hand influences the equilibrium of dehydrogenation-hydrogenation reactions that takes place on the metallic sites. For a given H_2/feed ratio, an increase in pressure leads to an increase in the partial pressure of hydrogen. This then leads to increased conversion rates of the aromatic structures to saturated products which will improve the quality of product (Raseev, 2003).

The feedstock is affected by certain parameters by the following ways. High hydrogen/feed ratios and high pressure is required if there is an excessive amount of aromatic hydrocarbons. Extremely low temperature, excessive hydrogen consumption and the severity of the process all affect the feedstock (Raseev, 2003).

Impurities also have an effect on the process. Impurities including nitrogen compounds, hydrogen sulphide and aromatic molecules present in the feed, have an impact on the hydrocracking reactions. An increase in nitrogen results in lower conversion. Ammonia decreases activity of the catalyst for the hydrocracking reaction which will lead to requiring higher operating temperatures (Cherzer & Gruia, 1996). This is due to the presence of nitogen in the feed that could dilute the feed to lower conversion due to lower reactant concentrations. Nitrogen may also compete for active adsorption sites on catalysts. Polymeric compounds have substantial inhibiting and poisoning effects. Polynuclear aromatics are hydrocarbons made up of fused aromatic ring molecules. These rings share one or more sides with each other and contain delocalized electrons. These hydrocarbons only contain carbon and hydrogen atoms. Polynuclear aromatics also pose a problem as even a small amount in the residue can deactivate the catalyst (Cherzer & Gruia, 1996). The proposed reaction mechanism for the vacuum residue hydrocracking process is shown below.

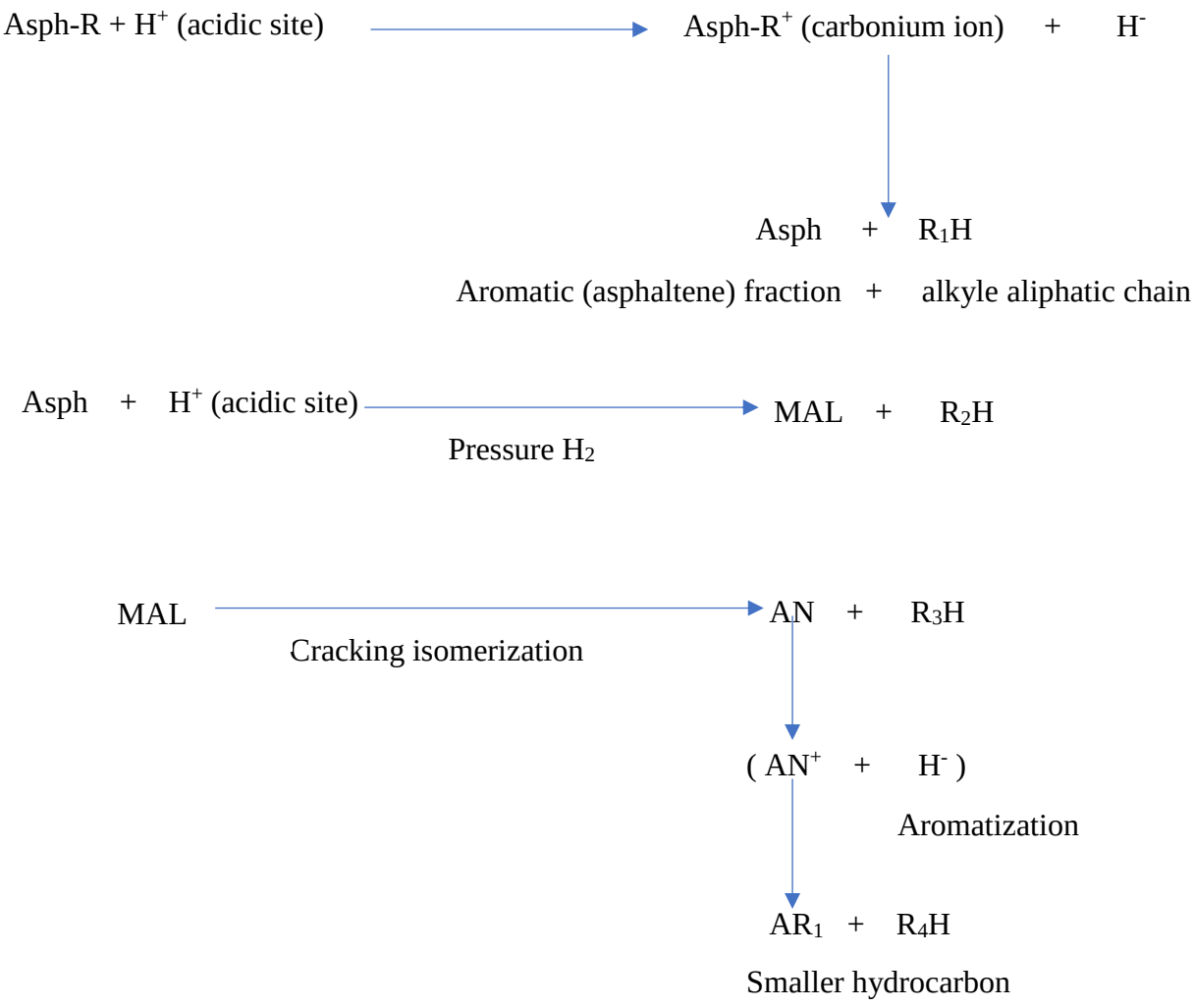

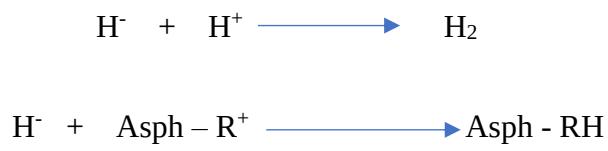

Figure 2.6 - Proposed reaction mechanism for vacuum residue hydrocracking (Cherzer & Gruia, 1996)

Asph = asphaltene or fused aromatic ring, R = alkyl chain, AN = hydroaromatic and MAL = maltene

Hydrocracking vs Catalytic Cracking

Catalytic and hydrocracking differ from each other beginning from the feedstock. Hydrocracking processes are able to handle a much wider range of feedstocks which is a huge advantage over catalytic cracking. It is also used to upgrade the heavy crude oil fractions such as heavy vacuum gas oil and vacuum distillation residue. Catalytic cracking struggles with cracking heavy residue due to the coking problems associated with the catalyst. Coking does lead to unfeasible results hence hydrocracking is favoured for heavy residue.

The processes also differ as well. The basis of catalytic cracking is carbon rejection, while hydrocracking is a hydrogen addition process, usually by the addition of steam (Sadeghbeigi, 2000). The catalyst used for each method differs as well, with catalytic cracking using an acid catalyst while hydrocracking uses a metal catalyst on an acid support. Acid catalysts such as zeolites contain natural acid sites that are able to catalyse cracking of hydrocarbons through the formation carbonium ion intermediates on the surface. Hydrocracking requires two types of sites, a metal site for activating surface hydrogen for insertion into the hydrocarbon molecule, and acid sites for the cracking. The support serves two functions, one to disperse the metal component of the catalyst which provides sufficient sites for hydrogen activation (support has high specific surface area and porous structure), and secondly to provide acid sites for cracking (Furimsky, 1998). Catalytic cracking is an endothermic reaction while hydrocracking is an exothermic reaction.

The two main processes associated with hydrocracking is the actual cracking of the material and hydrotreating. Hydrotreating is done to remove heteroatoms, while cracking is done to increase the H/C ratio of the hydrocarbons which results in a decrease of its molecular weight.

The products produced also differ as well. Catalytic cracking results in the production of paraffin's, iso– paraffin's, aromatics, naphthenes and olefins (Cornelius, 1985). Hydrocracking

on the other hand produces a decent amount of diesel fuel production. In hydrocracking the steam introduced provides a source of hydrogen and oxygen into the system. This helps reduce coke formation. The steam can be introduced by adding steam through a stream line once the feedstock in the reactor has reached its boiling point or an amount of water can be added to the feedstock prior to carrying out the reaction. This water will provide the hydrogen content as well as create a pressurised environment within the reactor, once it starts boiling at one hundred degrees Celsius.

Hydrocracking is the most favoured process due to the wide array of feedstocks it can use, but the cost for such a process is sometimes unfeasible to many. The following table summarises the differences:

Catalytic Cracking	Hydrocracking
Carbon rejection	Hydrogen addition
LPG/Gasoline	Kerosene/Diesel
Product rich in unsaturated components	Few aromatics, low S- and N-content in product

Table 2. 1 - Differences between Catalytic cracking and hydrocracking

Biological Process Technology Petroleum Residue upgradation

Biological processing of heavy residual fractions of crude oil provides less-harsh processing conditions and a greater selectivity for refining. These processes also require a smaller demand for energy and are environmentally friendly (Furimsky, 1998). Since it is seen that this technology offers higher selectivity to specific reactions and less harsh process conditions in refineries, it can be noted that the microorganisms are capable to biodegrade heavy fractions of petroleum residue (Gupta & Gera, 2015). A specific strain of Bacillus cereus has been documented to treat heavy oils. This biosurfactant producing bacterium utilises both anthracene and paraffin as samples of polycyclic and aliphatic aromatic hydrocarbons. Studies done by SARA showed that this bacterium decreased the amounts of asphaltenes, aliphatics and aromatics in vacuum residue (Gupta & Gera, 2015).

Nanoparticle Technology

In recent years nanotechnology has gained much interest as an alternative technology for in-situ heavy petroleum residue upgrading and recovery. Nanoparticle catalyst is one of the most

important industrial applications of nanotechnology. The nano-catalyst exhibit unique catalytic and sorption properties due to the high surface area-to-volume ratio as well as active surface sites. The use of multi-metallic nano catalyst in catalytic conversion or upgradation of heavy residue is a cost effective and environmentally friendly method to produce valuable oils that meet the required pipeline and industry standards. It is also possible that nano catalyst can be used as inhibitors to prevent asphalt precipitation and hence enhance oil recovery.

Future Developments

Studies have shown that crude oil will be heavier due to the high contents of impurities such as nitrogen, sulphur and other metals (Raseev, 2003). Current processes must be improved to allow hydrocracking of heavy oils into lighter and valuable products.

Factors such as properties of the feeds, contact time, operating conditions, catalyst activity and selectivity and certain chemical kinetic parameters, are important factors for achieving a desirable yield of the selected product. Combining these factors in a cost-effective manner is the main challenge for industry. Hydrocracking is the most effective method for upgrading heavy residue, however its effectiveness is dependent on the catalyst used. The catalyst should be able to endure metal and other impurities present within feeds, as well as showing great performance (activity, selectivity, stability and regenerability) and being cost effective (Cherzer & Gruia, 1996). Developments in fixed bed processes show that online catalyst replacement is more useful to a batch mode reactor. However, the process may not be efficient enough to handle heavy oils with higher metal impurities; improvements must be made in reactor design and operation conditions.

It is also seen that due to high investment, back mixing of the reactants, low reactor efficiency and high operating costs cause many issues in hydrocracking of heavy residue. The main steps to improve the situation includes optimization in reaction conditions, decrease costs in reactor design and using highly active and selective catalysts (Furimsky, 1998). Factors such as particle size, surface area, metal compositions and components, metal particle distribution and pore diameter all influence the activity and selectivity of the catalyst. The catalysts must also be reasonably priced, while having high mechanical strength and are recyclable. Studies have shown that molybdenum-based nanocatalyst with either an alumina or a silica support show resistance to coke formation (Pujado et al., 2006), hence will prove beneficial in the long term as well as being cost effective. For future developments, heavy residue technologies will likely

combine hydroprocessing techniques with other processes, such as thermal technologies or solvent de-asphalting. The field of nanotechnology will also be vital for finding a viable method for catalyst recovery.

2.3 Catalyst used in the upgrading of petroleum residues and heavy oils

Heavy crude oil contains large molecules called asphaltenes. These molecules contain highly condensable material, heterocyclic and aromatic rings which contain sulphur, nitrogen, oxygen and undesirable metals (Schacht et al., 2014). For the process of hydrogenation, catalyst usually contain nickel, tungsten, molybdenum and zirconium. Molybdenum based catalyst and nickel are widely used for refining processes such as hydrocracking or hydro-desulphurization. These catalysts usually require a support such us porous alumina or silica (Biasca, et al., 2003). These catalysts have acid-base properties which may lead to increased yields of gasoline and other light hydrocarbons in crude oil refining, while at the same time producing products that are environmentally friendly. Various catalyst used in heavy residue upgrading will be looked at in this section.

2.3.1 W-Zr Catalyst

W-Zr catalyst have been shown to be effective in the upgradation of crude oil. Experimental testing done by Schacht et al (2014), showed that the catalyst has a high activity in the removal of sulphur. However, the removal of the sulphur content is dependent on the type of feed and the operating conditions of the reaction. This high catalytic activity is due to the catalyst being acidic in nature, and the hydrocracking properties of the transition metals W and Zr (Joonaki, et al., 2012). The sulphur removal is caused by scission of the Carbon−Sulphur bonds, caused by extraction of thiophenic sulphur using the transition metal salts. The W-Zr catalyst has shown great ability to upgrade crude oil especially in hydro-desulphurization. It is still to be seen if it can upgrade heavy oil residue.

2.3.2 Molybdenum based catalyst

Molybdenum based catalyst such as NiMo or CoMo, have a variety of important applications in the petroleum industry. They are especially popular in the hydrodesulphurization of liquids derived from petroleum and coal sources. The catalyst is made up of MoS_2 supported on alumina, and promoted by cobalt or nickel. It is then prepared by sulfiding cobalt and

molybdenum oxides on alumina (IMOA, 2014). As the world supply of crude oil is further depleted and low-sulphur crudes are less available, molybdenum-based catalysts will gain popularity. The use of molybdenum is not only better for economical fuel refining, but also gives off less sulphur emissions leading to a safer environment (IMOA, 2014).

These catalysts are advantageous because they are resistant to poisoning by sulphur and catalyse the conversion of hydrogen and carbon monoxide from the pyrolysis of waste materials to alcohols in the presence of sulphur, under conditions that would poison precious metal catalysts (IMOA, 2014). These catalysts have not been used extensively in heavy residue upgrading, especially if the feeds have a low sulphur content, as they have a low selectivity towards the heavier components (Gang Yang & Eser, 2002).

2.3.3 Magnetite Nano-catalyst

The size of each of the particles of the heterogeneous catalyst determines the catalyst's selectivity, efficiency and specificity. Nano-catalyst have properties different from macroscopic systems due to a difference in specific area and also the presence of electrostatic charges surrounding them (Ramon, 2016).

In the refining processes of crude oil, the application of new technology catalyst such as magnetite nanoparticles has gained significant interest in recent years. These new catalysts contain various chemical and physical properties that are considered to be very effective catalytic agents for a wide array of reactions as they differ from the corresponding bulk phase. Some advantages of using a catalyst as such, is its high specific surface area of the particles, efficient dispersion of the catalyst within the reacting medium and the ease of recovery through magnetic separation are some of the benefits of utilizing these materials (Lokhat et al., 2015). Fe_3O_4 and Fe_2O_3 are new developments of magnetic nano-sized transition metal oxides to be used to oxidise various organic species. There are various methods available for the synthesis of iron oxide nanocatalysts of this nature, such as sol-gel processing, solution precipitation and water oil microemulsion method (Rana, 2007). Among these methods methods identified for the synthesis of Fe_3O_4 the chemical co-precipitation of Fe^{2+} and Fe^{3+} salts by addition of sodium hydroxide is the simplest and cheapest (Lokhat et al., 2015). Iron oxide nanocatalysts have been shown to have improved properties such as chemical stability and thermal stability, when supported with various transition metal oxides. Molybdenum is known to significantly improve the activity of some oxidation catalysts. The metal oxides can be incorporated into the

lattice structure through simple wet impregnation using a salt precursor solution (Lokhat et al., 2015).

2.3.4 Synthesis of Fe_3O_4 Magnetite Nano Particles (MNPs)

A viable method proposed by Khabazipour et al. (2016) for the production of Fe_3O_4 MNPs from aqueous solutions, is chemical co-precipitation. The method involves the mixing in a ratio of 2:1 ferric and ferrous ions, respectively in highly basic solutions at temperatures greater than 80°C. $FeCl_3.6H_2O$, $FeCl_2.4H_2O$, and HCl were dissolved in deionized water to prepare a stock solution of ferrous and ferric chloride. The solution is degassing by purging with nitrogen gas will be required as well. The stock formed should be slowly added to the ammonia solution under a nitrogen gas atmosphere, while stirring vigorously preferably with the use of a magnetic stirrer. Excess oxygen is to be removed by purging with nitrogen while maintaining a temperature at 80°C. After the reaction is complete, the Fe_3O_4 MNPs can be separated from the reaction solution magnetically. The product should then be washed with deionised water about four times. The obtained Fe_3O_4 MNPs is then dried for about in an oven for 120 minutes at 90°C.

In order to protect the iron oxide core from harsh acidic conditions, it is a necessity for the magnetite core to be coated with a silica layer prior to the synthesis of the mesoporous silica shell. To fabricate the $Fe_3O_4(SiO_2)$ MNPs, the MNPs that are synthesized must be dispersed in a mixture containing ethanol and concentrated ammonia. The $Fe_3O_4(SiO_2)$ nanoparticles is obtained after being washed with a solution of water-ethanol. $Fe_3O_4(SiO_2)$ is an integrated material of a mixed iron-silica oxide.

The synthesis of SBA-15 was performed according to the method reported by Zhao et al (1998), to obtain mesoporous magnetite nanoparticles (MMNPs**)**. Triblock copolymer pluronic P123 is used as direct-structuring agent. P123 is completely dissolved in distilled water. Then HCl and $Fe_3O_4(SiO_2)$ are to be added to the solution while continuously stirring. A small amount TEOS should be added immediately. The solution should then be transferred into the oven to dry under static conditions. Filtration of the product without washing and drying by vacuum is done. Lastly, the synthesized $Fe_3O_4(SiO_2)$ MMNPs is calcined and then ready to be used.

2.3.5 X-Ray Diffraction Analysis

"X-ray powder diffraction (XRD) is a rapid analytical technique primarily used for phase identification of a crystalline material and can provide information on unit cell dimensions. The analysed material is finely ground, homogenized, and average bulk composition is determined" (Brady & Boardman, 1995).

Diffraction methods used today are all based on generation of x-rays in an x-ray tube. The process involves directing the x-rays at the sample, while the rays diffracted are collected. These x-rays are directed at the sample, and the diffracted rays are collected. The angle calculated between the diffracted rays and incident rays is a key component to the process. X-ray diffractometers are the instruments that are used to generate diffraction patterns. The geometry of an x-ray diffractometer is such that the sample rotates in the path of the collimated x-ray beam at an angle θ while the x-ray detector is mounted on an arm to collect the diffracted X-rays and rotates at an angle of 2θ (Hluchy, 1999).

X-ray diffraction in this investigation was used to characterise the magnetite nanocatalyst, before and after the reaction. Apart from structure determination and quantitative phase analysis of the nano – particles, XRD also determines the effects of external factors on the structure of the nano-particles. The average crystallite size for a catalyst sample can be calculated using the Scherrer equation shown below (Lokhat et al., 2015):.

$$L = K\lambda / \beta\cos\theta \qquad \text{(equation 1)}$$

Where L is the crystallite diameter, K is the shape factor, λ is the incident X-ray wavelength, β is the full-width-at-half-maximum (in radians) of the highest intensity powder diffraction reflection, and θ is the corresponding half of a diffraction angle.

Due to the magnetic properties of the magnetite catalyst, x-ray diffraction analysis will determine whether there were any phase changes to the iron oxide. Also by analysis of the results generated it will be clear if the magnetite catalyst has lost its magnetic properties or not, providing an understanding whether the catalyst could be used again for the cracking reaction. The figure below provides some estimation of what an iron oxide diffraction pattern should look like.

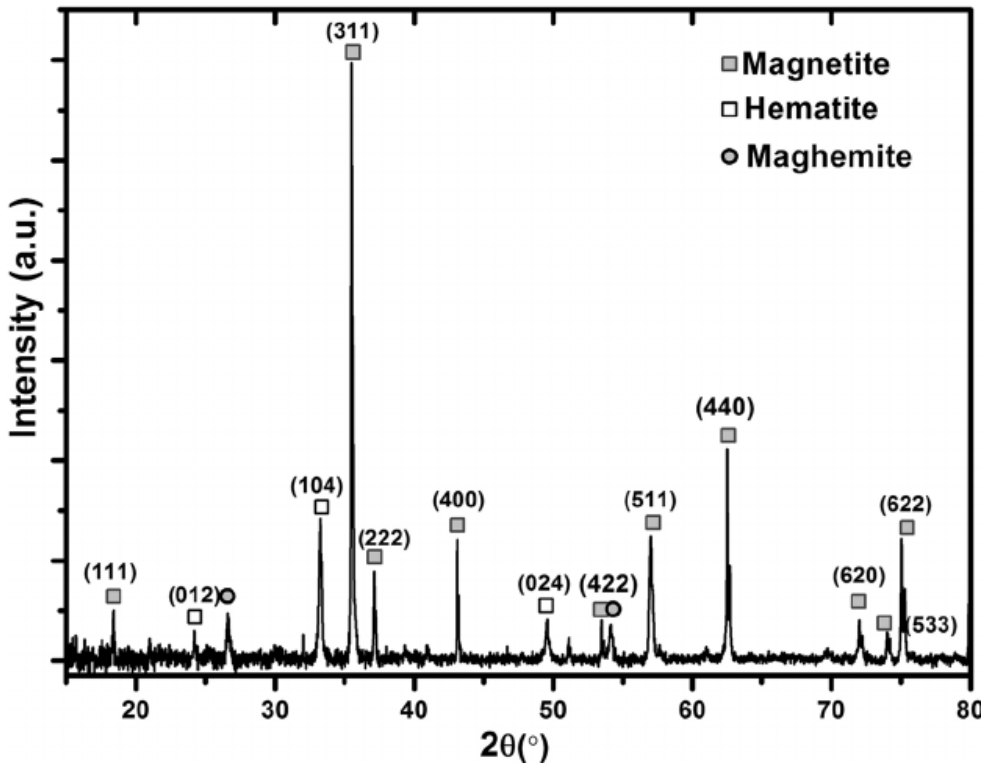

Figure 2.7 - Example of a XRD analysis of an iron oxide catalyst (Karami et al., 2013)

2.4 Characterisation of petroleum mixtures

2.4.1 GCMS Analysis

GCMS analysis involves a combination of gas chromatography and mass spectrometry in order to identify dissimilar components within a test sample. The gas chromatograph implements a capillary column which is dependent on the columns dimensions and the phase properties (Zeng et al., 2012). The chemical properties between components within the mixture and the relative affinity for the stationary phase of the column usually differ, which ultimately promotes separation of molecules as they pass through the column. The different molecules all have different retention times, which allows the mass spectrometer downstream to capture, ionise, deflect and detect the ionised molecules separately. Each molecule is broken down into ionised fragments and are detected by their mass-to-charge ratio.

Heavy oils which include resins and asphaltenes are the most difficult to analyze by GC because of their high boiling points. It has been reported however that a high temperature GC

technique in combination with MS has proven effective in heavy oil analysis (Zeng, et al., 2012). The method significantly extends the range of detectable hydrocarbons to approximately C_{120} compared to conventional GC which is limited to C_{35}. This is important in the study as short residue is composed of numerous components that are fairly unknown, so HTGC analysis will prove effective in characterisation of the residue and product samples.

There are various factors that could affect GC retention time and separation. These include: column temperature and temperature program, sample size and injection technique, column diameter and length, inlet temperature, carrier gas and carrier gas flow rates and the column's stationary phase,

It is advisable to keep the inlet temperature high so that vaporisation of the injected samples takes place, but also not too high that it leads to decomposition of the injected samples (Zeng, et al., 2012). Column temperature and temperature program are vital in terms of GC retention time and separation. The setup of the column temperature and temperature program is vital to make sure that all the molecules analysed are eluted and separated efficiently. High temperatures cause shorter retention times while a slower temperature ramp usually leads to better separation. The use of high speed carrier-gas flowrates leads to shorter retention times, which can cause peak co-elution. If the concentration of the injected sample is too high, the peaks in the chromatogram will be close together and appear crowded, which leads to inefficient separation, especially when the injected samples are crude oil samples. To rectify this issue, split injection techniques can be implemented. An excessive value for the split ratio (200), leads to a decrease in accuracy of the injection (Zeng, et al., 2012). The temperature programmed injection technique might be a good option due to the complexity of crude oil. Here the sample is introduced in the injector at low temperature followed by vaporization by a fast-programmed heating process. The split is open all in this case and the sample amount entering the column is proportional to the pre-set split ratio (Wang et al., 2010). All these factors have to be accounted for when analysing the product samples of the short residue after reaction in order to determine how much cracking has taken place,

2.5 Aquaprocessing

Aquaprocessing or AQP is a method whereby high conversion levels are achieved under the asphaltenes stability limit. This basically means that the process conditions are below the stability limit. In this process, water or steam is used as the source of hydrogen for hydrogenating the cracked components. The hydrogen is generated in-situ by the high

temperature decomposition of water, usually catalysed. In a study done by Fathi et al. (2013), the process was done in an open tubular pilot plant reactor using Arab Light Vacuum Residue.

AQP is catalytic process that utilises an ultradispersed catalytic metal active phase for steam cracking chemistry to maintain or improve the product stability and quality (Fathi.M., 2013). The catalysts generally involved for such processes are nickel, iron or molybdenum bases. In the study done by Fathi et al (2013), a nickel/potassium catalyst in the ratio 1:3 was utilised. The catalytic metal particulates were dispersed and combined to make a potassium promoted nickel catalyst in-situ. The function of such a catalyst is to generate hydrogen and oxygen radicals by breaking up the H_2O molecules in the steam, which then promotes hydrogen addition to the produced free hydrocarbon radicals (Fathi & Pereira-Almano, 2013)

2.5.1 Kinetic Modelling of Aquaprocessing

The kinetic modelling of aquaprocessing has been reported in the literature by Fathi et al (2013). The study involved a lumped kinetic model of five simulated distillation lumps cascaded under high space time velocities, which was investigated. An objective of the experiment involving AQP under various conditions was to develop a kinetic model that can be used to get a best estimate of the kinetic parameters. This in turn was used to develop a kinetic model that closely matches experimental results of the current investigation using the magnetite nanocatalyst. Since heavy oil upgradation follows first order kinetics (Singh, et al., 2005), the model proposed is composed of seven first order kinetic reactions generating 5 distinct clumps, based on boiling points, as shown in the figure below.

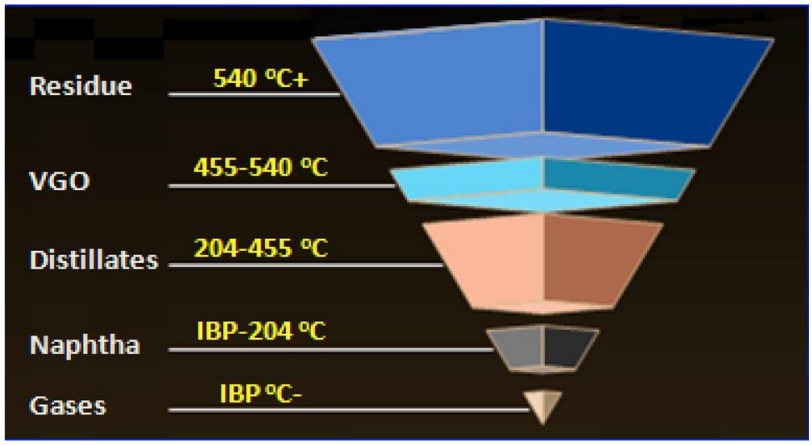

Figure 2.8 - Schematic of the cascaded kinetic model products distribution (Fathi et al.,, 2013)

The reactivity tests carried out by Fathi et al (2013), was done at 260 psi in a 100 cm^3 up flow isothermal tubular reactor. The liquid hourly space velocities (LHSV), for thermal cracking, were 2 and 2.5 h^{-1} at temperatures of 400, 405 and 408 ˚C. Considering that the minimum catalyst activation temperature of 430 ˚C was used, the experimental conditions at which the AQP tests was conducted was 435 ˚C and LHSV of 5-7.5 h^{-1}, 440 ˚C and LHSV of 6-8.5 h^{-1}, and 445 ˚C and LHSV of 8-10.5 h^{-1}.

The kinetic model proposed assumed negligible coke formation and asphaltene precipitation. Vacuum gas oil is a complex mixture and coke formation would lead to difficult mass balance calculations, so to neglect coke formation, the experimental conditions were chosen carefully as stated above. Other assumptions made were low residence time and lumping the products into five classes.

The following flow diagram is a representation of the kinetic model:

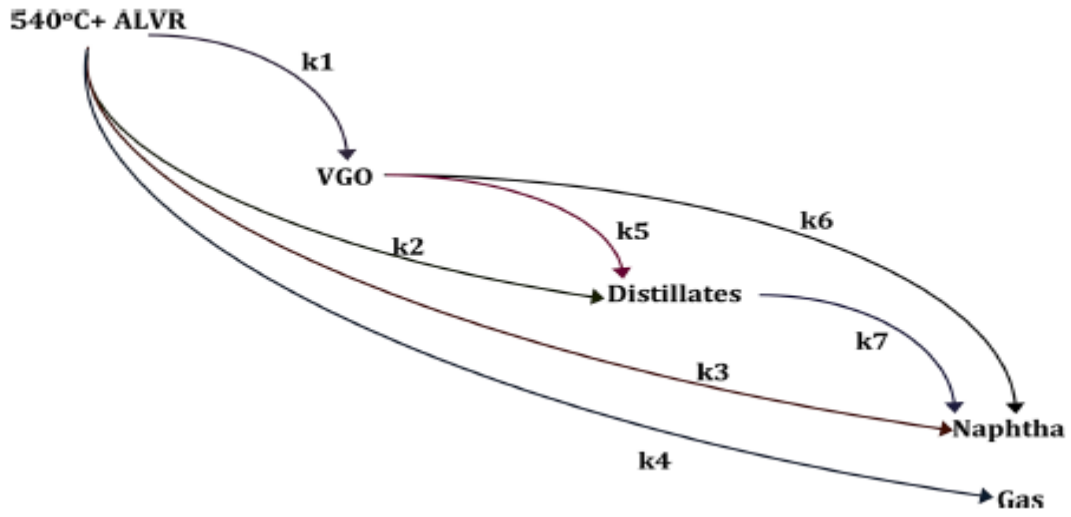

Figure 2.9 - Proposed lumped kinetic model (Fathi & Pereira-Almano, 2013)

The reaction pathways are shown in the above figure for the hydrocracking of vacuum residue over an unsupported nickel-based catalyst. The various products are obtained through both series and parallel reaction steps. The reaction pathways provide clarity on what reactions are favoured to produce the various fractions. For instance, a reaction pathway following k1 – k5-k7, will show substantial yields of vacuum gas oil, gas oil and naphtha products. However, if a pathway followed k3 only, it would result in large amounts of naphtha being formed with little or no vacuum gas oil and gas oil product.

Figure 2.9 above represents the proposed model configuration that employs seven first-order kinetic rate constants. The reactions are assumed to be first order (Singh et al, 2005), and given by the expressions below:

Reaction 1: A $\longrightarrow$ B

Reaction 2: A $\longrightarrow$ C

Reaction 3: A $\longrightarrow$ D

Reaction 4: A $\longrightarrow$ E

Reaction 5: B $\longrightarrow$ C

Reaction 6: B $\longrightarrow$ D

Reaction 7: C $\longrightarrow$ D

Where A – Vacuum residue

B- Vacuum gas oil

C- Gas oil

D- Kerosene

E- Gas

The material balances for each clump are given by the following set of ODE's:

$$\frac{dW_A}{dt} = -(k_1 + k_2 + k_3 + k_4) \times W_A$$

$$\frac{dW_B}{dt} = k_4 \times W_A - (k_5 + k_6) \times W_B$$

$$\frac{dW_C}{dt} = k_2 \times W_A + k_5 \times W_B - k_7 \times W_C$$

$$\frac{dW_D}{dt} = k_3 \times W_A + k_6 \times W_B$$

$$\frac{dW_E}{dt} = k_4 \times W_A$$

Where W_i is the mass fraction of the chemical lump.

The following table displays the Arrhenius parameters and activation energy:

	K1	K2	K3	K4	K5	K6	K7
Activation Energy (kJ/mol)	152	180	188	167	101	245	150
A (1/min)	2.315×10^{9}	1.454×10^{11}	2.934×10^{10}	0	1.22×10^{6}	4.118×10^{14}	6.284×10^{8}

Table 2. 2 - Arrhenius numbers and activation energy

Table 2.2 represents how much energy is required to shift the reaction into its respective fractions. The reaction pathways for k6 represents the highest activation energy. This means that the most energy is required to shift vacuum gas oil straight into naphtha, with little or no gas oil. This reaction is most likely to be favoured at high temperatures. The reaction pathway for k3 is quite interesting, as the activation energy shows that less energy is required to shift the reaction from vacuum residue into naphtha than vacuum gas oil into naphtha. The reaction pathways for k5 has the lowest activation energy, which means the least energy is required to shift the reaction from vacuum gas oil to gas oil.

CHAPTER 3

3.0 Experimental Methods and Apparatus

For this research, the performance of the unsupported magnetite nanocatalyst was investigated utilizing a batch reactor set up while the supported magnetite nanocatalyst was investigated utilizing a fixed bed reactor set up. The experimental setup for each reaction process can be seen in Appendix G, while the experimental method is explained below.

3.1 Batch Reactor Experimental

3.1.1 Materials

The following materials and equipment were utilised during the experimental work;

- Parr 5500 series compact batch reactor
- Parr 4848 reactor temperature controller
- Pressure gauge
- Thermocouple
- Stainless steel heating jacket
- Measuring cylinders
- Glass beakers
- Glass sample vials
- Cooling water inlet and outlet stream lines
- Spare valve seals
- Vapour trap
- Heat resistant gloves
- Nitrile gloves
- Gas chromatograph mass spectroscopy

- Plastic syringes
- Buchner funnel
- Filter paper

List of Materials

- Short residue as feedstock
- Toluene
- Molybdenum magnetite nanocatalyst
- Water
- Lubrication for reactor components
- Thread tape

3.1.2 Experimental Design

The following table shows each run specifications:

Run	Temperature(˚C)	Short residue(ml)	Toluene(ml)	Catalyst (g)	Water(ml)
1	350	7.5	7.5	2	7.5
2	360	7.5	7.5	2	7.5
3	370	7.5	7.5	2	7.5
4	380	7.5	7.5	2	7.5
5	390	7.5	7.5	2	7.5
6	400	7.5	7.5	2	7.5
7	380	7.5	7.5	1.5	7.5
8	360	7.5	7.5	1.5	7.5
No catalyst	400	7.5	7.5	2	7.5

Table 3. 1 - Batch reactor run specifications

The experimental plan for this investigation was to determine the temperature as well as the catalyst effects on the amount of cracking that has taken place. Previous investigations in undergraduate research was done from run 1 to run 6 (Section 4.2, Figure 4.3) to determine the temperature effects on the amount of cracking taking place (Maharaj, 2016). During the current

investigation, the catalyst ratio was investigated. Runs 1 to 6 investigated the effects of temperature at a fixed catalyst/residue ratio while runs 7 and 8 decreased the catalyst/residue ratio to compare to runs 2 and 4. A run was also done using no catalyst just to give an indication of how significant the use of a catalyst is in the experiment.

Since this was a first look at the performance of the magnetite catalyst for the aquaprocessing of heavy petroleum residues it was decided that the potentially major operating variables, i.e. temperature and ratio of catalyst/residue would be investigated using a simple one-variable-at-a-time (OVAT) approach, rather than a factorial experimental design for instance. This approach was necessary to determine the appropriate range of operating conditions for the aquaprocessing, which would have been required if a more elaborate design of experiments were used. The OVAT approach also allowed for better visualization of trends in the yield of products. Since the suggestion from collaborators on the project was to test an immobilized form of the magnetite catalyst in a continuous process, there was a natural progression with this approach to the study of the magnetite-silica catalyst.

3.1.3 Preparation of the feedstock

Due to the difficulty of working with short residue a method had to be devised to be able to get measurable quantities of the material.

The short residue (contained within a steel vessel) was heated on a heating mantel for approximately 30 minutes at 50˚C. Once the short residue becomes a less viscous liquid, 7.5 ml of the residue is poured into 7.5 ml of the toluene solvent. The solvent is in place to keep the residue in the liquid form. The residue/toluene mixture should be stirred using a metal rod to prevent settling of the residue and allow mixing. Water in the amount of 10 ml was then added to the mixture. The water provides the hydrogen content which is necessary for hydrocracking. Lastly, the amount of catalyst specified can be added to the feedstock. The heating mantle should be switched off and all materials should be stored in the fume cupboard provided. This completes the feed preparation.

The reason for only using 25ml of feedstock is to make sure the reaction takes place with a safe pressure range. One run prior to run 1 was done using 100 ml of feedstock. This resulted in a pressure of 180 bar which resulted in the reactor bursting. Hence using 25 ml of feedstock maintains a pressure around about 50 bar, which allows safe operation.

3.1.4 Reactor Experimental

The following steps provide a detailed explanation of how the experimental work was carried out in the reactor:

Firstly, with the assistance of the lab technicians the reactor was assembled, with all safety measures put in place to provide a safe working environment. The reactor cylinder must be clean and dry, to prevent impurities from entering the reactor. Once the reactor is clean, the feedstock can be added to the cylinder. The reactor must be sealed tight before turning on the reactor controller. The water stream line connected to a tap should then be opened, only to an extent where there is minimal flow. The reactor temperature controller can then be put on and then setting the temperature and impeller speed to the required specification. The impeller speed should be at 500rpm, if used at a higher speed the shaft will cease. So, using 500rpm is within a safe working range. Once the set reactor temperature is reached (approximately 3 hours), a reaction time of 1 hour is required. This allows cracking at the set temperature to occur. Once the reaction time is complete, the reactor controller can be switched off and the reactor can cool down. The reactor is usually allowed to cool overnight as dealing with a reactor at high temperatures is extremely dangerous.

3.1.5 GCMS Analysis

The next step is to do an analysis of each of the product samples using a GCMS. The analysis procedure is explained below:

After the completion of each run in the reactor, the product is collected in a glass vial and sent to the GCMS to be analysed. The product masses and volumes are recorded before commencement of analysis. The product sample contains water, toluene, catalyst and cracked short residue. Therefor a centrifuge had to be used to separate the liquids from each other to obtain a dry product sample. Once the sample has been separated in the centrifuge, a syringe was used to extract 1 ml of the cracked residue and placed in a 2ml sample vial. This vial is placed in the GCMS for analysis. Each product analysis takes approximately 86 minutes. The GCMS produces results in the form of an ion chromatogram, which further must be analysed. Using in-built software on the GCMS, each peak on the chromatogram can be identified, hence it is possible to determine what the product sample is made up of. The GCMS also provides a qualitative analysis of each sample, such as peak area and intensity. These are important for

fractional yield calculations. Once all data is recorded, the GCMS must be switched off and all glassware must be cleaned with toluene and water.

3.1.6 Catalyst Recovery

The catalyst from each sample had to be collected so that it could be sent for x-ray diffraction analysis to determine if there were any phase changes to the iron oxide. The following steps explains how this was done.

After each sample was done in the centrifuge, the catalyst would settle at the bottom of the glass vessel. This allows the catalyst from each sample to be easily collected. The catalyst contains impurities, so it should be cleaned. First the catalyst was soaked in toluene to remove residue from its surface. The solution is then filtered with a Buchner funnel under suction. Once the toluene has been filtered off, the catalyst is then soaked in acetone to remove the rest of the impurities. The solution once again is filtered under suction until lastly the catalyst is soaked in distilled water and filtered. The catalyst is then allowed to dry at 100˚C in an over for 90 minutes. Once dry, the catalyst is placed in a glass vial and sent to UKZN Westville Campus to be analysed by XRD analysis.

3.1.7 X-ray Diffraction

The particle size and size distribution of the nanocatalysts were measured with a Shimadzu SALD-3101 laser diffraction particle size analyser. X-ray powder diffraction (XRD) patterns for all materials were recorded using a PANalytical Empyrean X-ray diffractometer with a Co Kα (1.789 Å) radiation source (40 kV, 45 mA). The scans were performed at 25^{o}C in steps of 0.008^{o}, with a recording time of 6.98 s for each step (Lokhat et al., 2015)

3.2 Fixed Bed Reactor Experimental

3.2.1 Materials

The following materials and equipment were utilised during the experimental work;

- Heating wire
- Variac
- Measuring cylinders
- Glass beakers

- Glass sample vials
- Round bottom flask
- Heating mantle
- Centrifugal pump
- Heat resistant gloves
- Nitrile gloves
- Gas chromatograph mass spectroscopy
- Plastic syringes
- Thin wire mesh
- Insulation tape

List of Materials

- Short residue as feedstock
- Toluene
- Magnetite nanocatalyst on mesoporous silica support
- Water
- Lubrication for reactor components

3.2.2 Experimental Design

The performance of conventional nickel molybdenum and cobalt molybdenum catalyst was investigated to determine if the supported magnetite nanocatalyst will yield better results. The effect of temperature on the amount of cracking was investigated for these experiments. It must also be noted that a run at 400˚C was done using glass beads as an inert material to serve as a comparison.

NiMo Catalyst						
Run	**Temperature(˚C)**	**Short residue(ml)**	**Toluene(ml)**	**Catalyst (g)**	**Water(ml)**	**Flowrate (ml/minute)**
1	360	7.5	37.5	5	10	1
2	380	7.5	37.5	5	10	1
3	400	7.5	37.5	5	10	1

Table 3. 2 - Run specifications using the NiMo catalyst

CoMo Catalyst						
Run	**Temperature(˚C)**	**Short residue(ml)**	**Toluene(ml)**	**Catalyst (g)**	**Water(ml)**	**Flowrate (ml/minute)**
1	360	7.5	37.5	5	10	1
2	380	7.5	37.5	5	10	1
3	400	7.5	37.5	5	10	1

Table 3. 3 - Run specifications using the CoMo catalyst

Molybdenum doped magnetite nanocatalyst						
Run	**Temperature(˚C)**	**Short residue(ml)**	**Toluene(ml)**	**Catalyst (g)**	**Water(ml)**	**Flowrate (ml/minute)**
1	360	7.5	37.5	5	10	1
2	380	7.5	37.5	5	10	1
3	400	7.5	37.5	5	10	1

Table 3. 4 - Run Specifications using the Magnetite nanocatalyst on a mesoporous silica support

3.2.3 Feed Preparation

The feed was prepared in the same manner as the batch reactor experiments with minor differences Once the residue is heated up, 7.5 ml of residue is added to 37.5 ml of toluene. A 5:1 dilution ratio was used to ensure that the residue can flow smoothly through the experimental apparatus and not harden and stick to the equipment, which may lead to blockages. 10 ml of water is then added to the feed mixture to provide the hydrogen content required for hydrocracking. The feed is then prepared and ready to be used for the reaction process.

3.2.4 Reaction Process

It is vital to ensure that all tubes, pipes and equipment are clear from any blockages and clean before commencement of the experiment. As an initial step, toluene is fed into the pump to line the vessel, which ensures sufficient suction. The reactor tube is opened and a smaller tubular support is placed within the reactor tube and with a mesh covering the top of the support to hold up the catalyst. About 5 grams of catalyst is added to form a small bed as shown in figure G.7 of appendix G. Once that is complete, all connections between equipment such as tubes must be checked to make sure they are tightly sealed to prevent any leaks of fluid. The inlet tube to the reactor is wrapped in heating wire and then insulated so that it allows for vaporization of the toluene. The heating wire is connected to a variac that is set at 100 volts to allow the tube to be heated to 110 ˚C, which meets the boiling point of toluene. The reactor is then switched on and set to the required temperature using the inbuilt temperature controller, on the reactor.

Once the reactor and inlet tube to the reactor have reached their respective temperatures, the feed is then ready to be pumped into the reactor. The residue mixture, retained in a beaker, is then placed on a magnetic stirrer which ensures continuous mixing of each of the fluids to prevent separation. The inlet tube of the pump is then clamped and positioned within the feed beaker to ensure that it doesn't move away, which could lead to air entering the tube and can cause suction problems. The pump is then switched on and the flowrate is adjusted to the required value, using the flow controller inbuilt onto the pump. It is a continuous process, so once the pump has been switched on, the experiment will only stop when the feed mixture has been used up.

It is important to pay attention to the product collection beaker to make sure that fluid exits the system, and if not, it means that there is a blockage in the system. The experiment must be stopped immediately in this case. Initially toluene and water will exit the reactor and be collected. As the deep black residue begins exiting the reactor it is collected in a clean beaker to allow for more accurate yield calculations, while avoiding the water and toluene content as they are not being cracked in the process. The experiment then runs for 15 minutes, to allow for sufficient sample collection. Once enough product is collected, the reactor is then switched off as well as the variac and pump. The product is then transferred into a glass vial and sealed to prevent evaporation of the toluene. The mass of product is recorded and it is then stored in a refrigerator until ready to be analysed. The reaction system is then allowed to cool, usually

overnight. The tubing connected between the reactor and pump is then removed and washed with toluene. The pump is also washed with toluene to make sure the residue hasn't caused any blockages. The reactor tube is then removed and opened to remove the catalyst and then washed with toluene as well. Once all apparatus has been cleaned, the system is ready for a new run.

To record the mass of feed entering the reactor vessel, the pipeline connecting the pump and reactor must be separated. The pump is then switched on, and the amount of residue exiting the pump outlet is regarded as the feed mass entering the reactor vessel. This mass was assumed to be the same for all runs.

3.2.5 GCMS Analysis

The next step is to do an analysis of each of the product samples using a GCMS. The same approach was used for both the supported and unsupported catalyst products. The analysis procedure is explained below:

After the completion of each run in the reactor, the product is collected in a glass vial and sent to the GCMS to be analysed. The product masses and volumes are recorded before commencement of analysis. The product sample contains water, toluene, catalyst and cracked short residue. Due to the low dilution ratio implemented when using the unsupported catalyst a centrifuge had to be used to separate the liquids from each other to obtain a dry product sample. The products from the supported catalyst experimental did not have to go through this step. Once the sample is done in the centrifuge, a syringe is used to extract 1 ml of the cracked residue and placed in a 2ml sample vial. This vial is placed in the GCMS for analysis. Each product analysis takes approximately 86 minutes. The GCMS produces results in the form of an ion chromatogram, which further must be analysed. Using in-built software on the GCMS, each peak on the chromatogram can be identified, hence it is possible to determine what the product sample is made up of. The GCMS also provides a qualitative analysis of each sample, such as peak area and intensity. These are important for fractional yield calculations. Once all data is recorded, the GCMS must be switched off and all glassware must be cleaned with toluene and water.

3.3 Synthesis of the supported and unsupported magnetite nanocatalysts

3.3.1 Supported Catalyst

The following procedure was used to synthesize the 15wt% Fe3O4/SiO2 catalyst.

Firstly, iron nitrate is produced by mixing ferric chloride and nitric acid. It was necessary to heat the solution to about 50-70°C to drive off any HCl that may be produced. The solution is then diluted with deionised water to a more appropriate concentration (based on number of moles of Fe required to load 15 wt% Fe3O4 onto the amount of silica being used). Silica particles are then introduced (average specific surface area 280 m^2/g). The mixture will need to be stirred overnight. The mixture is then filtered under suction and dried at 10°C/min to 300 °C under air (hold half hour). Lastly the particles are treated with 5% H_2 in N_2 (10 °C/min to 400°C), then only N_2 for 30 min at 400 °C.

It must be noted that after the last calcination step the catalyst reverted to the Fe_2O_3 state (reddish brown). The catalyst requires pre-reduction under H_2 before use in the cracking experiments. The catalyst was exposed to H_2 gas for 1 hour at 400°C within the reaction vessel to allow for pre-reduction back into the Fe_2O_4 state.

3.3.2 Unsupported Catalyst

The procedure to synthesize the magnetite nanoparticles, done by Lokhat et al (2015), was based on the method of co-precipitation of a stoichiometric mixture (2:1 ratio) of Fe^{3+} and Fe^{2+} salts with NaOH.

$FeCl_2$ was prepared by dissolving steel wool in a diluted solution of HCl, while in the presence of a nitrogen atmosphere. The nitrogen atmosphere prevents oxidation during the preparation. A similar procedure was utilised to produce $FeCl_3$ with a few drops of hydrogen peroxide added, just to force the transition to the 3+ state. These iron salt solutions were then combined in a 1:1 ratio, within an open beaker, while adding constantly NaOH in a dropwise manner. After agitation of the mixture, a dark greenish grey precipitation of $Fe(OH)_2$ was produced. This was then transferred into a beaker of fresh water with an adjusted pH between 13-14,

which was achieved by adding NaOH. Oxidation of the mixture to Fe_3O_4 was achieved by aerating the vessel while also agitating the mixture under the action of an ultrasonic bath.

To prepare the molybdenum doped magnetite nanocatalyst, an appropriate amount of ammonium molybdate was added to the dry magnetite to produce a slurry. After agitation of the slurry, it was centrifuged and the solid material was allowed to dry overnight. Calcination of the product, in a furnace at 500˚C, was necessary as well. This allowed the ammonium molybdate precursor to decompose to the metal oxide. The iron oxide then in the Fe_2O_3 state was then heated under hydrogen until molybdenum doped Fe_3O_4 was produced.

CHAPTER 4

4.0 Results & Discussion

The main aim of this project was to investigate the performance of supported and unsupported magnetite nanocatalyst for the hydrocracking of heavy petroleum residue. The yields of the products calculated should also be compared to results simulated for a conventional hydrocracking reaction using kinetics from literature in order to determine how effective, the magnetite catalysts are. A hydrocracking reaction was chosen over conventional catalytic cracking procedures as the hydrogen content results in less coke being formed. This undesirable coke formation is also limited using a molybdenum doped magnetite nanocatalyst. The scope of this investigation does not account for the amount of coke formed, but rather the catalyst itself and whether it can be regenerated or not after the cracking reaction. Investigation into the use of the molybdenum doped magnetite nanocatalyst was done previously at undergraduate level. At postgraduate level, the program was then extended considering the catalyst ratio on the yields of products. The use of an magnetite catalyst on a silica support was also investigated, in order to determine if such a catalyst would be effective for industrial use. The results for both of the cases is discussed below.

4.1 Feed Analysis

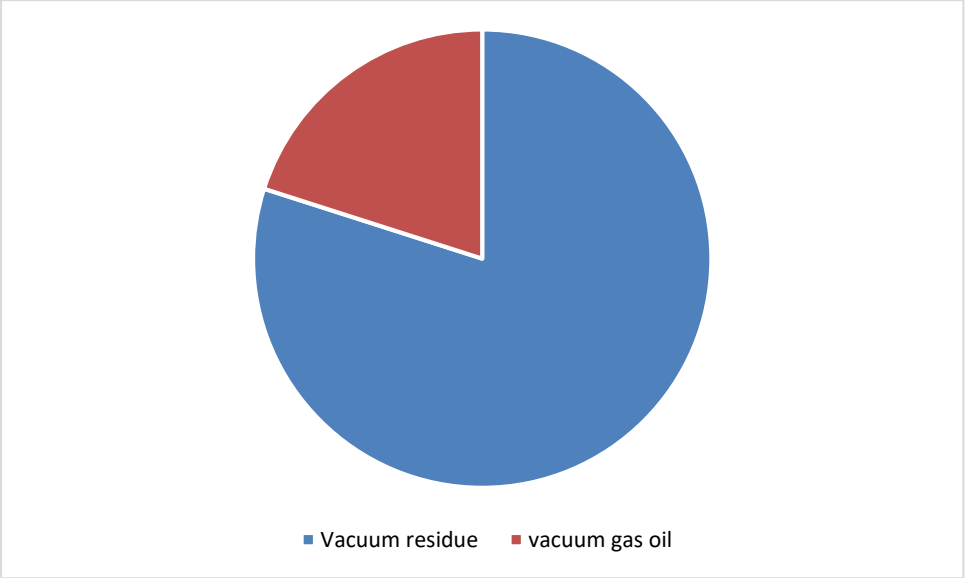

Figure 4. 1 - Pie chart illustrating mass fraction composition of feed

The aim of this experiment was to investigate the extent to which the temperature and catalyst affected the cracking of petroleum residue. From figure 4.1, above, it is clear that the petroleum residue feed is made up primarily of vacuum residue (79.87%) - the heaviest boiling components, with the remainder being vacuum gas oil. This is expected as short residue is the bottoms product from the vacuum distillation column, hence the large amount of vacuum residue. This composition was assumed constant for all the samples created during the duration of this experiment. This assumption; however, could contribute toward inaccuracies discussed with the results obtained. Characterization of the feed, shown in table C.1 in appendix C indicates that the short residue obtained from SAPREF has little or no sulphur.

4.2 Unsupported Catalyst Results

The temperature effects as well as catalyst:residue ratios were investigated on the yield of products formed after the cracking reaction. Figure 4.2 displays all the runs carried out in specific order. Previous investigations were done on the temperature effects on the amount of cracking taking place, which is shown in Figure 4.3. In the current programme, analysis on the catalyst to feedstock ratio was investigated depicted in figures 4.4 and 4.5. Figure 4.6 is the simulated composition profiles, figure 4.7 being simulated fractional yields, while figure 4.8 is the XRD analysis.

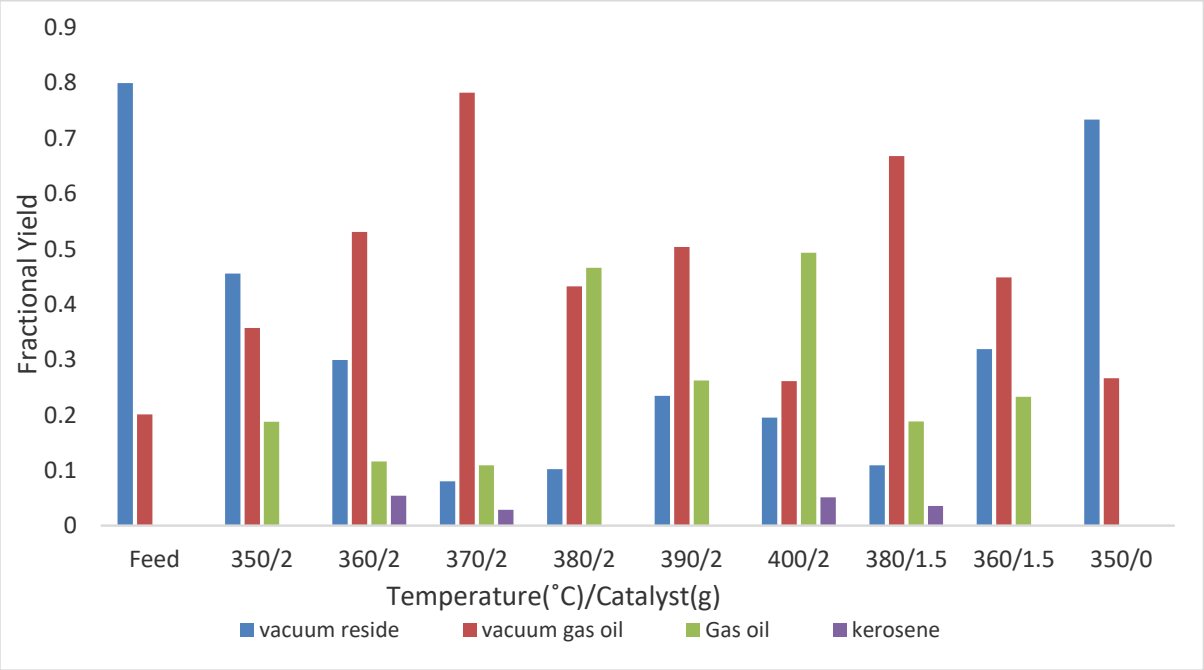

Figure 4. 2 - Fractional yields of cracking products for all experimental runs

A Parr 5500 series compact batch reactor was utilised throughout the experimental work to carry out the hydrocracking reaction. The feed to the reactor consisted of short residue mixed with toluene and water. The solvent chosen was toluene, which kept the short residue in a liquid form due to the high viscosity of the residue. The solvent also ensured that the residue could be transferred to the reaction vessel for processing and that the reaction mixture could be agitated during the heating up period. The specified amount of catalyst was lastly added to the feedstock. Usually steam is added to the reactor to provide the hydrogen content for hydrocracking, however this resulted in the pressure reaching a hazardous limit of approximately 180 bar. Due to this only a small amount of water was added to provide the hydrogen content and produces a pressurised environment when boiling temperature is reached.

The basis of the post run analysis was to determine the fractional yields of the products formed after the cracking process had been completed. A gas chromatograph mass spectrometer (GCMS) was used for analysis of products. The GCMS produced results in the form of a total ion chromatograph. The area of the peaks was used to calculate the respective fractional yields of each fractional group. Each fractional group was identified by using its respective boiling point (Appendix C).

The temperatures for each run were varied between 350˚C and 400˚C. Even though the reactor can handle temperatures up to 450˚C, the current temperature range was chosen in order to determine if cracking can occur at lower temperatures than conventional cracking and aquaprocessing.

Figure 4.2 shows the fractional yields of each run. The fractional yields were based on the feed mass of 6.467 grams. The mass of the sample was measured prior to the reaction and after the reaction was completed, and it was calculated that the mass of product lost to gas was negligible, hence fractional yields are based on the feed mass. The reactor and set up acted as a closed system hence, negligible mass loss was assumed. A run was also done using no catalyst, at 400˚C, with the feedstock to determine if cracking of the short residue can take place or not. From Figure 4.2, the run carried out with no catalyst produced a fractional yield of 73.4% vacuum residue and 26.6% of vacuum gas oil. It is quite evident by this result that without the use of a catalyst that the amount of cracking taking place is insufficient to shift the product into the lighter fractions.

Analysis of Figure 4.2 indicates that as temperature increases so does the amount cracking, as the amount of vacuum residue decreases significantly at higher temperatures. It is also clear that as temperature increases sufficient cracking occurs to shift it into the lighter fractions as the amount of gas oil increases greatly. A closer look into the temperature effects are shown in the figure below.

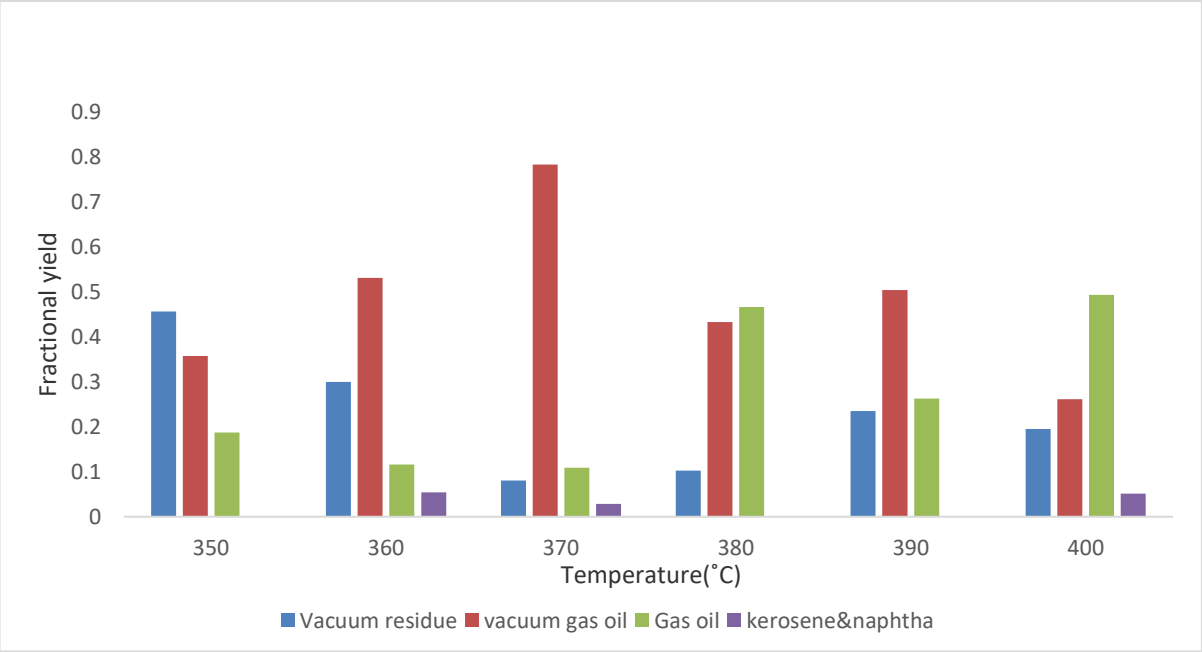

Figure 4. 3 - Fractional yields varying Temperature with Catalyst/Feedstock ratio of 0.3

Six runs were carried out maintaining a catalyst to feedstock ratio of 0.3 (feed mass is 6.467g) as shown in figure 4.3. This was done in order to determine the temperature effects on the cracking reaction. From the trend observed, it can be seen that as the temperature increases so does the amount of desirable gas oil and kerosene. Even though the run at 360˚C shows a greater amount of kerosene than the run at 380˚C, the overall shift into lighter fractions is greater at the higher temperature. The amount of heavier vacuum gas oil also decreases as temperature increases which shows that greater amount of cracking occurs at higher temperatures as there is a shift into the lighter fractions. The run carried out at 400˚C showed the best results with a fractional yield of 6% of kerosene, 49.3% of gas oil, 26.1% of vacuum gas oil and 19.5% of vacuum residue. It is also noted that at higher temperatures there is also higher amounts of vacuum residue than in the lower temperature runs. This is most likely due to the greater range of vacuum residue components being produced. The result at 380˚C compared quite favourably to that of 400˚C which is a positive indication that sufficient

cracking occurs at low temperatures compared to conventional methods (450˚C) (Fathi.M., 2013).

Clearly it has been established that temperature plays a vital part in the amount of cracking that takes place. Investigation whether the amount of catalyst has any effect on the extent of cracking taking place was then done. The figures below depict the results.

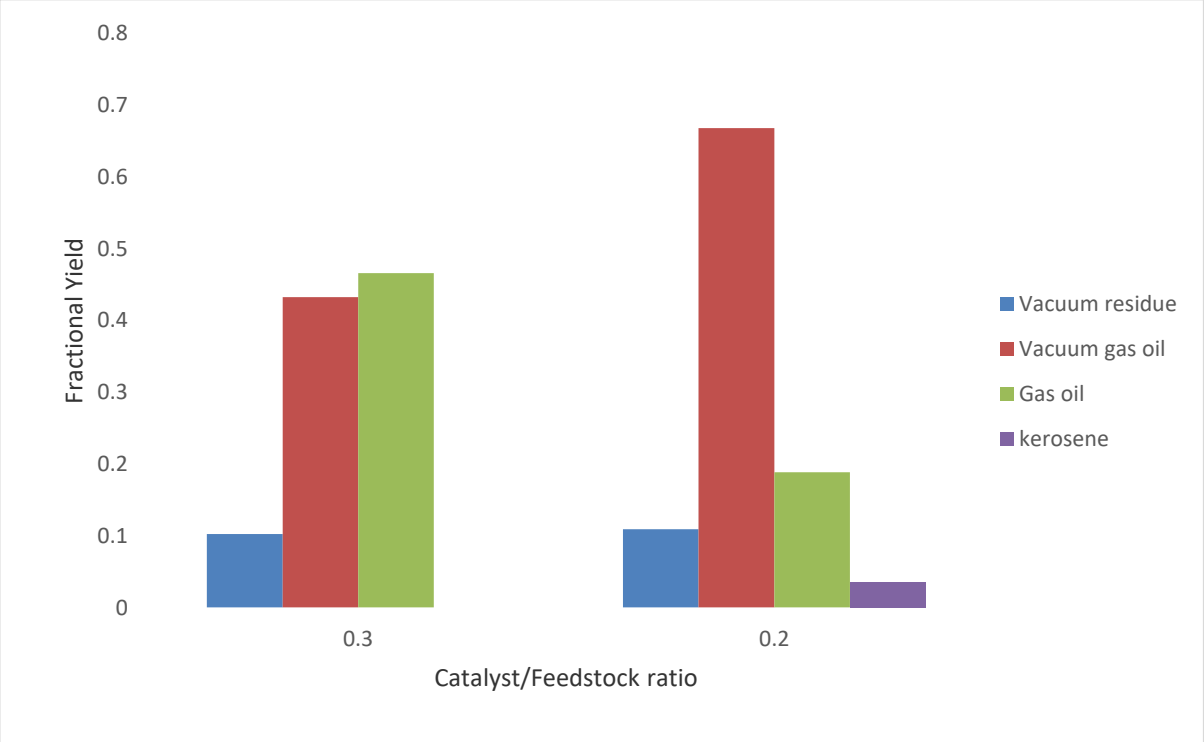

Figure 4. 4 - Fractional yields varying catalyst to feedstock ratio at 380˚C

Two runs were carried out with a catalyst amount of 1.5 grams on order to determine if the catalyst to feedstock ratio has any effect of the fractional yield of desirable products. Figure 4.4 shows the results carried out at 380˚C. The trend observed was that as the catalyst to feedstock ratio increases to does the fractional yield of gas oil and the amount of heavier components decreases. The amount of vacuum gas oil of the high feedstock to catalyst ratio is 28.4% greater than that of the 0.3 ratio run and the gas oil of the 0.3 ratio run is 24.2% greater than that of the 0.2 run. Even though kerosene is present in the lower ratio run (3.4%), the high catalyst ratio run produced a much higher yield of desirable products achieving a yield of 46.6% gas oil.

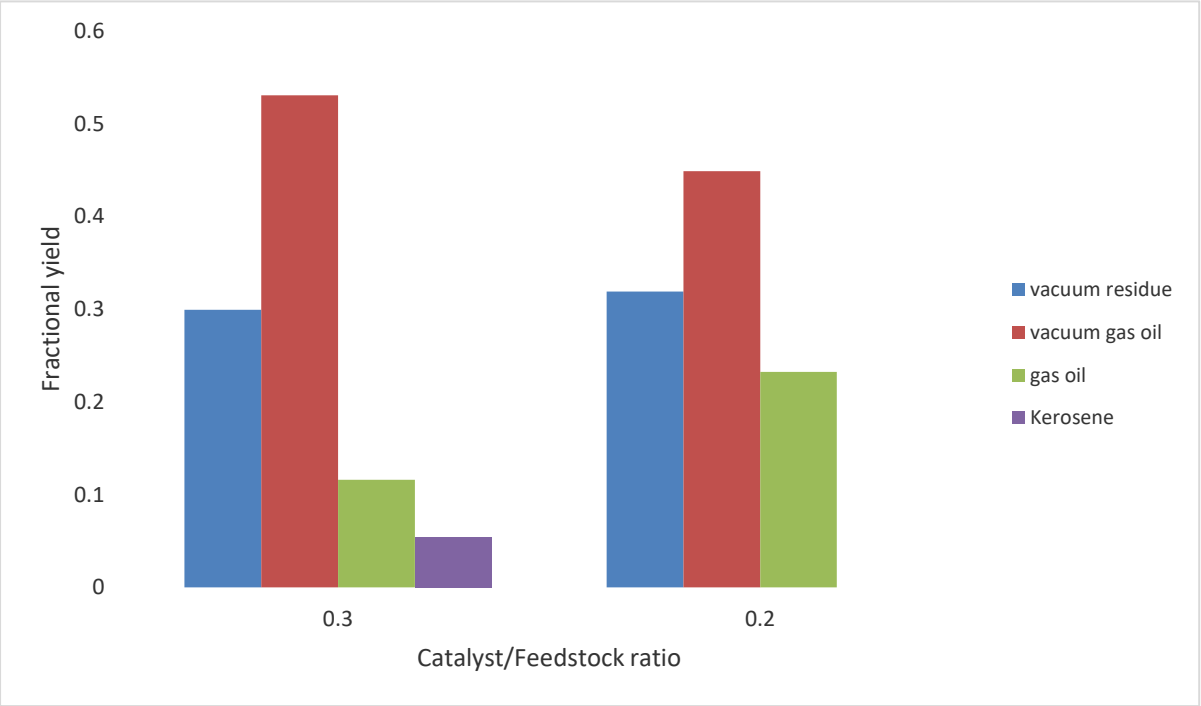

Figure 4. 5 - Fractional yields varying catalyst to feedstock ratio at 360˚C

Figure 4.5 shows the results for varying the catalyst to feed ratio at 360˚C. This result is very interesting as the lower ratio run produced the more desirable result. The run at a lower ratio resulted in a greater shift into the lighter fractions as seen with the greater amount of gas oil formed and lower amount of vacuum gas oil. There is some kerosene present in the 0.3 ratio run which shows that the more catalyst present, the greater the tendency of the reaction to shift into the desirable fractions (gas oils and kerosene).

From the results of varying the catalyst to feedstock ratio the high temperature-high catalyst combination produced improved gas oil yields over the low temperature-high catalyst ratio combination. It is evident that there appears to be strong interactions between reaction temperature and the catalyst to feedstock ratio. At low temperatures, mild cracking of the short residue occurs which is insufficient to shift it into the lighter desirable fractions, as seen with the high amount of vacuum residue still present at 360˚C. This results in a larger proportion of vacuum residue available to be converted to vacuum gas oil. However, at higher temperatures (380˚C and above) the residue is converted into the lighter fractions quite extensively.

In order to see if the experimental results achieved could be accepted, it was compared to results of simulations based on the aquaprocessing kinetics in the presence of an ultra-dispersed nickel/potassium catalyst, developed by Fathi et al (2013). The transformation of vacuum residue most likely proceeds through a parallel and series route as proposed by Fathi et al

(2013). The set of ODE's representing the lumped component balances were solved using the ode15s function is Matlab, which can be seen in Appendix E. The conversion of vacuum residue to vacuum gas oil dominates the reaction scheme, and the main pathway to gas oil is from vacuum gas oil, and not directly from the vacuum residue, this is evident by the product distribution as shown in the figure below.

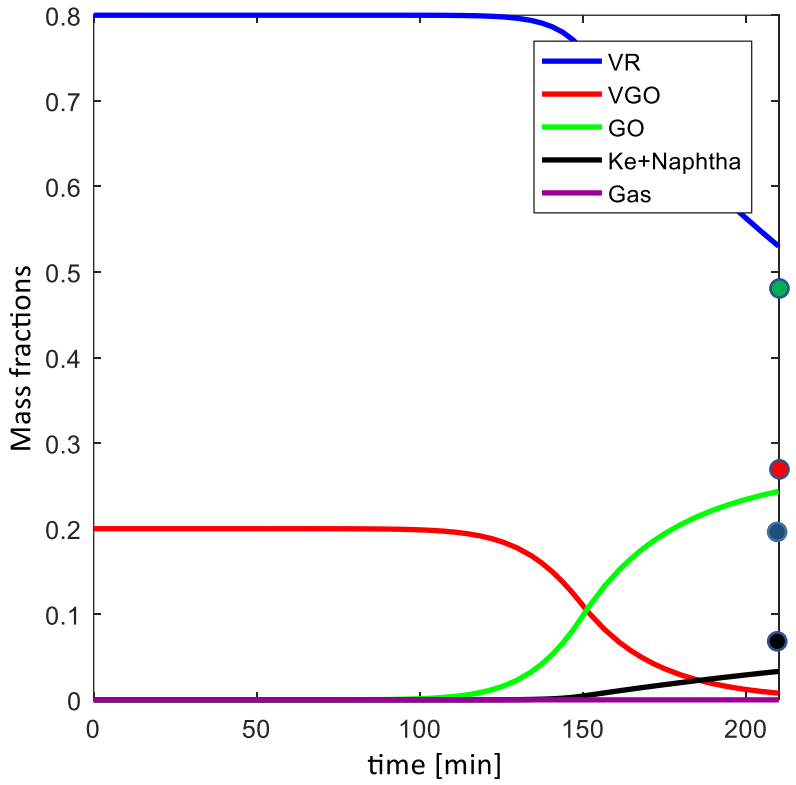

Figure 4. 6 - Simulated composition profile at 400˚C with dotted data representing experimental results at the same conditions.

The simulated composition profiles at 400 ˚C can be seen in figure 4.6. The rest of the composition profiles can be seen in Appendix F. All the profiles follow a similar trend hence the need to show one result. From the simulated composition profiles, it is evident that minimal cracking occurs during the heating up period (150 minutes). Once reaction temperature was reached it is clear that cracking has taken place, with the amounts of vacuum residue and vacuum gas oils sharply decreasing while the fractional yield of gas oil increases significantly. Even though cracking has clearly taken place, the experimental results at the same temperature indicate that the unsupported magnetite nanocatalyst is much more effective in the cracking of short residue as opposed to the Nickel/Potassium catalyst, used in the aquaprocessing method of Fathi et al. (2013). The reaction favours a shift from the vacuum residue to vacuum gas oil,

with the main pathway to gas oil being from the vacuum gas oil. This is evident as there is a significant decrease in vacuum residue shifting into the vacuum gas oil and then forming a large amount of gas oil. It is also clear that the experimental results show significantly greater amounts of lighter components (gas oil) than simulated results. This is more evident by analysis of the fractional yields produced by the simulations, as depicted below:

Figure 4. 7 - Fractional Yield results from simulated profiles with dotted data representing experimental results.

The data above was extracted from the composition profiles in Appendix F, while the dotted data represents the fractional yields of experimental results at the same conditions. The objective of carrying out the simulations using literature data is to compare the performance of

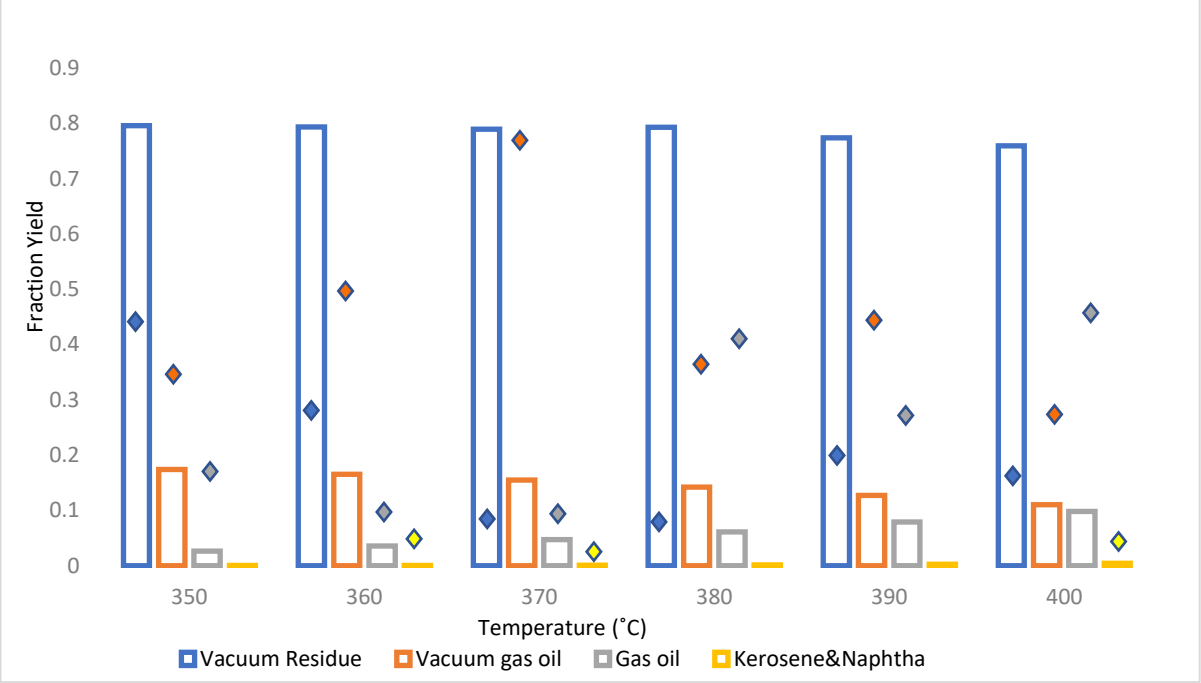

a previously used aquaprocessing catalyst (nickel/potassium) to the magnetite catalyst used in this study, at the same reaction conditions. From analysis of just the simulated yields, it is quite clear that over the entire temperature range, minimal cracking is taking place over. It is however noticed that the amounts of gas oil increased significantly over the temperature range. The amount of vacuum residue still present at each temperature is large, this could mean that the major reactions catalysed by nickel/potassium are less sensitive to the change in temperature than when the magnetite was used (in the temperature range considered). The result at 400 ˚C is the most favourable with the greatest number of light components, and the least vacuum residue. However, experimental results for the current catalytic system appear to be far superior than the simulated yields using literature kinetics. At every single temperature, experimental yields for the vacuum residue is less than the simulated yields, while there are clearly greater

amounts of lighter components present in the experimental results. This further proves the efficiency of the molybdenum doped magnetite nanocatalyst in upgrading the short residue.

One of the objectives of this investigation was to determine if the catalyst could be regenerated or not, in order to be used again. X-ray diffraction (XRD) analysis was carried out on the magnetite supported nanocatalyst in order to determine if any phase changes has occurred on the iron oxide.

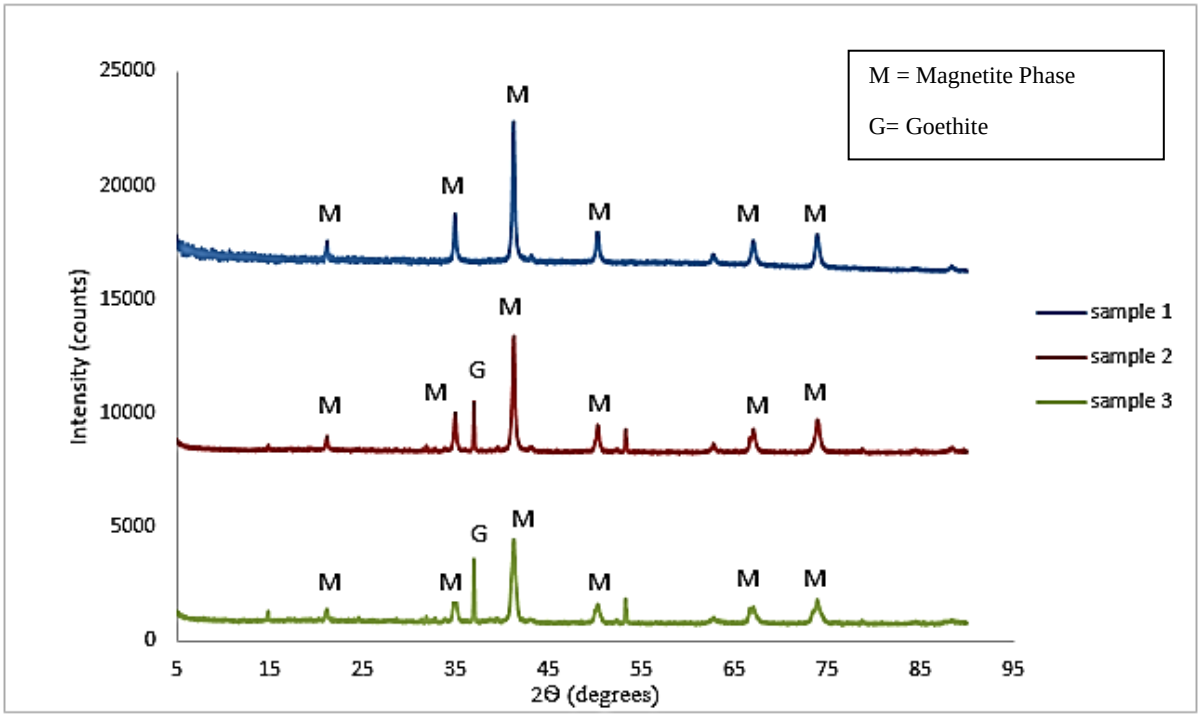

Figure 4. 8 - X-ray diffraction patterns for sample 1) post-run catalyst sample 2) fresh Mo iron oxide nanocatalyst sample 3) fresh Mo iron oxide nanocatalyst

Figure 4.8 is the results for XRD analysis. Sample 2 and 3 is the analysis done on the original traces and sample 1 is the catalyst analysis after it went through the cracking reaction. Analysis of the XRD patterns from the two original traces show that the dominant iron oxide phase is magnetite, while there is a small amount of goethite in the molybdenum nanocatalyst. From the result from sample 1 it is evident that the iron oxyhydroxide phase is removed. This proves a positive result as oxyhydroxides are not active for any cracking reaction. The catalyst is relatively stable in the presence of pure oxygen and relatively high temperatures, since no major phase changes has taken place. The positive results mean that the catalyst can be used again, as it also maintains its hydrocracking properties. It is also noticed that there is no conversion to a sulphur oxide phase which usually is contained within short residue. Therefore, this also proves that the short residue supplied from SAPREF may have a little sulphur contained with it. Analysis of the results achieved in this investigation it can be concluded that petroleum

residue, namely short residue can be cracked into lighter desirable fractions using an unsupported molybdenum magnetite nanocatalyst.

4.3 Fixed Bed Reactor Results

Batch results proved using the unsupported magnetite nanocatalyst that sufficient cracking does take place. In order to determine if the process can be scaled up and used in industry, a magnetite nanocatalyst on a mesoporous silica support was synthesised and implemented in a fixed bed reactor set up to see if short residue can be upgraded efficiently on a larger scale. The same temperature range of 350 to 400 degrees Celsius was investigated to compare results to that of the batch reactor set up results. Conventional catalyst namely nickel molybdenum and cobalt molybdenum were also used to compare if the supported magnetite catalyst is more effective in upgrading the short residue. The temperature effects on the amount of cracking was investigated while holding the catalyst mass constant. The feed composition was the same as the batch reactor experimental. All fractional yields are based on the feed mass, due to the mass lost to gas products being negligible.

4.3.1 Cobalt Molybdenum

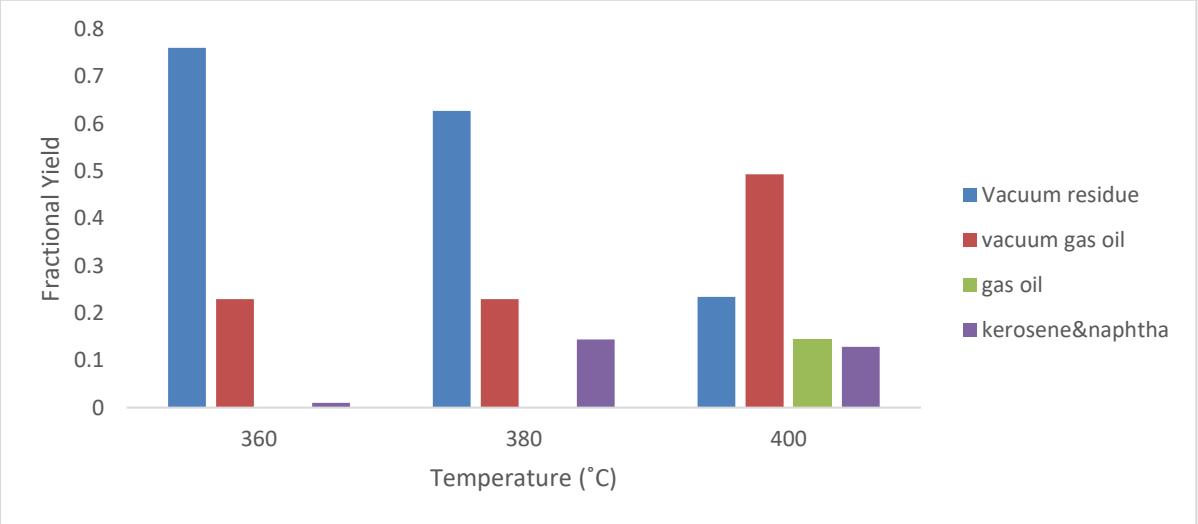

Figure 4. 9 - Fractional yield comparison using cobalt molybdenum catalyst

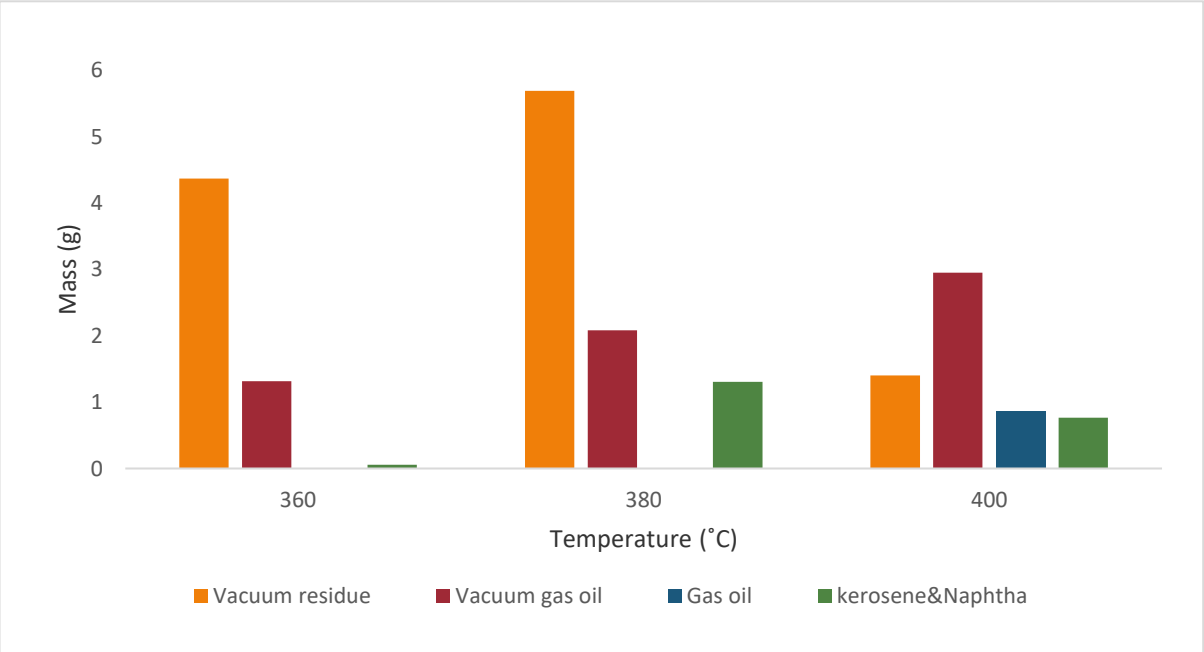

Figure 4. 10 - Mass comparison using cobalt molybdenum catalyst

From Figures 4.9 and 4.10, it is apparent that the cobalt molybdenum catalyst operated optimally at 400°C. This is evident as this sample returned the lowest fractional yield (23.4%) and mass (1.391g) of vacuum residue after the sample had been introduced into the reactor. This means that more of the vacuum residue was cracked into smaller components when the reactor operated at 400°C with the cobalt molybdenum catalyst. This sample also returned the highest fractional yield of vacuum gas oil (49.3%) and gas oil (14.5%) and the second highest fractional yield of kerosene and naphtha product (12.8%) - these being more valuable than the vacuum residue.

It was expected that better cracking would occur at the higher temperatures since the particles involved in the reaction would have more energy and thus more motion. This would result in the reaction proceeding quicker (Fogler, 2011). Additionally, the cobalt molybdenum catalyst was capable of cracking more vacuum residue than the nickel molybdenum catalyst operating at its optimal conditions as well as over the entire temperature range.

4.3.2 Nickel Molybdenum

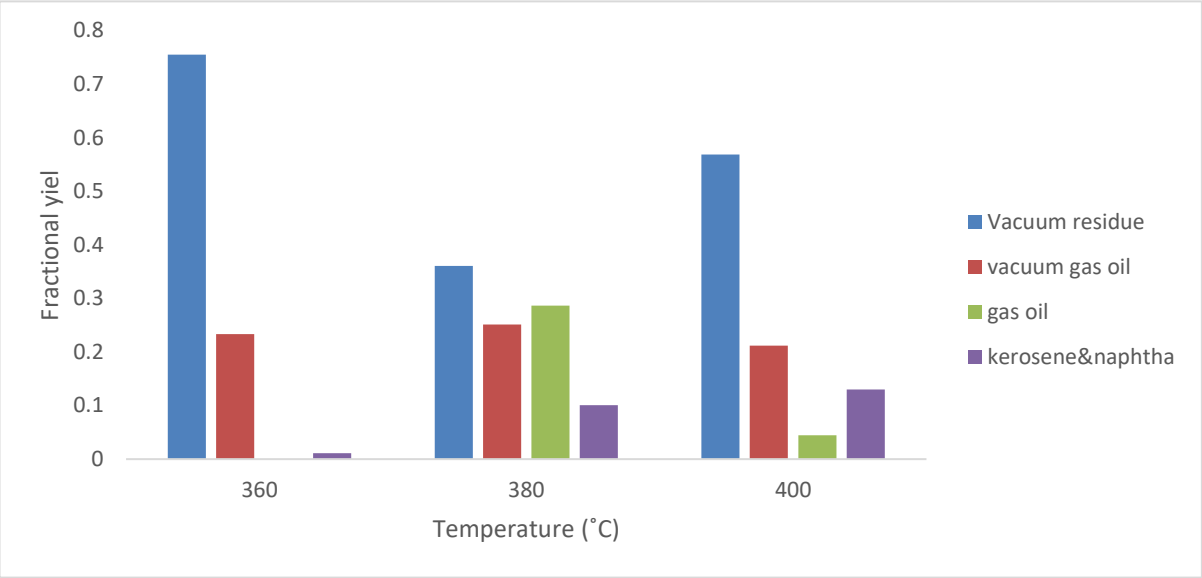

Figure 4. 11 - Fractional yield comparison using nickel molybdenum catalyst

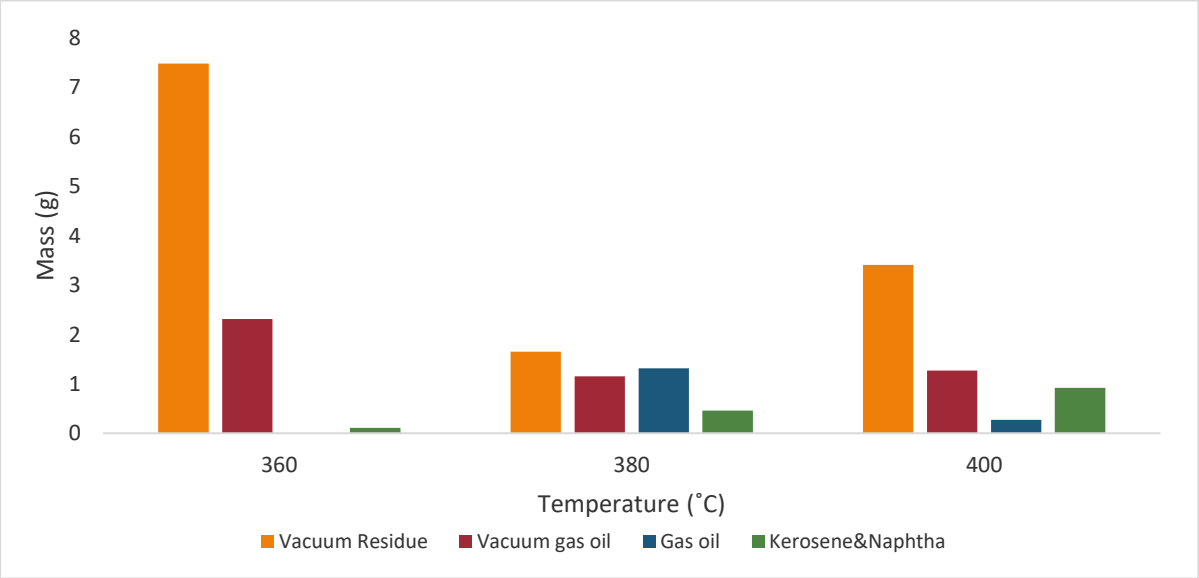

Figure 4. 12 - Mass distribution using nickel molybdenum catalyst

From Figures 4.11 and 4.12, it is evident that the nickel molybdenum catalyst operated optimally at 380°C. This was deduced since the sample retrieved when the reactor had been operated at 380°C returned the lowest fractional yield of vacuum residue (36.1%). This suggests that more of the vacuum residue had been cracked into lighter components. Furthermore, this sample returned the highest fractional yield of the more valuable vacuum gas oil (25.1%), gas oil (28.7%) and kerosene (10.1%) - this is desirable. This proves to be a very positive result as operating at lower temperatures uses up less energy,

Intuitively, it was expected that the optimal temperature for catalytic cracking would occur at the highest temperature (400°C), however, this was not the case for the runs using the nickel molybdenum catalyst. It is possible that the high temperature at which the reactor was operating could have caused sintering of the catalyst. Sintering is the loss of catalytic surface area caused by the catalytic phase to develop crystallite growth or loss of support area due to support collapse and of catalytic surface area due to pore collapse on crystallites of the active phase. Sintering of a catalyst occurs at temperatures close to 500°C but the effect is more pronounced in the presence of water (Argyle & Bartholomew, 2015). It is also possible that poisoning of the catalyst occurred if the equipment was not thoroughly cleaned and impurities were left in the system. Coking of the catalyst could have also occurred since petroleum residue is made up of hydrocarbons which can degrade into coke. Additionally, the nickel molybdenum catalyst was capable of producing more lighter components than the cobalt molybdenum catalyst operating at its optimal conditions.

4.3.3 Magnetite Nanocatalyst on a Mesoporous Silica Support

In the case for the fixed bed set up, the feed composition is the same as the batch set up. However, the mass of the feed was calculated by a different method as explained in Chapter 3. The mass was therefore 10.4 grams and yield calculations were based on this mass assuming negligible mass loss to gas.

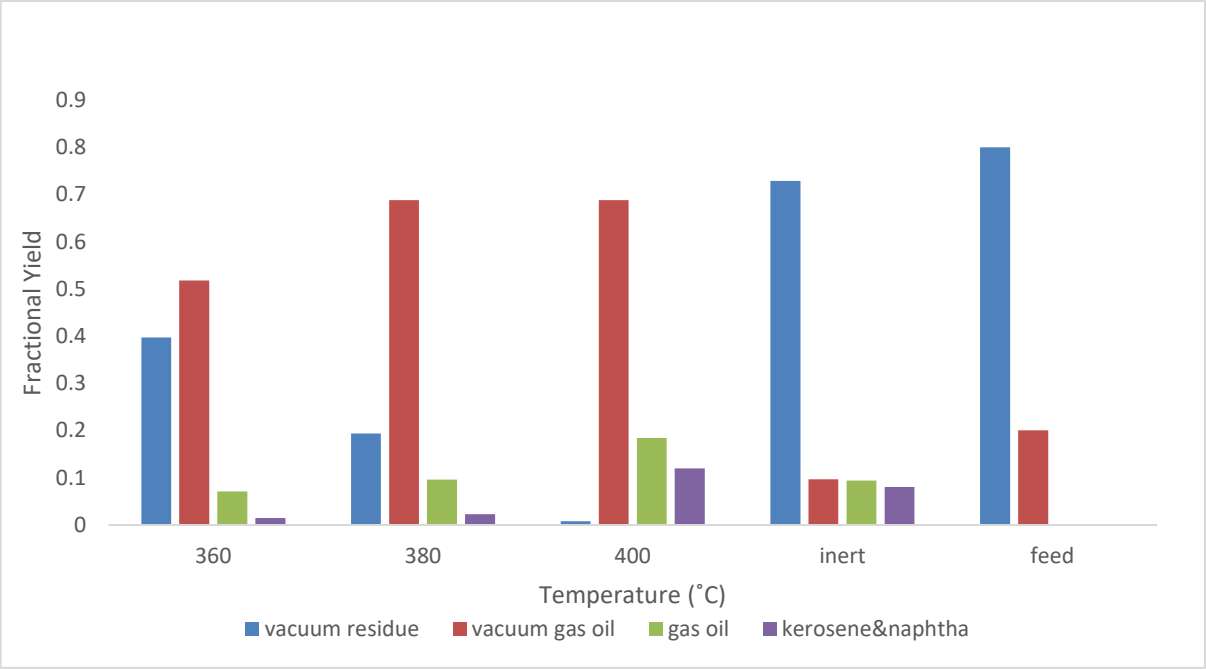

Figure 4. 13 - Fractional yield comparison using the supported magnetite nanocatalyst

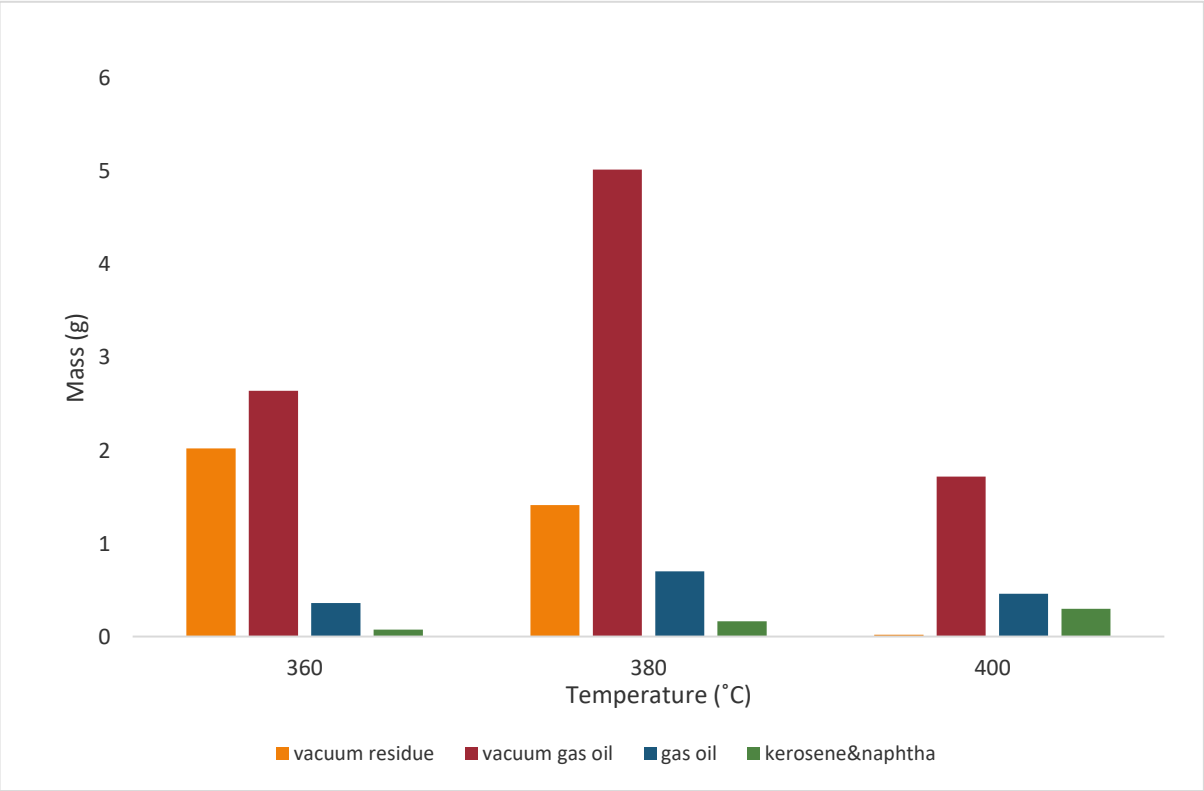

Figure 4. 14 - Mass distribution using the supported magnetite nanocatalyst

From analysis of Figures 4.13 and 4.14, it is evident that as the temperature increases so does the extent of cracking taking place. This is clearly shown as the amount of vacuum residue decreases steadily from 79.9% in the feed to 39.7% at 360 ˚C, 19.4% at 380 ˚C and just 0.8 % at 400˚C. It is also shown that the reaction favours the shift from vacuum residue into vacuum gas oil as it has the highest yield at all temperatures. Experimental results at 400 ˚C are optimal due to the extent the vacuum residue has been upgraded, as well as the amount lighter components such as gas oil (18.4%) and kerosene and naphtha product formed (11.9%).

In Figure 4.13, a run was done using glass beads as an inert material at 400°C, to determine the extent of cracking that can take place without a catalyst. The result indicates that even though small amounts of gas oil (9.4%) and kerosene and naphtha product (8.1%) was formed, there is still a large amount of vacuum residue present. Clearly without a catalyst, the heavy residue feed cannot be shifted into the lighter more desirable fractions.

4.3.4 Comparison Between Hydrocracking Catalysts

One of the objectives of this project was to compare the supported magnetite nanocatalyst to that of conventional catalysts. It was shown that the nickel molybdenum yields more favourable results than the cobalt molybdenum, especially achieving optimum results as just 380°C. The following figures summarise results using each catalyst at each temperature to indicate which provided the best yields.

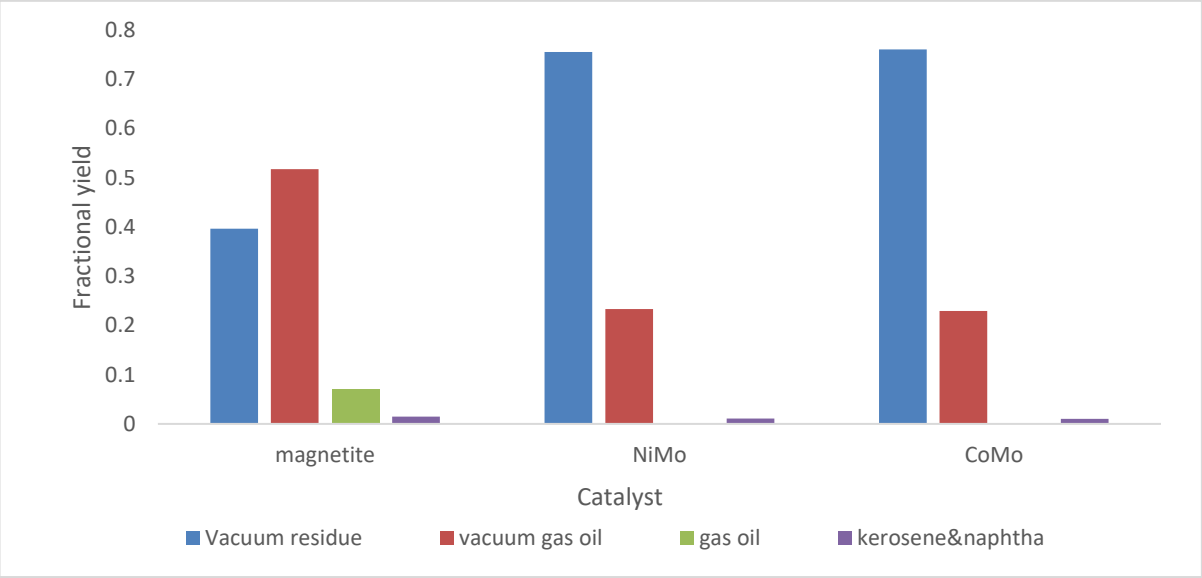

Figure 4. 15 - Fractional yield comparison at 360˚

Analysis of results at 360 ˚C clearly show that the supported magnetite catalyst yields much better results in terms of the amount of vacuum residue that has been upgraded into lighter products. The NiMo and CoMo show almost identical yields in products. It is evident that at lower temperatures minimal cracking occurs which is insufficient to shift the reaction into its lighter components, when using conventional catalysts.

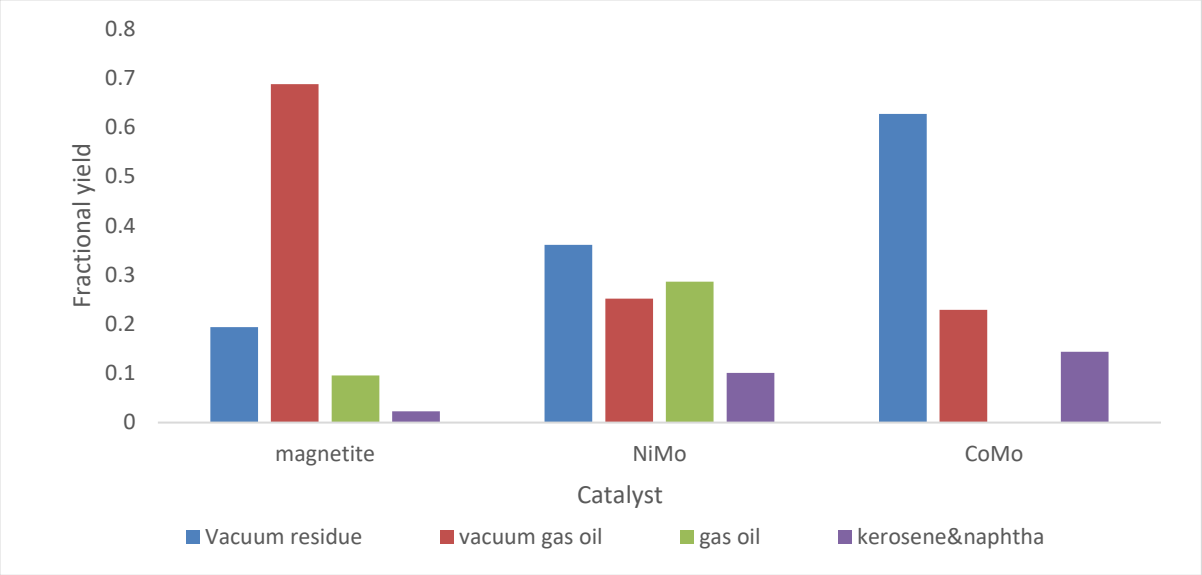

Figure 4. 16 - Fractional yield comparison at 380˚C

At the intermediate temperature of 380˚C results prove to be rather interesting. Clearly the CoMo catalyst performed the worst as there are still large amounts of vacuum residue that had not been upgraded. The magnetite catalyst proved efficient in shifting the vacuum residue into the lighter fractions, mainly vacuum gas oil. However, even though the NiMo catalyst yielded higher amounts of vacuum residue, it produced the greatest amount of the lighter gas oil, kerosene and naphtha products. This result is the most favourable at 380 ˚C.

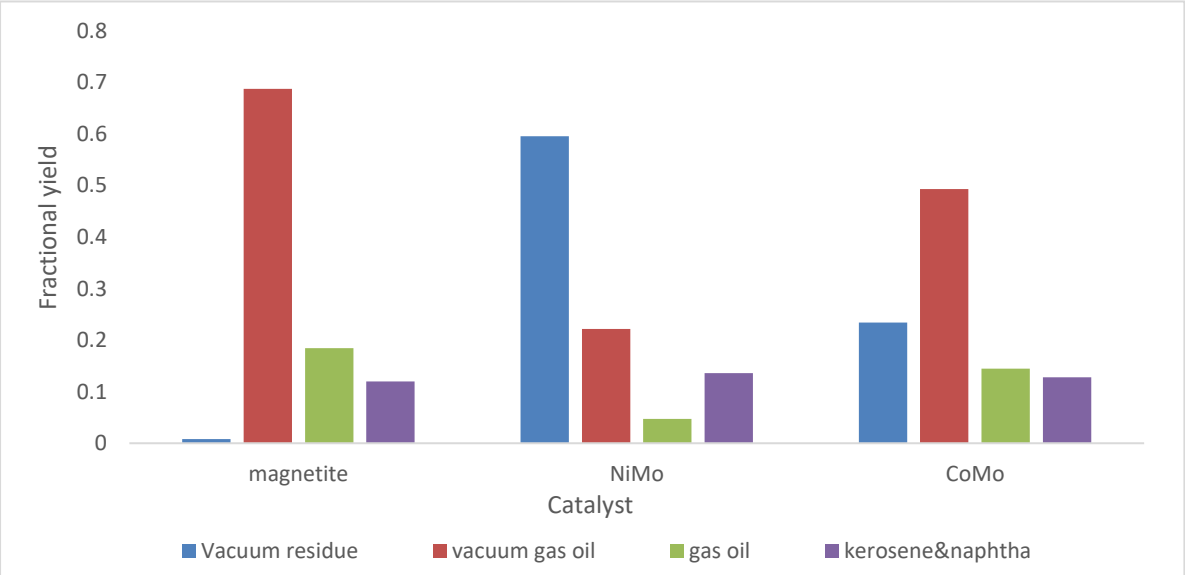

Figure 4. 17 - Fractional yield comparison at 400˚C

At higher temperatures, there is more energy available to break down the heavier components into the lighter, more desirable components. Hence, the best results for each catalyst should be at 400˚C. This was not the case for NiMo as explained in section 4.3.2. In figure 4.17 it is evident that the NiMo catalyst performed the worst with high amounts of vacuum residue still

present. Even though it produced the most kerosene and naphtha product, it failed to shift the vacuum residue into the lighter fractions sufficiently. The supported magnetite catalyst yielded the optimum results as almost all the vacuum residue has been upgraded into lighter components. It also yielded a combined number of light components (gas oil, kersosene and naphtha) of 30.3 % compared to the 27.4% combined amount produced using the CoMo catalyst. The supported magnetite catalyst proved to be the most consistent over the temperature range investigated, proving to efficiently upgrade the short residue into its lighter fractions as compared to conventional catalysts. This is evident as the amount of vacuum residue decreased consistently as temperature increases, shifting the short residue into the lighter fractions.

4.3.5 Supported vs Unsupported Catalyst results

From the analysis of the individual results of the supported and unsupported magnetite nanocatalysts, it is evident that mechanisms are in place to facilitate the cracking process. The unsupported molybdenum based catalyst serves two functions; one being to generate hydrogen in-situ and the other facilitating cracking and hydrogenation of the cracked components.

The presence of iron in the catalyst, catalyses hydrogen generation in-situ. In figure 4.8, it is evident that the surface of the catalyst was reduced as seen with the oxidised iron phase that was removed. This confirms the splitting of the water molecules and that hydrogen generation occurred on the magnetite nanocatalyst. Molybdenum being a component implemented mostly in hydrotreating catalysts appears to be participating in hydrogenation of the cracked components. In terms of the actual cracking taking place there are two mechanisms that are evident. One mechanism being thermal cracking that is taking place, as in the run where no catalysts was used still resulted in some cracking taking place. The other mechanism being cracking by the iron oxide catalyst and the presence of molybdenum.

In terms of the supported magnetite nanocatalyst, in-situ hydrogenation is taking place due to the presence of iron within the catalyst. There is no molybdenum present, but it appears that the strong acid sites on the silica support is facilitating cracking and hydrogenation. This is evident by the results achieved using the supported catalyst and comparisons between supported and unsupported magnetite catalysts are discussed in this section.

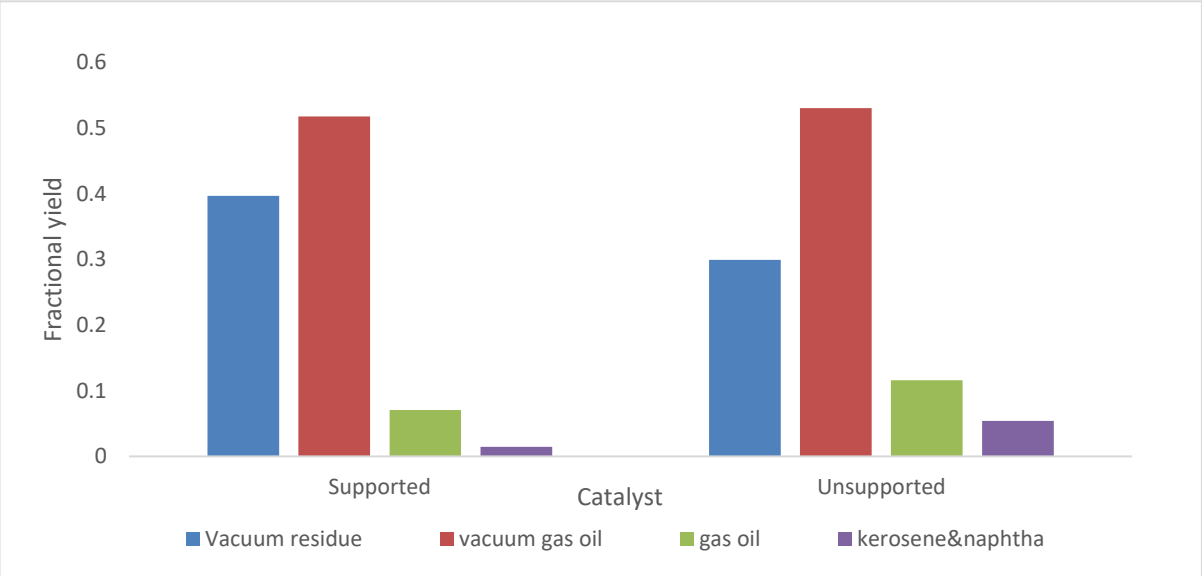

Figure 4. 18 - Supported vs unsupported catalyst results at 360˚C

From the above figure, the yield of each fractional group compares quite favourably to each other. The unsupported catalyst did provide better results with a yield of vacuum residue 9.8% less than the supported catalyst with an increase of 4.5% and 4% of gas oil, kerosene and naphtha products respectively. Hence, at low temperatures the molybdenum doped magnetite nanocatalyst proves more effective in upgrading the short residue.

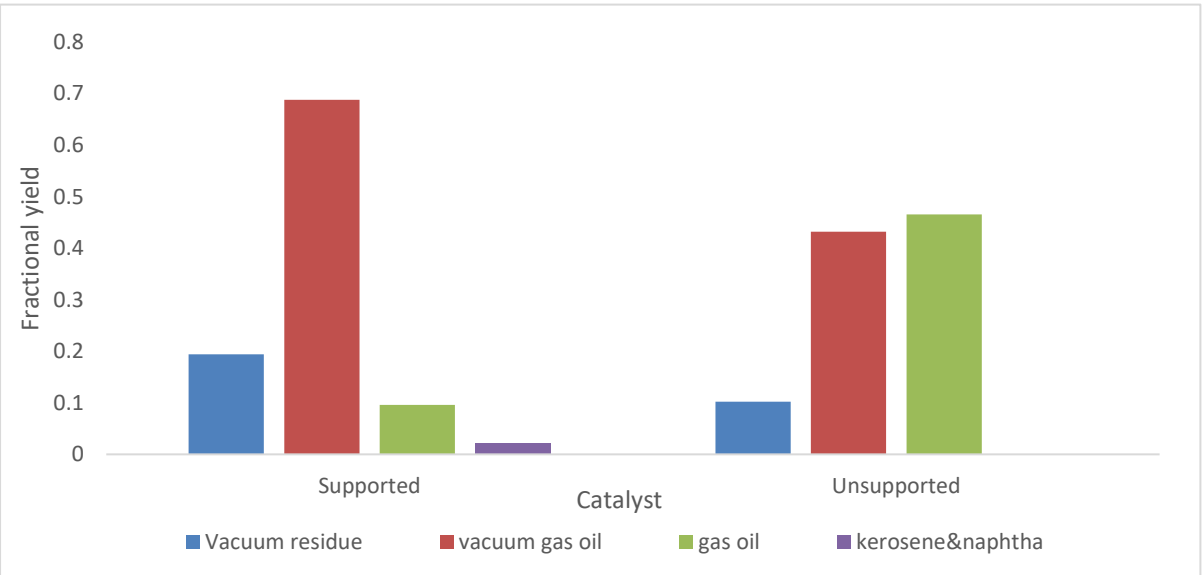

Figure 4. 19 - Supported vs unsupported results at 380 ˚C

At the intermediate temperature of 380˚C, it is apparently clear that the unsupported catalyst effectively shifts the short residue into its lighter fractions. The supported magnetite catalyst does break down the vacuum residue to a decent extent, but not enough to sufficiently shift it into the gas oil, kerosene and naphtha fractions. The unsupported catalyst yields an increase of

36.9% gas oil compared to the supported catalyst. By analysis of figure 2.9 in section 2.5.2, the result indicates that the supported catalyst largely favours the shift from vacuum residue into vacuum gas oil (k1), while the unsupported catalyst further shifts the reaction from the vacuum gas oil to the gas oil fraction quite extensively (k1-k2-k5).

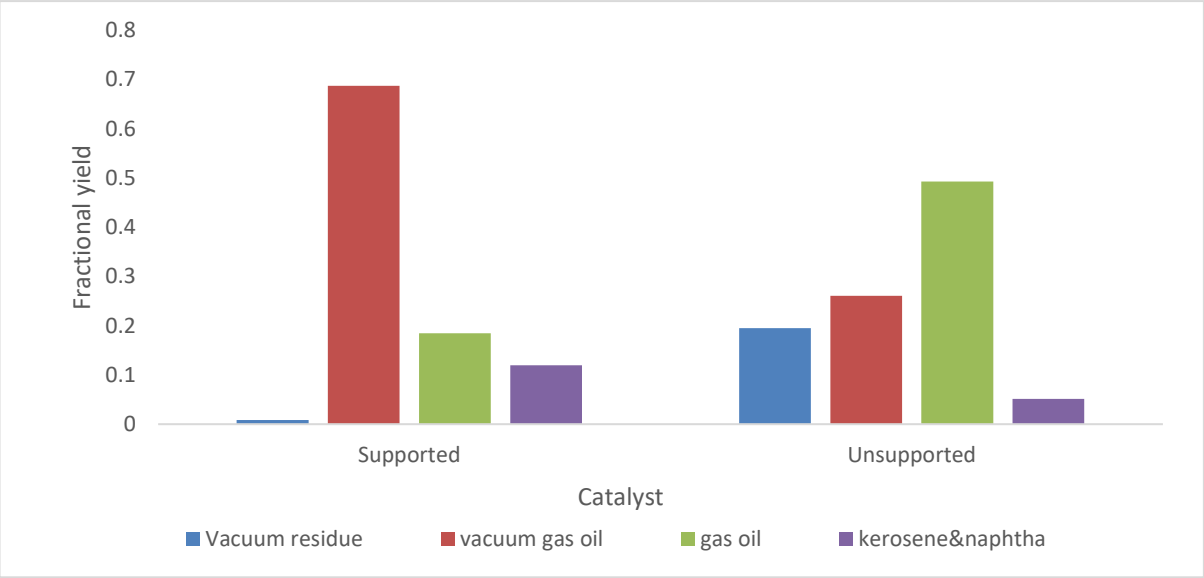

Figure 4. 20 - Supported vs unsupported results at 400 ˚C

For both catalyst, the result as the highest temperature of 400˚C provided optimal results. Both were effective in upgrading the vacuum residue into lighter components, however the supported catalyst proved to be far better than any catalyst in breaking down the vacuum residue. As explained in the result at 380˚C, the supported catalyst seems to be favouring the shift into vacuum gas oil extensively while the unsupported catalyst further shifts the reaction into the gas oil fraction. This trend is confirmed over the entire temperature range as the supported catalyst yields more vacuum gas than the other fractions. Even though the supported catalyst does produce slightly more kerosene and naphtha product, it also yields 30.8% less gas oil than the unsupported catalyst. Ultimately both catalyst is quite effective in cracking the heavy residue into lighter components. They however seem to be favouring different reaction routes. The magnetite nanocatalyst on a mesoporous silica support proved best in shifting the vacuum residue into the lighter fractions, mostly vacuum gas oil. The molybdenum doped magnetite nanocatalyst on the other hand yielded the greatest amount of lighter desirable products (gas oil, kerosene and naphtha). The result is positive as the unsupported catalyst was implemented in a batch scale set up that can't be used in industry. Hence the use of the supported catalyst proved that magnetite based catalyst is more effective than current

commercial catalyst, in the hydrocracking of short residue especially that magnetite based catalyst is far cheaper to synthesise that nickel or cobalt based catalysts.

XRD analysis was done on the supported catalyst to determine the iron oxide phase present within the catalyst. The result is depicted below:

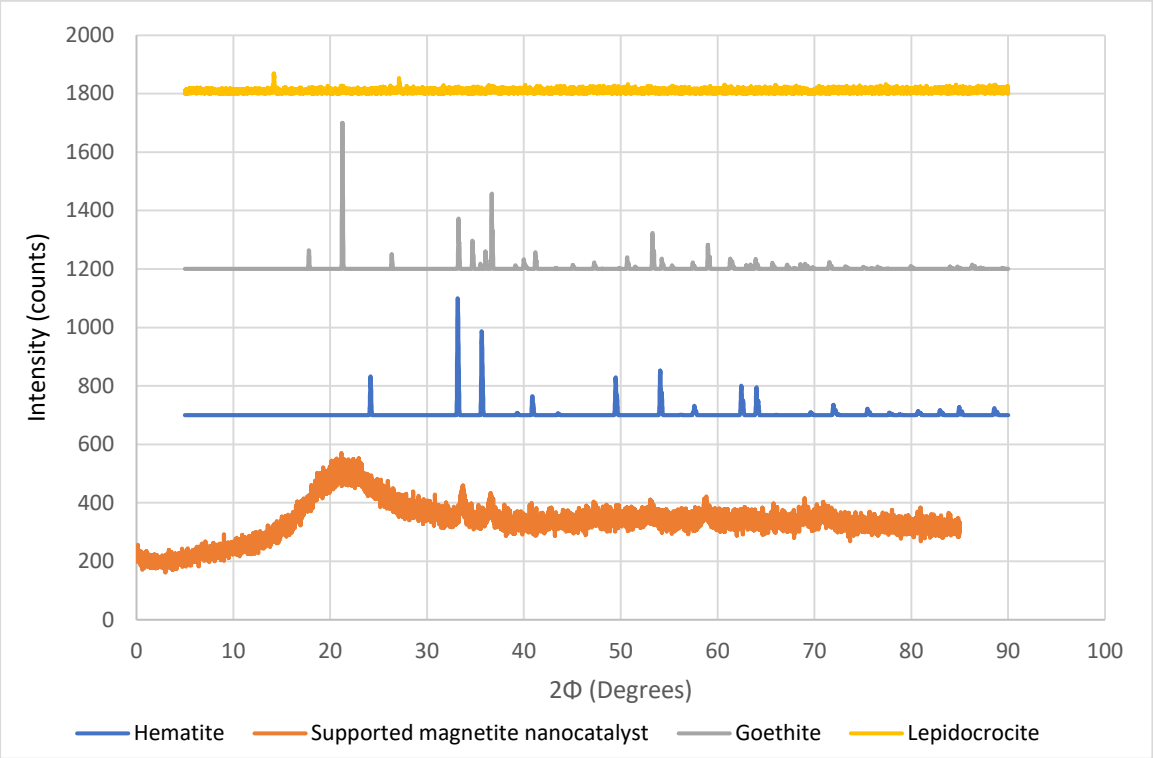

Figure 4. 21 - XRD patterns for the supported magnetite nanocatalys

It is quite evident that the resolution of the supported magnetite XRD pattern is poor. This is due to the presence of the amorphous silica support. The amorphous silica is clearly masking the iron components present. As shown in figure A.4 of appendix A, the supported catalyst was red in colour, hence it was compared other iron oxides that are also red in colour. These being iron oxyhydroxides such as goethite, lepidocrocite and hematite. At least five diffraction peaks match those that appear on standard hematite, hence hematite was present within the catalyst used.

CHAPTER 5

5.1 Conclusions

- A viable method was devised to prepare the feedstock using a solvent to residue ratio of 1:1 for the batch reactor set up and 5:1 for the fixed bed reactor set up.
- Vacuum residue was successfully cracked within a relatively low temperature range (350-400˚C) and pressure range(40-50bar) using the molybdenum doped magnetite nano-catalyst.
- In the batch tests, the most prominent fractions in the products were vacuum gas oil and gas oil.
- The maximum yield of favourable products, in the batch tests, were obtained at a reaction temperature of 450˚C and for a catalyst/residue ratio of 2 grams.
- The ultrafine dispersed catalyst is several times more active for hydrocracking of heavy petroleum residues than conventional heterogeneous catalysts e.g. Ni-Mo/Al_2O_3.
- Successfully simulated aquaprocessing in a batch reactor using available kinetic data which compared favourably to experimental yields.
- The unsupported magnetite nanocatalysts was proved to be much more efficient in the upgrading of the vacuum residue compared to the Nickel/Potassium catalyst used in aquaprocessing.
- XRD analysis proved that the catalyst could be recovered and used again due to no major changes to the iron oxide phase.
- Conventional catalysts namely NiMo and CoMo proved inefficient to break down the heavy vacuum residue effectively compared to the magnetite nanocatalyst on a mesoporous silica support.
- The most prominent fraction for the fixed bed tests, was vacuum gas oil.
- The most favourable results achieved in the fixed bed tests were achieved at a temperature of 400 ˚C and 5 grams of catalyst.
- The yields of the unsupported catalyst proved to be slightly more favourable than the supported catalyst yields.
- The iron present in both supported and unsupported magnetite catalysts are involved in in-situ hydrogen generation.

- The strong acidic site on the silica support serves the same purpose as the molybdenum in the unsupported catalyst. These being participation in hydrogenation and cracking.
- It can be concluded that the process can be scaled up from a batch set up using a unsupported magnetite catalyst, to industry level processes, as proved by the use of the supported catalyst in a fixed bed set up.

5.2 Recommendations

- Each run should be carried multiple times to get a better understanding on the conversion of heavy petroleum residue to lighter fractions.
- A larger temperature range should be used in order to determine what the optimum temperature is for the cracking of residues.
- A better method of separating the product residue from water and toluene should be devised. Maybe drying the product sample over magnesium oxide will provide a better result for the batch tests.
- Diluting the product, from the batch tests, with a small amount of toluene will make it easier to analyse by the GCMS.
- Incorporating molybdenum into the supported magnetite catalyst may improve yields extensively.
- Varying the flowrates in the fixed bed set up to determine if efficient cracking can occur at a higher flowrate.

\

References

1. Argyle, M. D. & Bartholomew, C. H., 2015. Heterogeneous Catalyst Deactivation and Regeneration: A Review. *Catalysts*, 5(1), p. 26.
2. Atkins.L, T, H. & C, B., 2010. *Heavy crude oil global analysis and outlook to 2030,* Houston: Hart Energy consulting report.
3. Biasca, F. et al., 2003. *In upgrading heavy crude oils and residue to transportation fuel,* s.l.: SAF Pacific Inc.
4. Billon, A., Norel, F. & Peries, J., 1997. *Use of solvent deasphaling process in residue conversion schemes,* Beijing: 15th world congress.
5. Brady, J. B. a. B., 1995. Introducing Mineralogy Students to X-ray Diffraction Through Optical Diffraction Experiments Using Lasers. *Geology education v43,* pp. 471-470.
6. Cherzer, J. & Gruia, J., 1996. *Hydrocracking Science and Technology.* New York: Marcel Dekker.
7. Cornelius.S, 1985. *Manual of Mineralogy (20th ed.).* London: Wiley.
8. Engelhard, K., n.d. *FCCU Reactor and Transfer Line Coking.* [Online] Available at: http://www.refiningonline.com/
9. EnggCyclopedia, 2012. *Vacuum distillation Unit.* [Online] Available at: www.enggcylcopedia.com/2012/01/crudeoilrefining [Accessed 8 August 2017].
10. Enkhsaruul, B., 1992. *Cracking Behavior of Asphaltene in the presence of Iron Catalyst supported on Mesoporous Molecular sive with different pore diameters.* s.l.:s.n.
11. Fathi.M., P.-A., 2013. Kinetic Modeling of Arab Light Vacuum Residue Upgrading by Aquaprocessing at High Space Velocities. *I&CE research,* pp. 4-37.
12. Fathi, M. & Pereira-Almano, P., 2013. Kinetic Modeling of Arab Light Vacuum Residue Upgrading by Aquaprocessing at High Space Velocities. *Industrial & Engineering Chemistry Research,* Volume 52, pp. 612-623.
13. Fogler, H., 2011. *Essentials of Chemical Reaction Engineering.* 2nd ed. United States: Prentice Hall.
14. Furimsky, E., 1998. *Adnavced petroleum refining.* 1 ed. New Dehli: Khanna Publishers.
15. Gang Yang, M. & Eser, S., 2002. *Upgrading a High Asphaltene Content Petroleum Residue by Hydrogenation with a NiMo-supported Catalyst,* Pennsylvania: Fuel Science Program and The Energy Institute.
16. Gary, J., 2004. *Petroleum Refining Technology and Economics (2nd ed.).* London: s.n.

17. Gupta, R. & Gera, P., 2015. Process for the upgradation of petroeum residue: Review. *International Journal of Advanced Technology in Engineering and Science,* 3(2), pp. 550-562.

18. Hildebrand, E., 1972. *Materials Selection for Petroleum Refineries and Petrochemical Plants, Mater. Prot. Perform., Vol 11.* s.l.:s.n.

19. Hluchy, M., 1999. The Value of Teaching X-ray Techniques and Clay Mineralogy to Undergraduates. *Geoscience Education, v. 47,* pp. 236-240.

20. IMOA, 2014. *Molybdenum compounds in catalysts.* [Online] Available at: http://www.imoa.info/molybdenum-uses/molybdenum-chemistry-uses/catalysts.php [Accessed 24 April 2017].

21. Joonaki, E., Ghanaatian, S. & Zargar, G., 2012. A New Approach to Simultaneously Enhancing Heavy Oil Recovery and Hindering Asphaltene Precipitation. *Iranian Journal of Oil & Gas Science and Technology,* Volume 1, pp. 40-47.

22. Khabazipour, M., Shariati, S. & Safa, S., 2016. SBA and KIT-6 Mesoporous Silica Magnetite Nanoparticles: Synthesis and Charaterization. *Synthesis and Reactivity in Inorganic, Metal-Organic, and Nano-Metal Chemistry*, 46(5).

23. Kister, H. Z., 1992. *Distillation Design.* s.l.:McGraw-Hill.

24. Lokhat D et al, 2015. Preparation of iron oxide nanocatalysts and application in the liquid phase oxidation of benzene. *Polish Journal of Chemical Technology,* 17(2), pp. 44-45.

25. NPTEL, n.d. *Crude Oil Distillation.* [Online] Available at: www.nptel.com/lecture3/crudeoildistillation [Accessed 12 July 2017].

26. P.Pujado, D. S. J. a. P., 2006. *Handbook of Petroleum Processing, First Edition.* s.l.:Springer.

27. Pereira, P. M. R. et al., 1999. *Steam conversion process and catalyst.* United States, Patent No. 5,885,441.

28. Ramon, D. J., 2016. *Universitat d'Alacant.* [Online] Available at: http://m.personal.ua.es/en/djramon/nanocatalysts-impregnated-on-magnetite

29. Rana, M. S., 2007. *A review of revent advances on process technologies for upgrading heavy oils and residue, vol 86.* George: Wiley.

30. Rana, M., Samano, V. & Anchetya, J., 2007. A review of recent advances on process technologies for upgrading of heavy oils and residua. *Fuel,* Volume 86, pp. 1201-1217.

31. Raseev, S., 2003. *Hydrocracking in Thermal and Catalytic Processes in Petroleum refining,* s.l.: Marcel Dekker, Inc.

32. Sadeghbeigi, R., 2000. *Fluid Catalytic Cracking Handbook (2nd ed.).* s.l.:Gulf Publishing.

33. Sahu, R. et al., 2015. A review of recent advances in catalytic hydrocracking of heavy residues. *Journal of Industrial and Engineering Chemistry,* pp. 33-46.

34. Sathya, P., 2012. *Catalytic Cracking: Fluid Catalytic Cracking And Hydrocracking,* Dehli: nptel.

35. Sathya, P., 2013. *Thermal Cracking, Visbreaking and Delayed coking.* [Online] Available at: www.nptel.com/lecture4/reactortechnology [Accessed 24 April 2017].

36. Schacht, P., Diaz-Garcia, L., Aguilar, J. & Ramirez, S., 2014. Upgrading of Heavy Crude Oil with W-Zr catalyst. *Advances in Chemical Engineering and Science,* Volume 4, pp. 250-257.

37. Shen, H., Ding, Z. & Li, R., 1997. *Thermal conversion - An Efficient Way For Heavy Residue Processing,* Beijing: s.n.

38. Sieli, G., 1998. *Visbreaking the next generation,* s.l.: Foster wheeler publication.

39. Singh, J., Kumar, M. M., Saxena, A. K. & Kumar, 2005. Reaction pathways and product yields in mild thermal cracking of vacuum residues. *Chem.Eng.J,* 108(3), pp. 250-268.

40. Trambouze, P. & Euzen, J., 2004. *Chemical Reactors: From design to operation.* 1 ed. Paris: Editions Technip.

41. Zeng, H., Zou, F., Lehne, E. & Zhang, D., 2012. Gas Chromatograph Applications in Petroleum Hydrocarbon Fluids. In: D. M. A. Mohd, ed. *Advanced Gas Chromatography - Progress in Agricultural, Biomedical and Industrial Applications.* s.l.:InTech, pp. 368-385.

APPENDICES

Appendix A: Photos of equipment and Materials

Figure A. 2 - Picture of GCMS

Figure A. 1 - Parr 5500 series compact batch reactor and reactor controller

Figure A. 3 - Molybdenum doped magnetite nanocatalyst powder

Figure A. 4 - Supported Iron Oxide Catalyst

Appendix B: Total Ion Chromatograms

Unsupported Catalyst Data

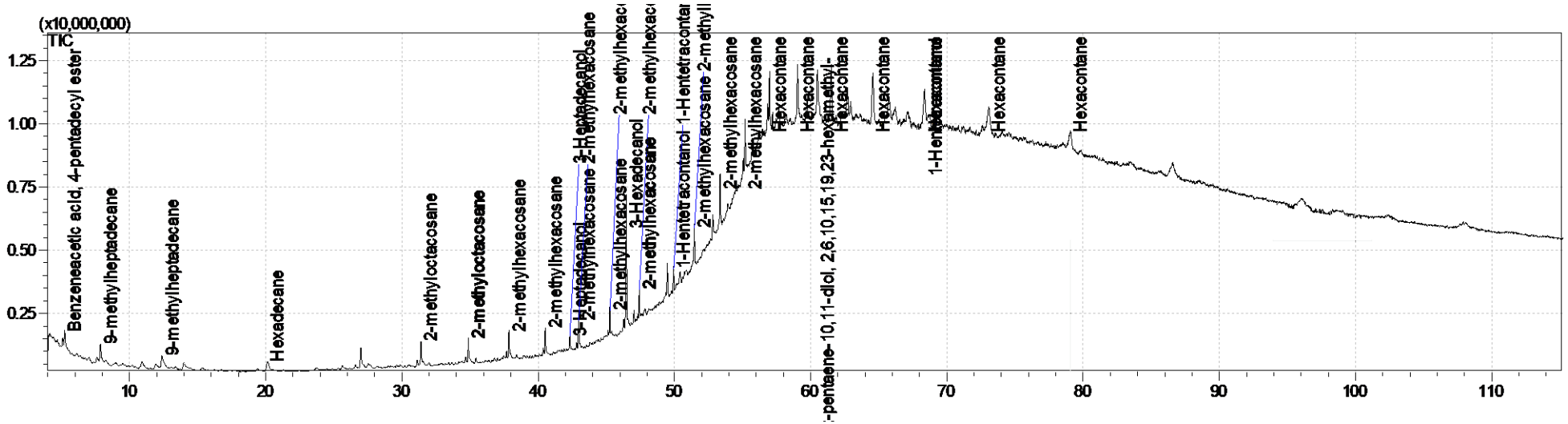

Figure B. 1 - Run 1 total ion chromatogram

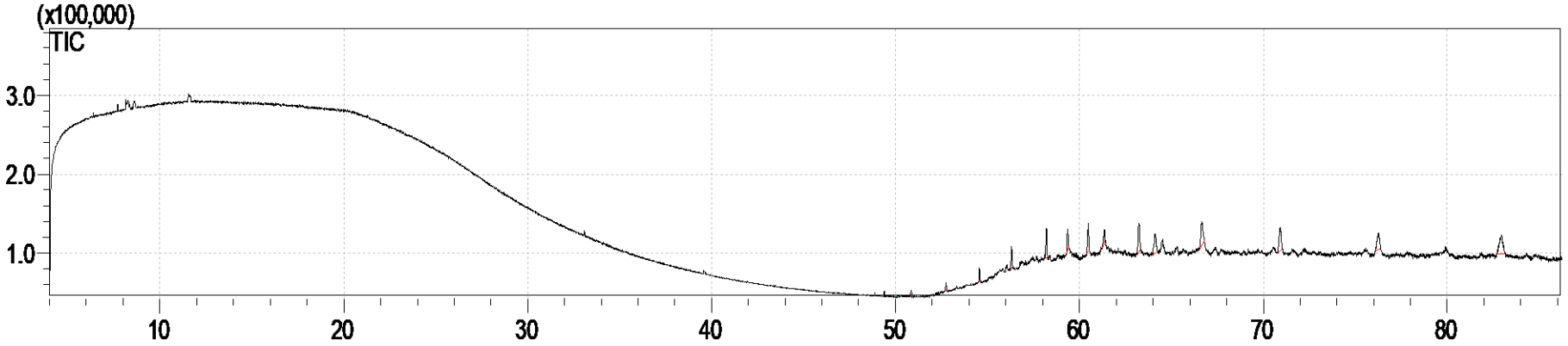

Figure B. 2 - Feed total ion chromatogram

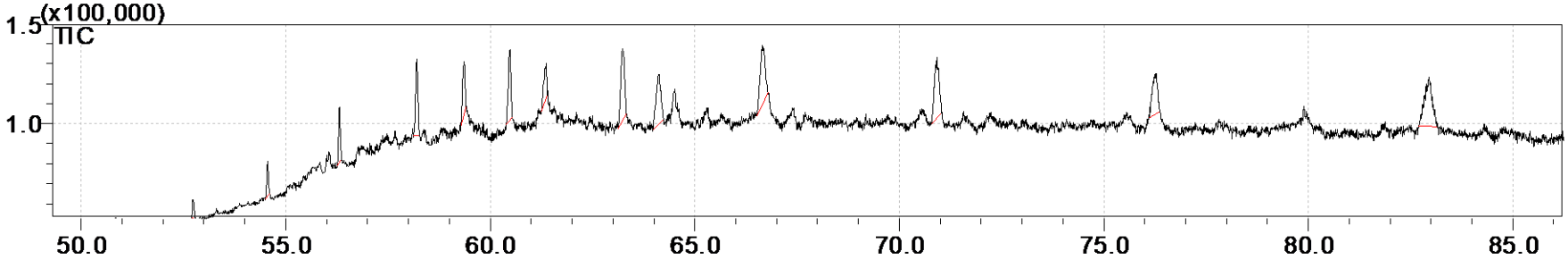

Figure B. 3 - Zoomed in image of feed

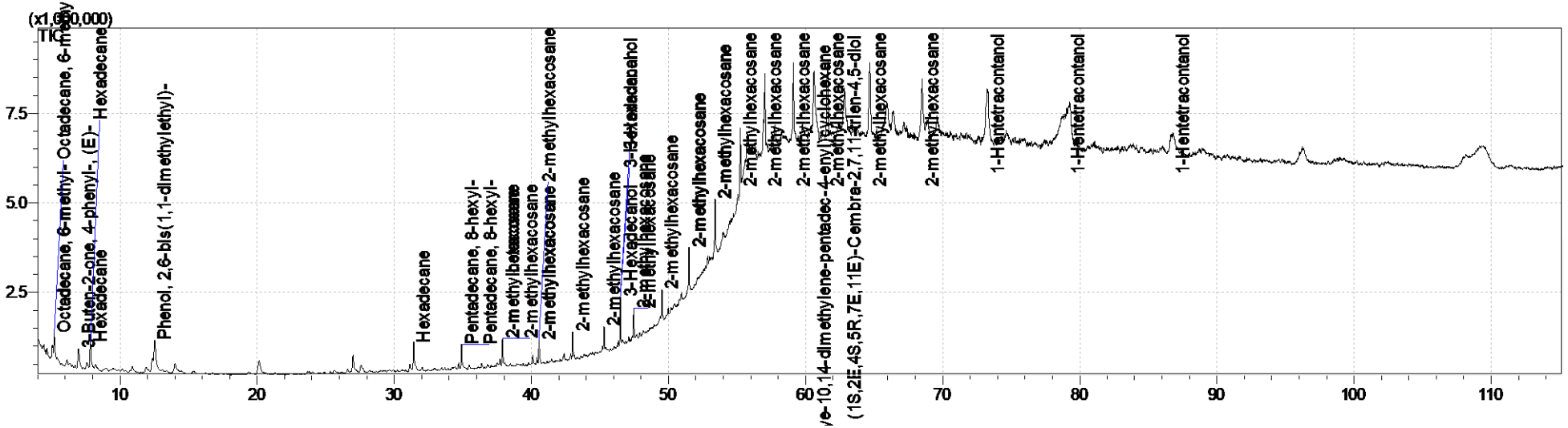

Figure B. 4 - Run 2 total ion chromatogram

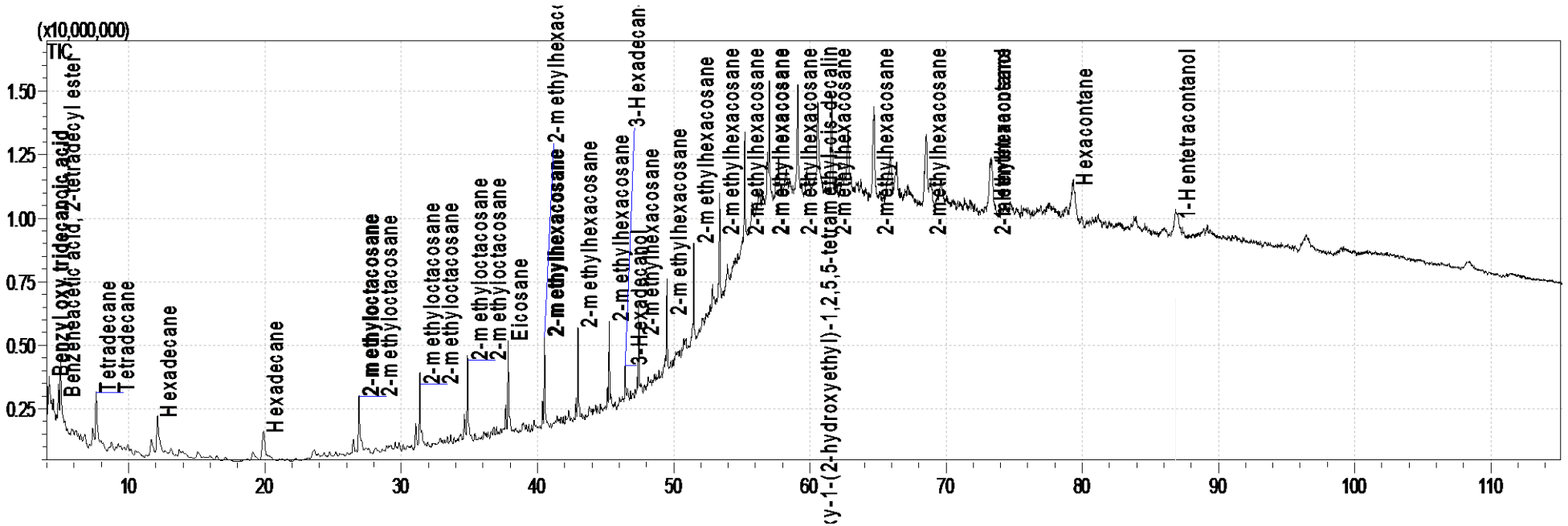

Figure B. 5 - Run 3 total ion chromatograms

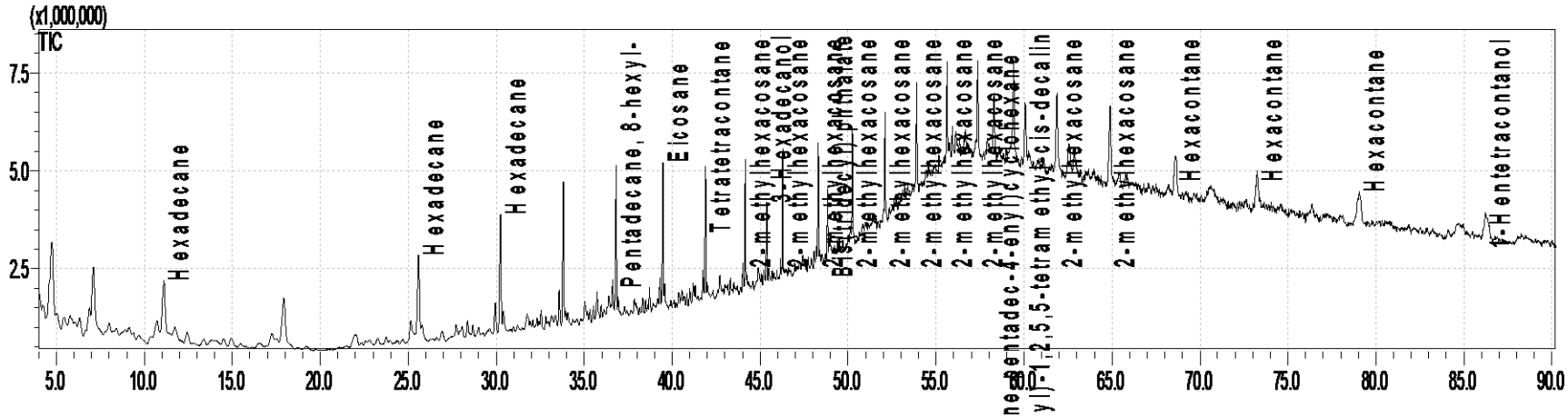

Figure B. 7 - Run 4 total ion chromatogram

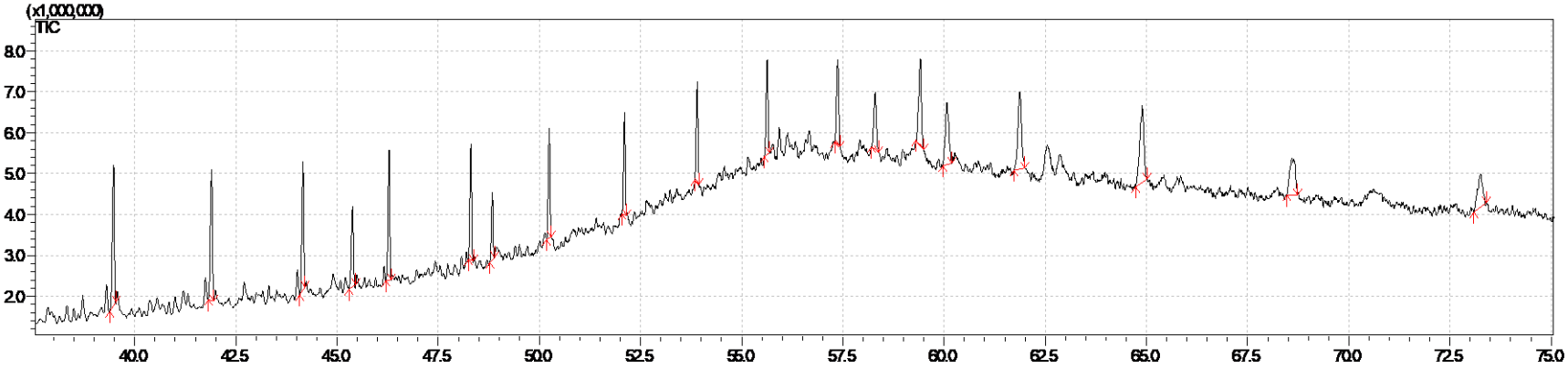

Figure B. 6 - Zoomed in chromatogram of run 4

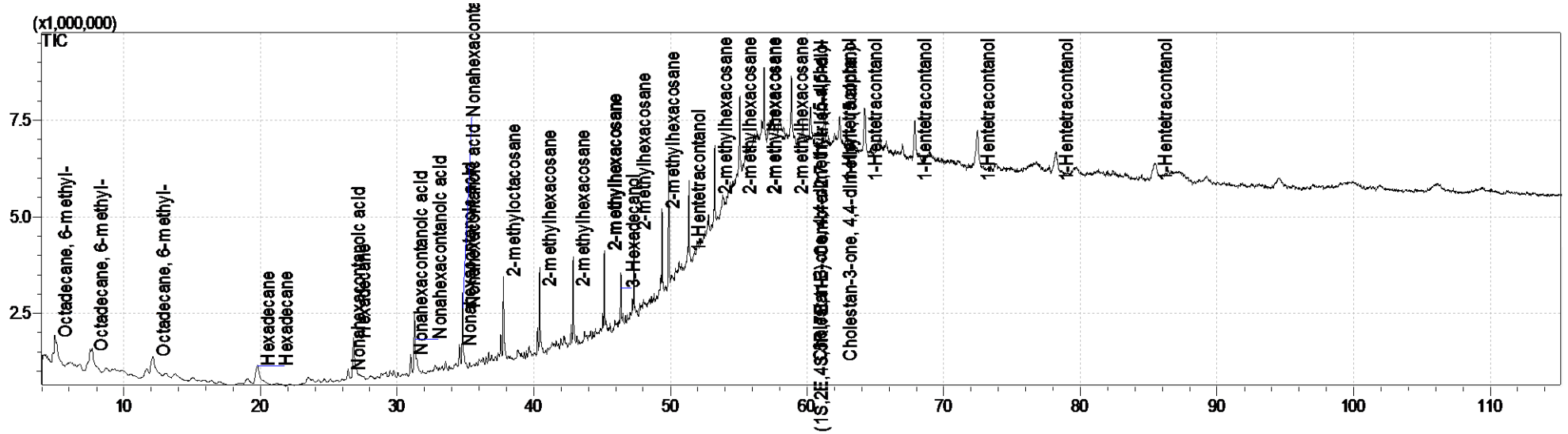

Figure B. 8 - Run 5 total ion chromatogram

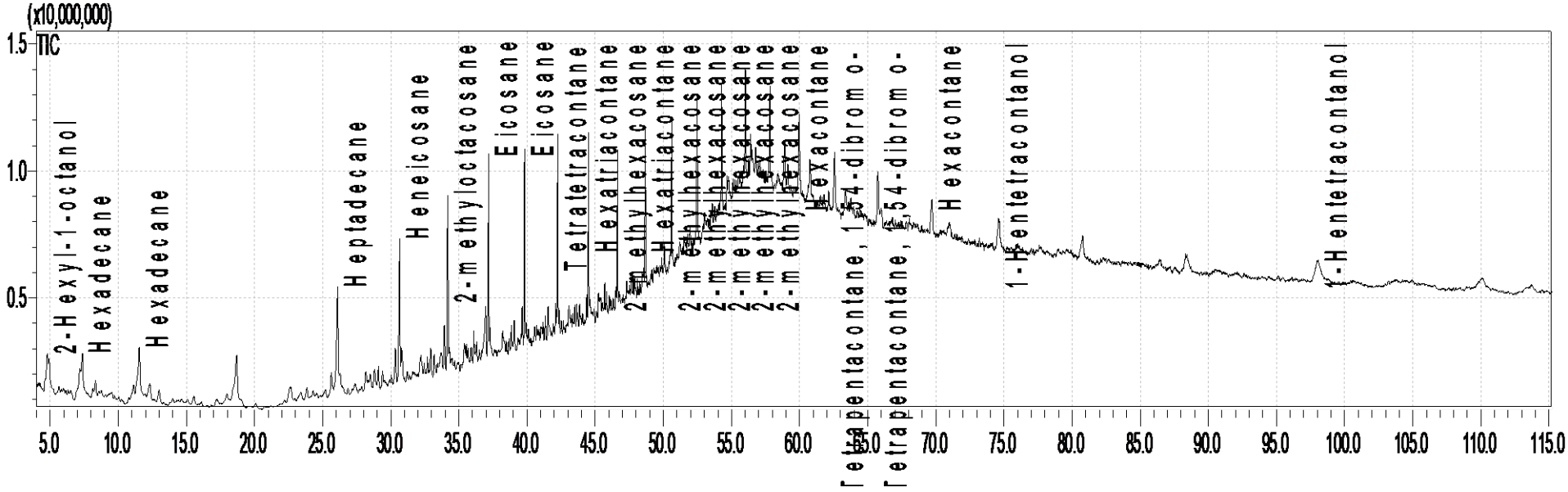

Figure B. 9 - Run 6 total ion chromatogram

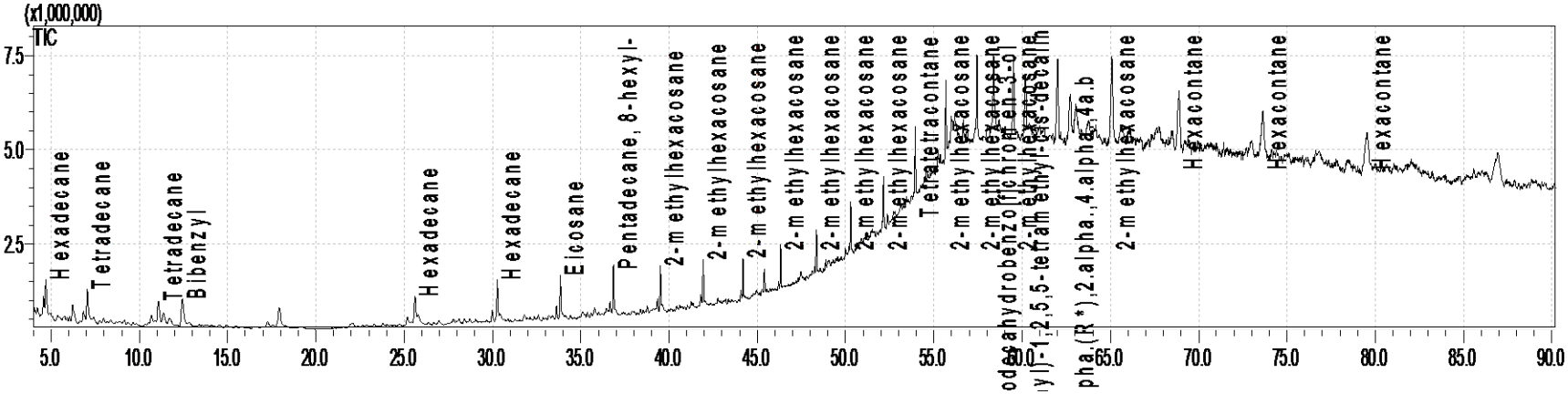

Figure B. 10 - Run 8 total ion chromatogram

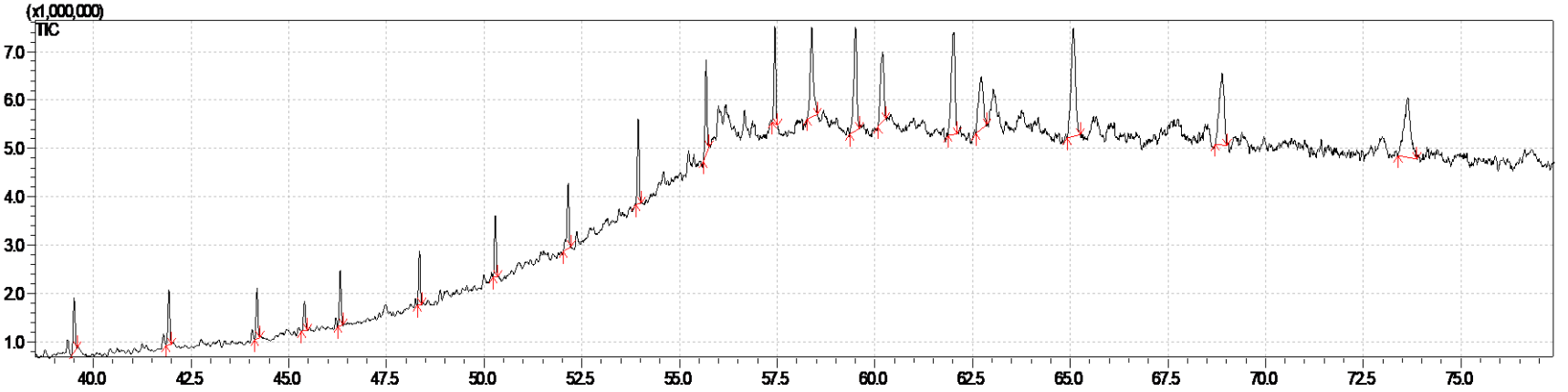

Figure B. 11 - zoomed in chromatogram of run 8

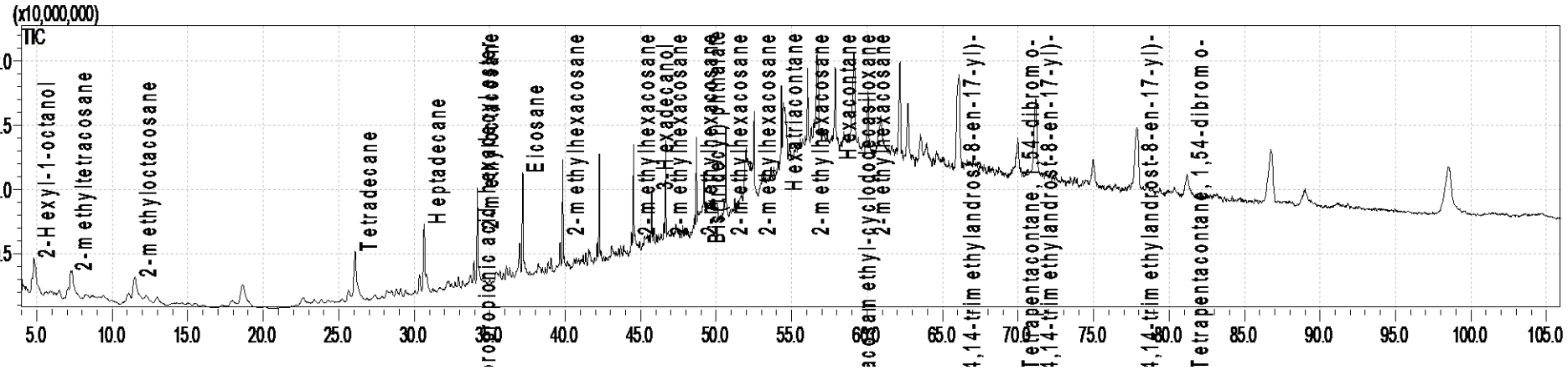

Figure B. 12 - Run 7 total ion chromatogram

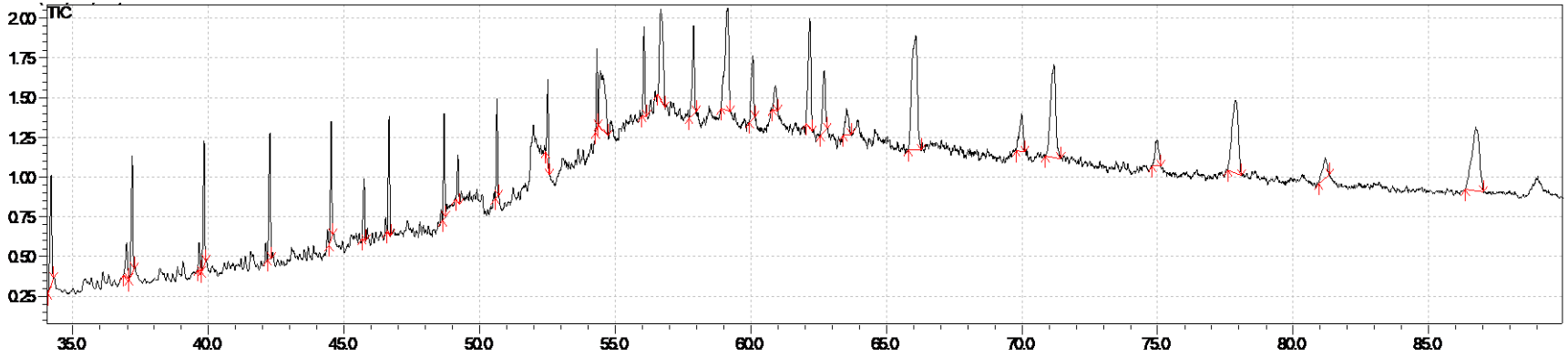

Figure B. 13 - zoomed in chromatogram of run 7

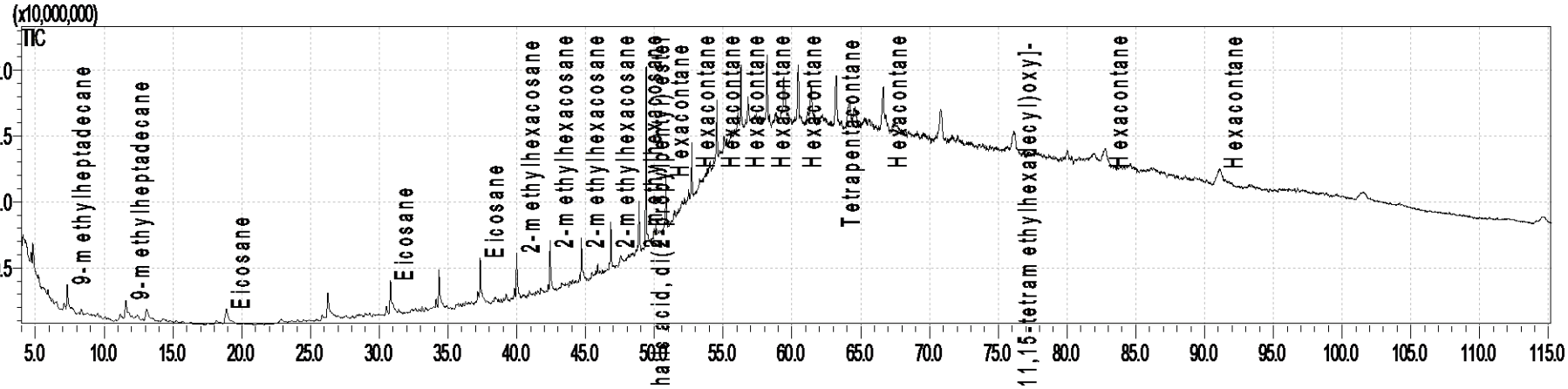

Figure B. 14 - No catalyst total ion chromatogram

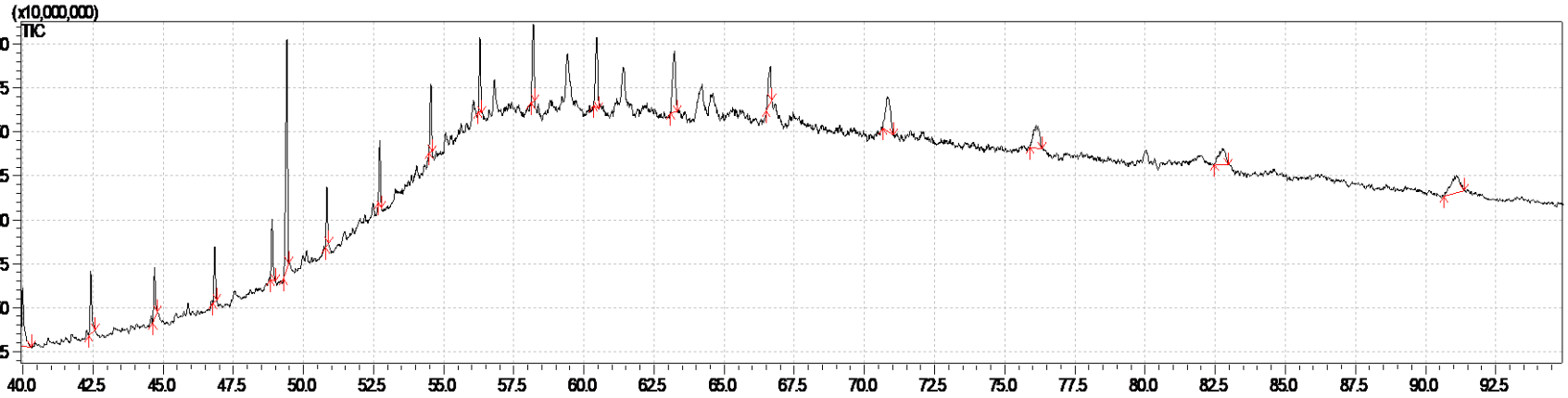

Figure B. 15 - zoomed in chromatogram of no catalyst run

Fixed Bed Reactor Data

Nickel Molybdenum

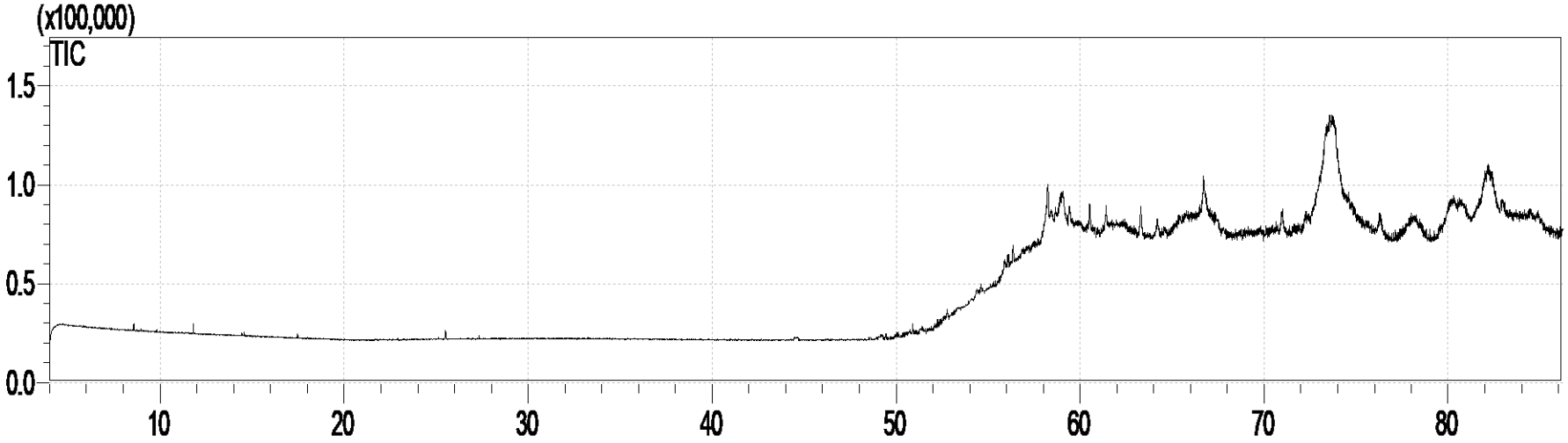

Figure B. 16 - NiMo 360 ˚C total ion chromatogram

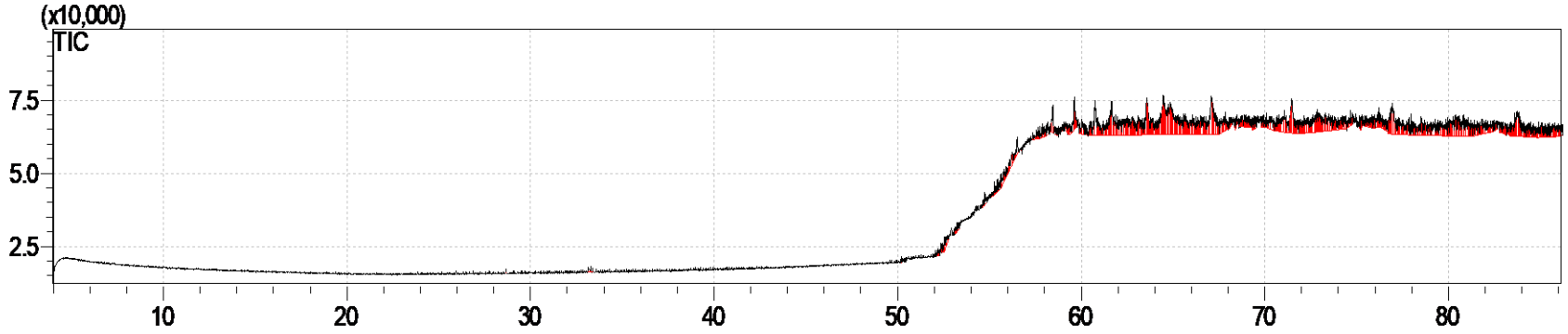

Figure B. 17 - NiMo 380 ˚C total ion chromatogram

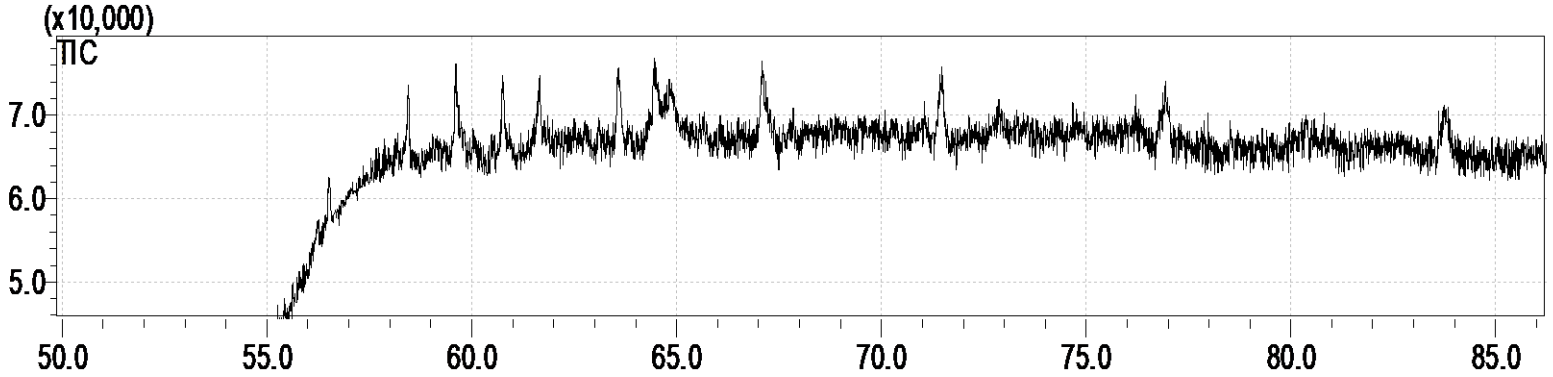

Figure B. 18 -Zoomed in NiMo 380 ˚C total ion chromatogram

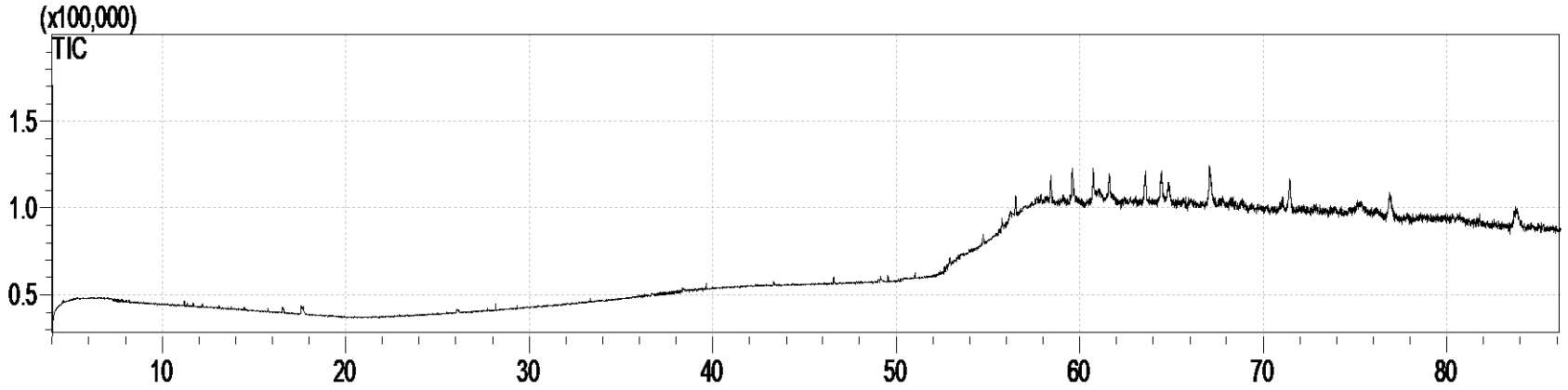

Figure B. 19 - NiMo 400 ˚C total ion chromatogram

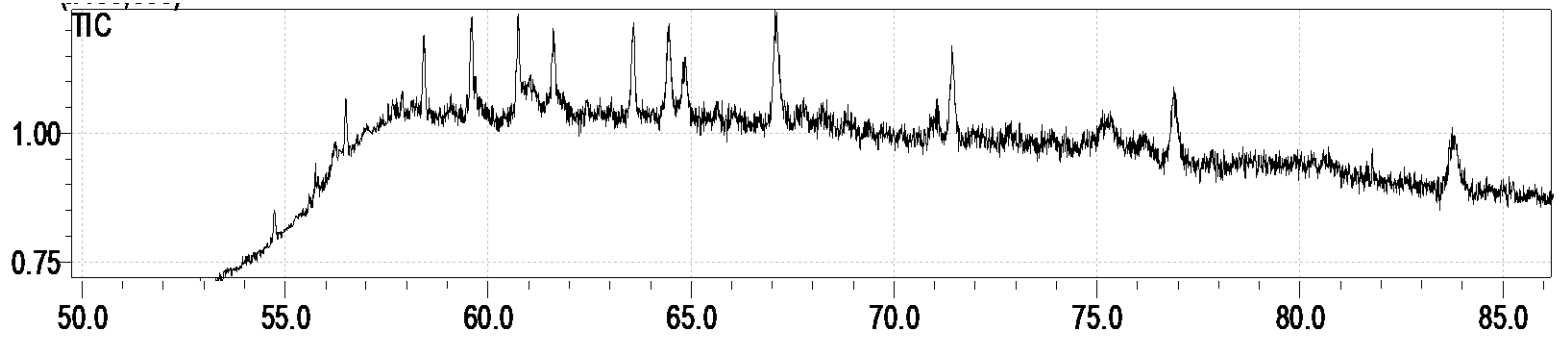

Figure B. 20 -Zoomed in NiMo 400 ˚C total ion chromatogram

Cobalt Molybdenum

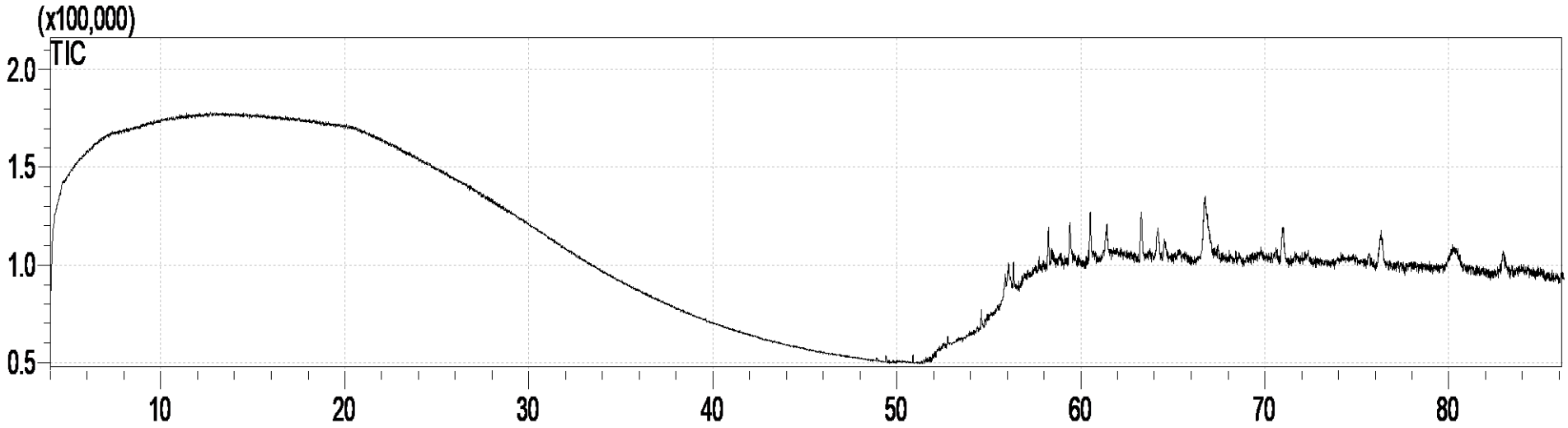

Figure B. 21 - CoMo 360 ˚C total ion chromatogram and zoomed in

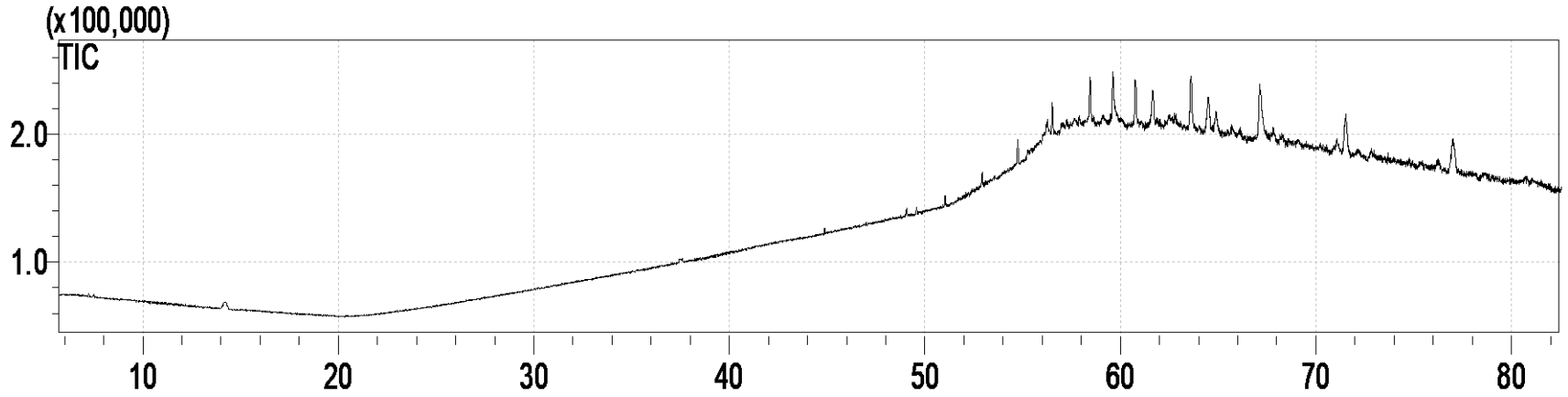

Figure B. 22 - CoMo 380 ˚C total ion chromatogram

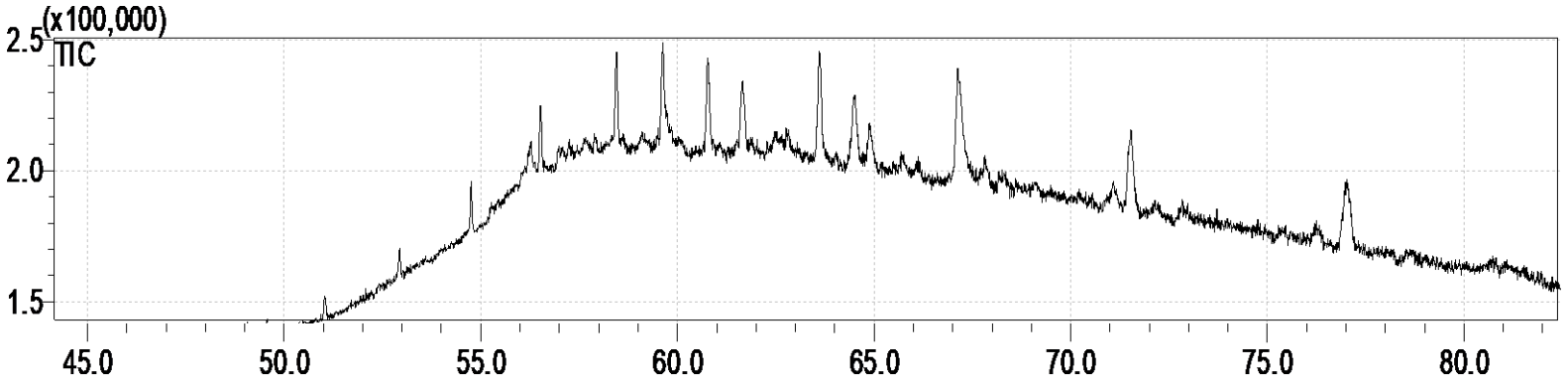

Figure B. 23 - Zoomed in CoMo 380 ˚C total ion chromatogram

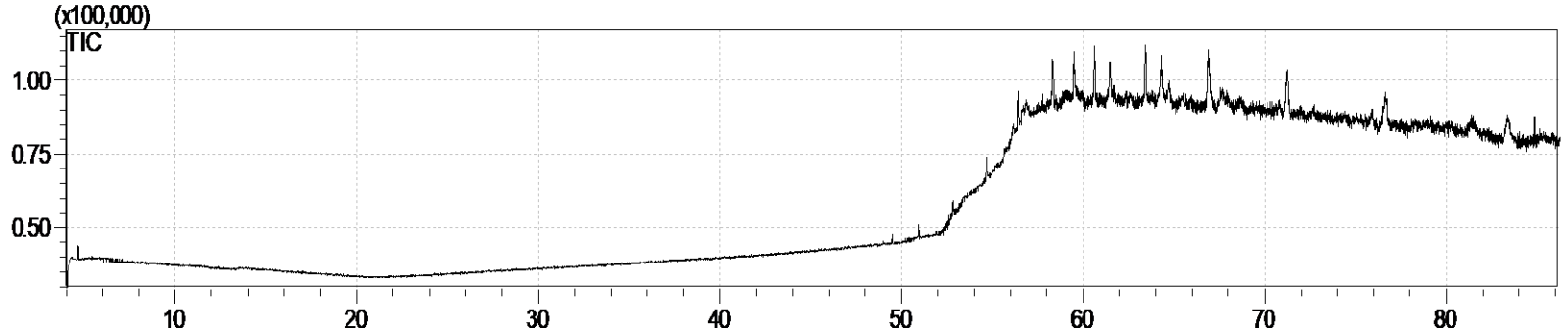

Figure B. 24 - CoMo 400 ˚C total ion chromatogram

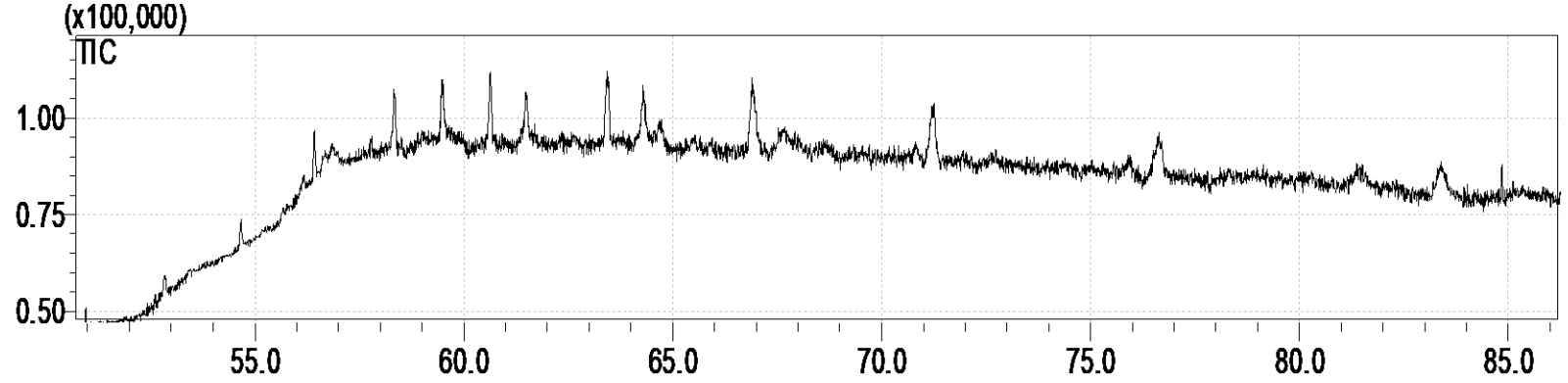

Figure B. 25 - Zoomed in CoMo 400 ˚C total ion chromatogram

Supported Magnetite Nanocatalyst

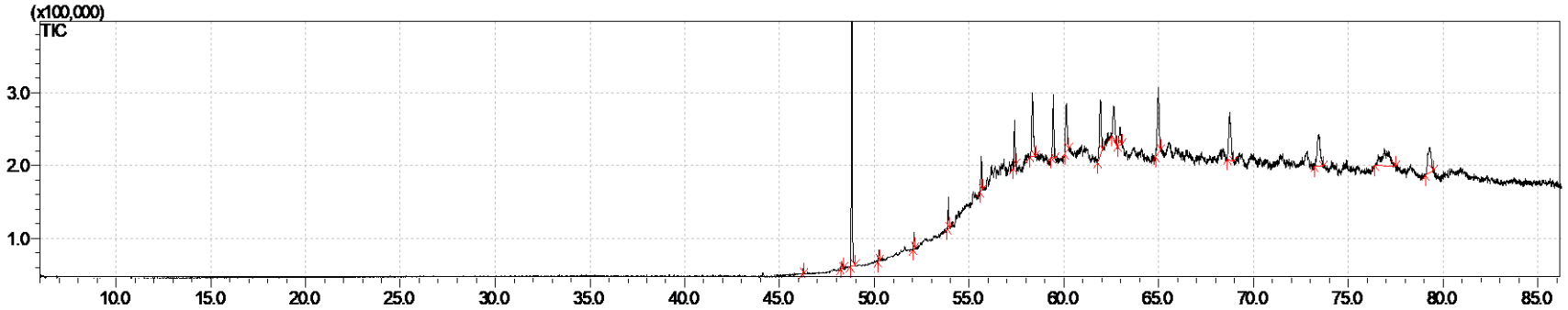

Figure B. 26 - Supported magnetite 360 ˚C total ion chromatogram

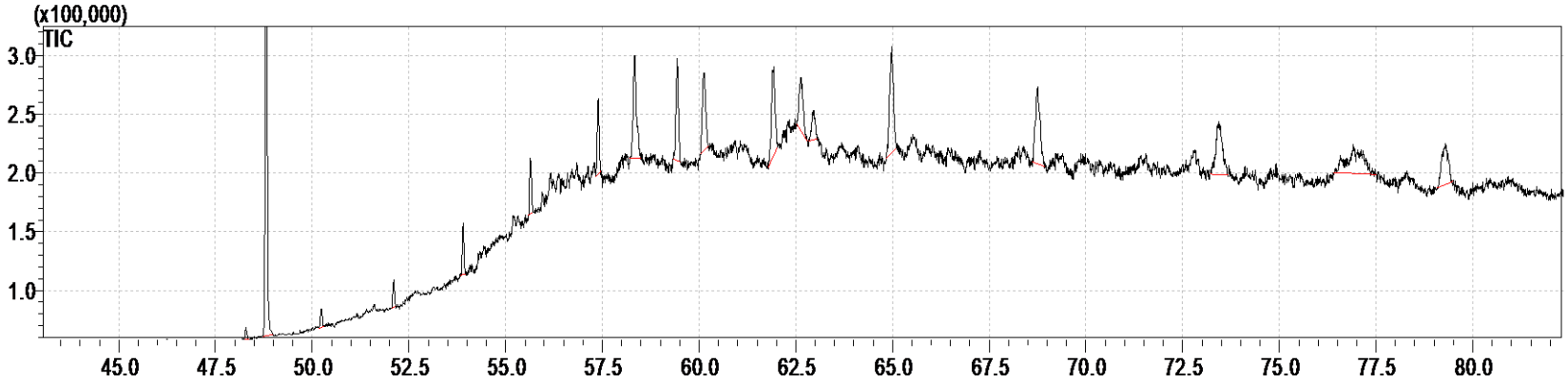

Figure B. 27 - Zoomed in Supported magnetite 360 ˚C total ion chromatogram

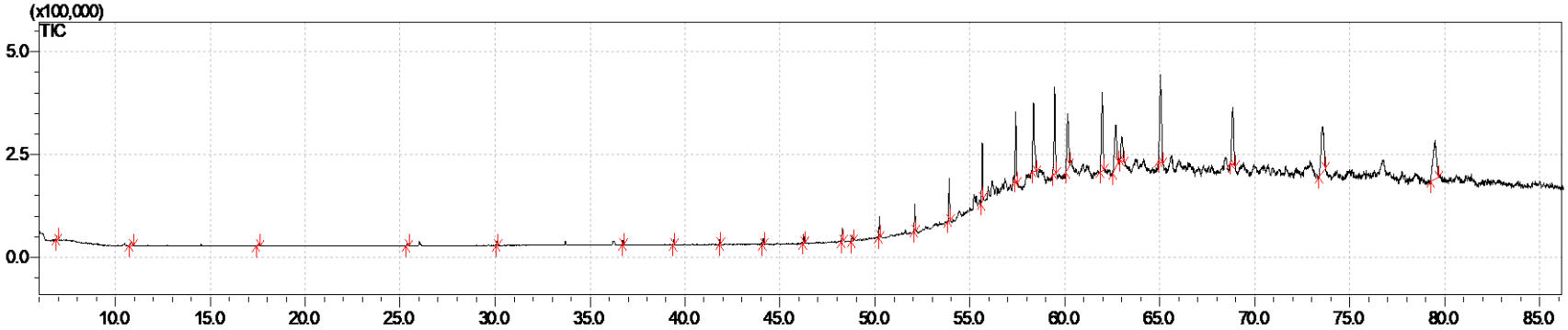

Figure B. 28 - Supported magnetite 380 ˚C total ion chromatogram

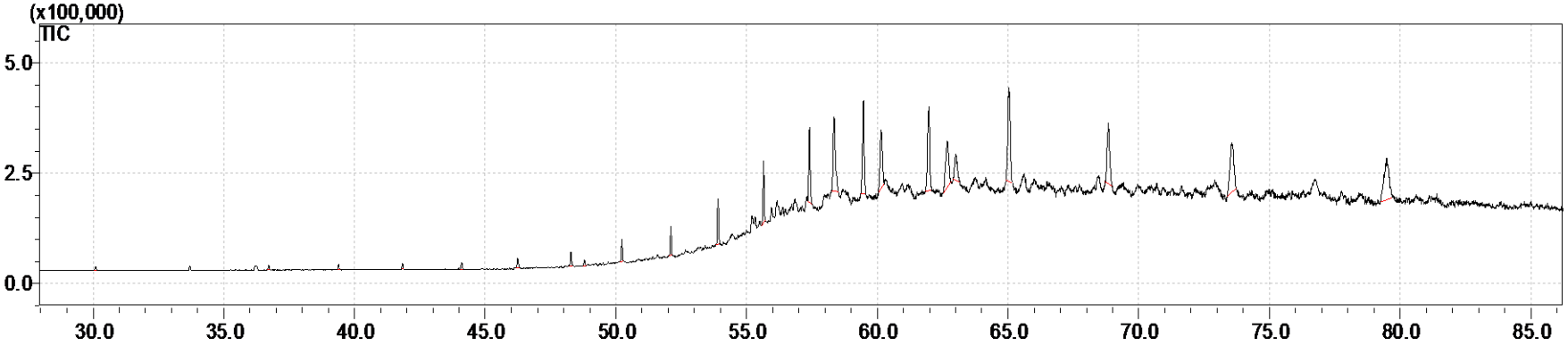

Figure B. 29 - Zoomed in Supported magnetite 380 ˚C total ion chromatogram

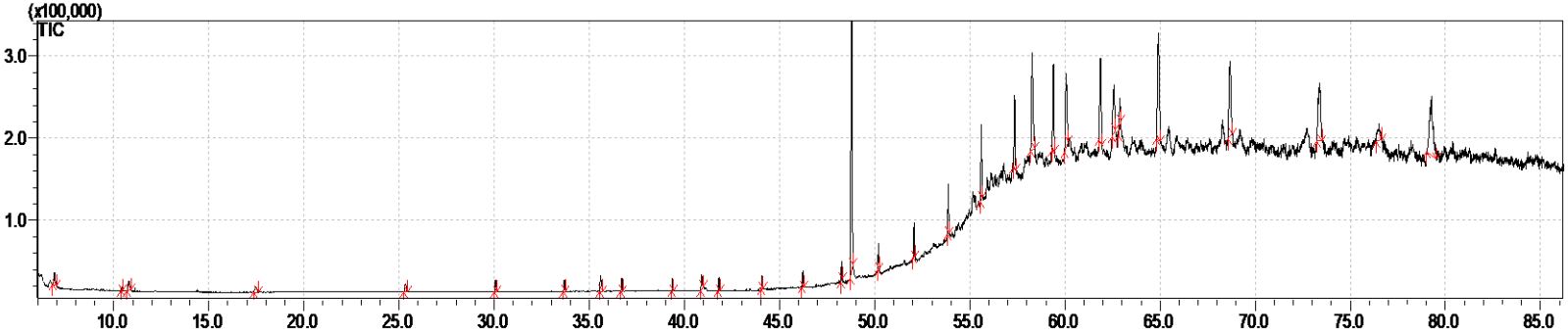

Figure B. 30 - Supported magnetite 400 ˚C total ion chromatogram

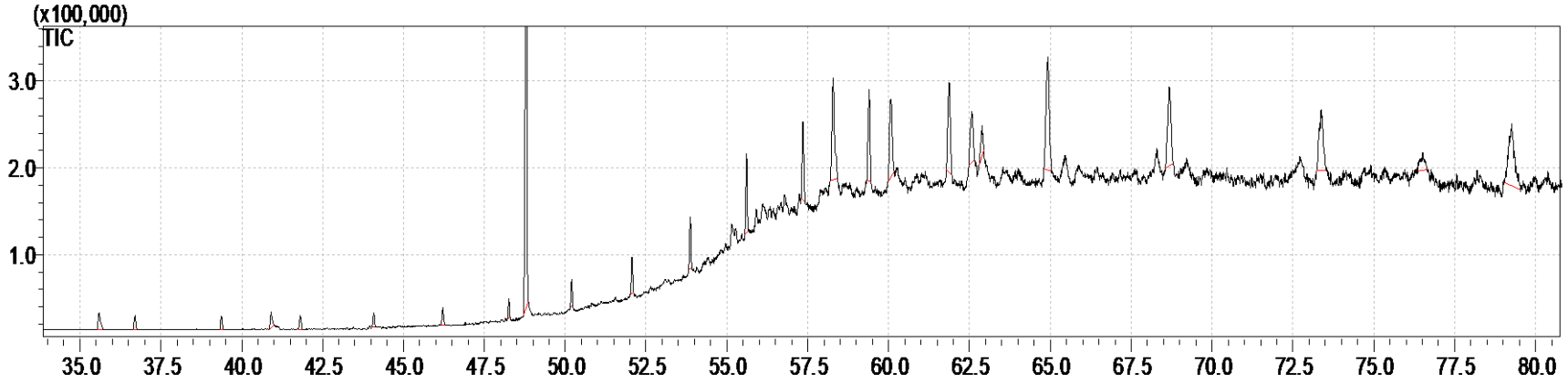

Figure B. 31 - Zoomed in Supported magnetite 400 ˚C total ion chromatogram

Inert Glass Beads

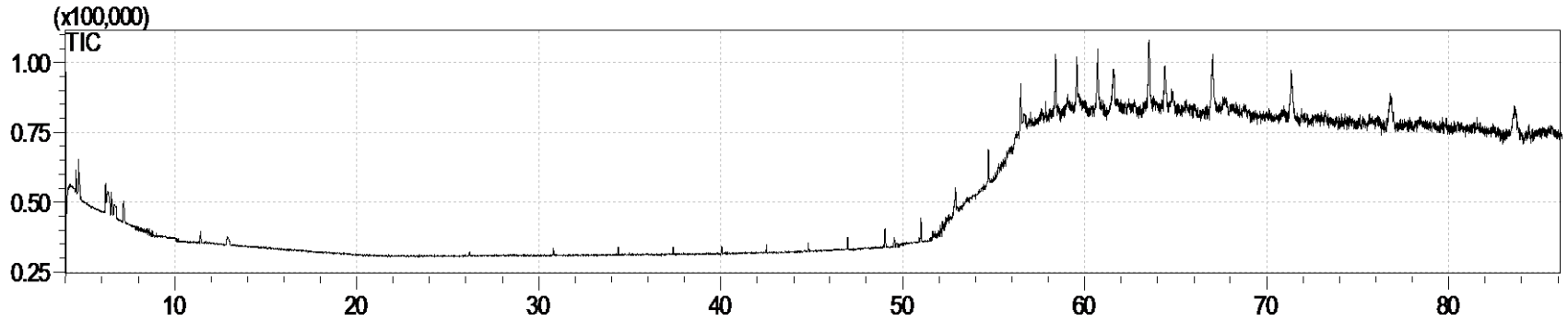

Figure B. 32 - Inert catalyst total ion chromatograms

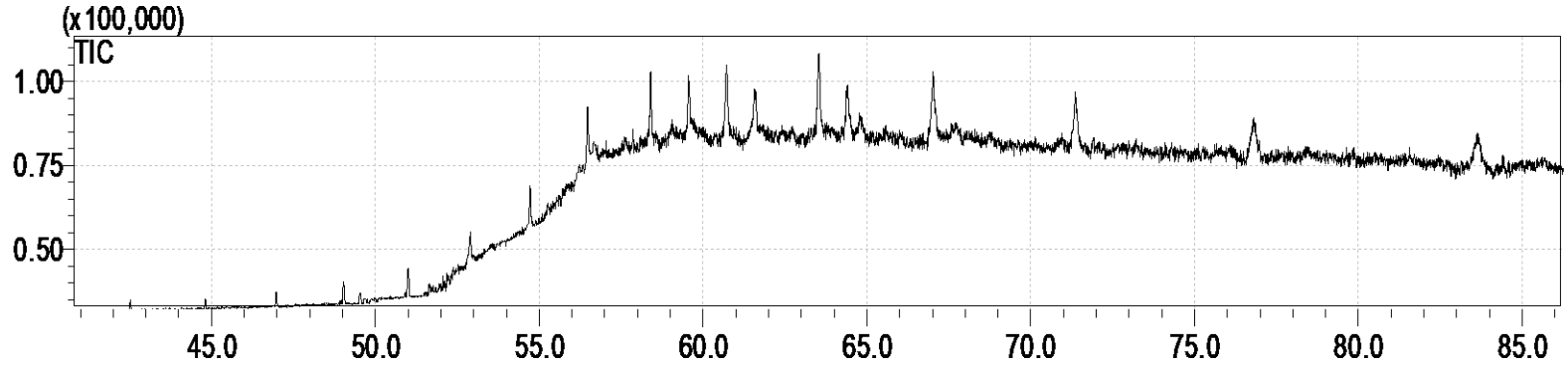

Figure B. 33 - Zoomed in Inert catalyst total ion chromatograms

Appendix C: Peak analysis from GCMS

Time (min)	Mol Formula	Name	Boiling Points(˚C)	Peak Area	Mass fraction
48,878	C3OH52O2	Tetracosapentaene, 2,6,10,15,19,23-hexamethyl-	380	2023	0,0009
49,394	C3OH52O2	Tetracosapentaene, 2,6,10,15,19,23-hexamethyl-	381	18134	0,0085
50,848	C3OH52O2	Tetracosapentaene, 2,6,10,15,19,23-hexamethyl-	382	22940	0,0107
52,731	C3OH52O2	Tetracosapentaene, 2,6,10,15,19,23-hexamethyl-	382	27417	0,0128
54,559	C69H138O2	Nonahexacontanoic acid	702	49198	0,0230
56,314	C69H138O2	Nonahexacontanoic acid	702	80931	0,0379
58,204	C69H138O2	Nonahexacontanoic acid	702	152523	0,0714
59,364	C3OH52O2	Tetracosapentaene, 2,6,10,15,19,23-hexamethyl-	380	115881	0,0543
60,48	C3OH52O2	Tetracosapentaene, 2,6,10,15,19,23-hexamethyl-	380	153030	0,0716
61,37	C3OH52O2	Tetracosapentaene, 2,6,10,15,19,23-hexamethyl-	380	89190	0,0418
63,238	C69H138O2	Nonahexacontanoic acid	702	233216	0,1092
64,124	C69H138O2	Nonahexacontanoic acid	702	203076	0,0951
66,647	C69H138O2	Nonahexacontanoic acid	702	247019	0,1157
70,915	C69H138O2	Nonahexacontanoic acid	702	246010	0,1152
76,274	C69H138O2	Nonahexacontanoic acid	702	180287	0,0844
82,955	C69H138O2	Nonahexacontanoic acid	702	314959	0,1475
		Total Area		2135834	

Table C. 1 - Feed peak analysis

Batch Reactor Data

Time(min)	Form	Name	Boiling Points(˚C)	Peak Area	Mass fraction
5,5	C23H38O2	Benzeneacetic acid, 4-pentadecyl ester $$ 1-Propyldodecyl phenylacetate # $$	462	2773083	0,0148
8	C18H38	9-methylheptadecane	313	4441043	0,0237
12,5	C18H38	9-methylheptadecane	313	3959734	0,0211
20	C16H34	Hexadecane $$ n-Cetane $$ n-Hexadecane $$ Cetane $$	620	3248273	0,0173
27	C29H60	2-methyloctacosane	436	4549469	0,0242
31,4	C29H60	2-methyloctacosane	436	3819222	0,0203
34,8	C21H44	Pentadecane, 8-hexyl- $$ 8-n-Hexylpentadecane $$ 8-Hexylpentadecane # $$	337	3762784	0,0200
37,9	C27H56	2-methylhexacosane	381	3812304	0,0203
40,5	C27H56	2-methylhexacosane	381	4155963	0,0221
42,2	C17H36O	3-Heptadecanol	309	2371623	0,0126
43	C27H56	2-methylhexacosane	381	4622330	0,0246
45,2	C27H56	2-methylhexacosane	381	3684549	0,0196
46,5	C16H34O	3-Hexadecanol	304	20642879	0,1099
47,5	C27H56	2-methylhexacosane	381	4217506	0,0225
49,5	C27H56	2-methylhexacosane	381	4751431	0,0253
50	C41H84O	1-Hentetracontanol	572	2822152	0,0150
51,5	C27H56	2-methylhexacosane	381	4697374	0,0250
53,4	C27H56	2-methylhexacosane	381	6676816	0,0356
55,2	C27H56	2-methylhexacosane	381	6885419	0,0367
57	C60H122	Hexacontane	620	7611841	0,0405
59	C60H122	Hexacontane	620	8539736	0,0455
60,5	C30H52O2	Tetracosa-2,6,14,18,22-pentaene-10,11-diol, 2,6,10,15,19,23-hexamethyl	513	12432951	0,0662
61,5	C60H122	Hexacontane	620	15191666	0,0809
64,5	C60H122	Hexacontane	620	18221643	0,0970
68,5	C60H122	Hexacontane	620	12077250	0,0643
73	C60H122	Hexacontane	620	10316632	0,0549
79	C60H122	Hexacontane	620	7494903	0,0399
		Total Area		187780576	

Table C. 2 - Run 1 peak analysis

Time	Form	Name	Boiling Points	Peak Area	Mass fraction
5,2	C19H40	Octadecane	317	2732673	0,0118
7	C10H10O	3-Buten-2-one, 4-phenyl-, (E)-	261	3424827	0,0148
7,8	C16H34	Hexadecane	286	4028307	0,0174
12,5	C14H22O	Phenol, 2,6-bis(1,1-dimethylethyl)- $$ Phenol, 2,6-di-tert-butyl	256	9088340	0,0394
31	C16H34	Hexadecane	286	3409322	0,0148
35	C21H44	Pentadecane	270	2499277	0,0108
37,8	C27H56	2-methylhexacosane	381	3189620	0,0138
40,5	C27H56	2-methylhexacosane	381	2686361	0,0116
43	C27H56	2-methylhexacosane	381	2587979	0,0112
45,3	C27H56	2-methylhexacosane	381	2248754	0,0097
46,5	C16H34O	3-Hexadecanol	304	5027614	0,0218
47,5	C27H56	2-methylhexacosane	381	2913105	0,0126
49,5	C27H57	2-methylhexacosane	381	2703719	0,0117
51,5	C27H58	2-methylhexacosane	381	3805689	0,0165
53,4	C27H59	2-methylhexacosane	381	6841771	0,0296
55,2	C27H60	2-methylhexacosane	381	7035908	0,0305
57	C27H61	2-methylhexacosane	381	13193050	0,0571
59	C27H62	2-methylhexacosane	381	11728167	0,0508
60,5	C33H56	1,1,6-trimethyl-3-methylene-2-(3,6,9,13-tetramethyl-6-ethenye-10,14-dimethylene-pentadec-4-enyl)cyclohexane		16141812	0,0699
61,5	C27H62	2-methylhexacosane	381	15209625	0,0659
62,6	C20H34O2	(1S,2E,4S,5R,7E,11E)-Cembra-2,7,11-trien-4,5-diol $$ 12-Isopropyl-1,5,9-trimethyl-4,8,12-cyclotetradecatriene-1,2-diol # $$	218	9086254	0,0394
64,5	C27H62	2-methylhexacosane	381	17401886	0,0754
68,5	C27H59	2-methylhexacosane	381	14786683	0,0640
73	C41H84O	1-Hentetracontanol	572	18072396	0,0783
78,5	C41H84O	1-Hentetracontanol	572	39011353	0,1690
87	C41H84O	1-Hentetracontanol	572	12009068	0,0520
		Total Area		230863560	

Table C. 3 - Run 2 peak analysis

Time	Form	Name	Boiling Points	Peak Area	Mass fraction
4	C20H32O3	Benzyl oxy tridecanoic acid $$ 13-(Benzyloxy)tridecanoic acid # $$	435	5851456	0,0124
5	C22H36O2	Benzeneacetic acid, 2-tetradecyl ester $$ 1-Methyltridecyl phenylacetate # $$	440	10955678	0,0232
7,6	C14H30	Tetradecane $$ n-Tetradecane $$	254	13564643	0,0288
12,2	C16H34	Hexadecane $$ n-Cetane $$ n-Hexadecane $$ Cetane $$	286	14357969	0,0305
20	C16H34	Hexadecane $$ n-Cetane $$ n-Hexadecane $$ Cetane $$	286	11668314	0,0248
27	C29H60	2-methyloctacosane	436	18368204	0,0390
31,5	C29H60	2-methyloctacosane	436	17875460	0,0379
35	C29H60	2-methyloctacosane	436	15557387	0,0330
38	C20H42	Eicosane $$ n-Eicosane $$ Icosane # $$ n-Icosane $$	343	15013819	0,0319
40,5	C27H56	2-methylhexacosane	381	14677633	0,0311
43	C27H56	2-methylhexacosane	381	15616765	0,0331
45,2	C16H34O	3-Hexadecanol	304	10412588	0,0221
47,5	C27H56	2-methylhexacosane	381	8006107	0,0170
49,5	C27H57	2-methylhexacosane	381	2752654	0,0058
51,5	C27H58	2-methylhexacosane	381	16247411	0,0345
53,5	C27H59	2-methylhexacosane	381	20058731	0,0426
55	C27H59	2-methylhexacosane	381	16710046	0,0355
57	C27H59	2-methylhexacosane	381	26881677	0,0570
59	C27H59	2-methylhexacosane	381	30394732	0,0645
60,5	C16H30O2	(1R,2R,8S,8Ar)-8-hydroxy-1-(2-hydroxyethyl)-1,2,5,5-tetramethyl-cis-decalin	370	32184220	0,0683
61,5	C27H59	2-methylhexacosane	381	29896136	0,0634
64,5	C27H59	2-methylhexacosane	381	25072070	0,0532
68,5	C27H59	2-methylhexacosane	381	23773913	0,0504
73,5	C27H59	2-methylhexacosane	381	37644613	0,0799
78,5	C60H122	Hexacontane	620	23517526	0,0499
87	C41H84O	1-Hentetracontanol	572	14228634	0,0302
		Total Area		471288386	

Table C. 4 - Run 3 peak analysis

Time(min)	Formula	Name	Boiling Points(˚C)	Peak Area	Mass fraction
4,75	C25H52	2-methyltetracosane	381	33049978	0,0965
7,13	C14H30	Tetradecane	253	31062188	0,0907
11,105	C16H34	Hexadecane	286	26646663	0,0778
17,94	C16H34	Hexadecane	286	16514090	0,0482
25,59	C17H36	Heptadecane	302	13743728	0,0401
30,25	C16H34	Hexadecane	286	14995267	0,0438
33,38	C20H42	Eicosane	342	14679268	0,0429
36,82	C21H44	Pentadecane	270	13691684	0,0400
39,48	C20H42	Eicosane	342	11994593	0,0350
41,9	C27H56	2-methylhexacosane	416,85	11327443	0,0331
44,16	C27H56	2-methylhexacosane	416,85	9881679	0,0289
45,38	C16H34O	3-Hexadecanol	304	6857891	0,0200
46,29	C27H56	2-methylhexacosane	416,85	9600824	0,0280
48,31	C27H56	2-methylhexacosane	416,85	8392008	0,0245
48,305	C34H58O4	Bis(tridecyl) phthalate	477	4630036	0,0135
52,2	C27H56	2-methylhexacosane	416,85	7120129	0,0208
53,89	C27H56	2-methylhexacosane	416,85	7455864	0,0218
55,62	C27H56	2-methylhexacosane	416,85	7497910	0,0219
57,38	C27H56	2-methylhexacosane	416,85	7697311	0,0225
58,3	C33H56	1,1,6-trimethyl-3-methylene-2-(3,6,9,13-tetramethyl-6-ethenye-10,14-dimethylene-pentadec-4-enyl)cyclohexane		6286577	0,0184
59,4	C27H56	2-methylhexacosane	416,85	9678491	0,0283
60,07	C16H30O2	(1R,2R,8S,8Ar)-8-hydroxy-1-(2-hydroxyethyl)-1,2,5,5-tetramethyl-cis-decalin	353,66	9265397	0,0271
61,88	C27H56	2-methylhexacosane	416,85	11940276	0,0349
64,89	C27H56	2-methylhexacosane	416,85	13409019	0,0392
68,6	C60H122	Hexacontane	620,2	8774989	0,0256
73,25	C60H122	Hexacontane	620,2	7109992	0,0208
79,7	C60H122	Hexacontane	620,2	9111952	0,0266
86,21	C41H84O	1-Hentetracontanol	572	9963816	0,0291
		Total Area		3,42E+08	

Table C. 5 - Run 4 peak analysis

Time(min)	Formula	Name	Boiling point(˚C)	Peak Area	Mass Fraction
5	C19H40	Octadecane	317	10065579	0,0436
7,5	C19H40	Octadecane	317	12060287	0,0522
12	C19H40	Octadecane	317	6447491	0,0279
20	C16H34	Hexadecane	286	6505391	0,0281
26,5	C69H138O2	Nonahexacontanoic acid	557	1872471	0,0081
27	C16H34	Hexadecane	286	9899701	0,0428
31	C69H138O2	Nonahexacontanoic acid	557	3036606	0,0131
31,5	C69H138O2	Nonahexacontanoic acid	557	2505904	0,0108
34,5	C69H138O2	Nonahexacontanoic acid	557	2593586	0,0112
35	C69H138O2	Nonahexacontanoic acid	557	1475914	0,0063
37,5	C29H60	2-methyloctacosane	436	13972221	0,0605
40,5	C27H56	2-methylhexacosane	436	12515488	0,0542
42,5	C27H56	2-methylhexacosane	381	10517713	0,0455
45	C27H56	2-methylhexacosane	381	4480580	0,0194
46,5	C16H34O	3-Hexadecanol	304	3865832	0,0167
47,5	C27H56	2-methylhexacosane	381	9660194	0,0418
49,5	C27H56	2-methylhexacosane	381	8830756	0,0382
50	C34H58O4	Bis(tridecyl) phthalate $$ 1,2-Benzenedicarboxylic acid, ditridecyl ester $$ Phthalic acid, ditri	285	11644904	0,0504
51,5	C41H84O	1-Hentetracontanol	572	9700404	0,0420
53,25	C27H56	2-methylhexacosane	381	6366476	0,0275
55	C27H56	2-methylhexacosane	381	10674143	0,0462
56,8	C27H56	2-methylhexacosane	381	5510177	0,0238
58,8	C27H56	2-methylhexacosane	381	6101228	0,0264
60	C29H50O	Cholestan-3-one	502	7642449	0,0331
61,5	C29H50O	Cholestan-3-one	502	8398192	0,0363
62,5	C41H84O	1-Hentetracontanol	572	4024300	0,0174
64	C41H84O	1-Hentetracontanol	572	9172000	0,0397
68	C41H84O	1-Hentetracontanol	572	6675377	0,0289
72,5	C41H84O	1-Hentetracontanol	572	10760808	0,0466
78	C41H84O	1-Hentetracontanol	572	7304702	0,0316
85,5	C41H84O	1-Hentetracontanol	572	6538684	0,0283
		Total Area		230819558	

Table C. 6 - Run 5 peak analysis

Time(min)	Formula	Name	Boiling point(˚C)	Peak Area	Mass Fraction
4,82	C14H30O	2-Hexyl-1-octanol	195	29015510	0,0510
7,37	C16H34	Hexadecane	286	37286857	0,0656
11,55	C16H34	Hexadecane	286	20258372	0,0356
18,71	C16H34	Hexadecane	286	24161788	0,0425
26,05	C17H36	Heptadecane	302	36296825	0,0639
30,65	C21H44	Heneicosane	305	40789178	0,0718
34,18	C29H60	2-methyloctacosane	413	34264708	0,0603
37,18	C20H42	Eicosane	343	36385555	0,0640
39,825	C20H42	Eicosane	343	27750349	0,0488
42,25	C36H74	Hexatriacontane	497	25207866	0,0443
44,51	C34H70	Tetratriacontane	285	22768174	0,0400
46,65	C27H56	2-methylhexacosane	416,85	20579040	0,0362
48,68	C27H56	2-methylhexacosane	416,85	19836350	0,0349
50,62	C27H56	2-methylhexacosane	416,85	17720538	0,0312
52,48	C27H56	2-methylhexacosane	416,85	22958873	0,0404
54,29	C27H56	2-methylhexacosane	416,85	14160486	0,0249
56,02	C27H56	2-methylhexacosane	416,85	12843484	0,0226
57,83	C27H56	2-methylhexacosane	416,85	14787711	0,0260
59,97	C60H122	Hexacontane	620,2	17685756	0,0311
62,58	C60H122	Hexacontane	620,2	14181722	0,0249
65,75	C60H122	Hexacontane	620,2	11230125	0,0197
69,72	C60H122	Hexacontane	620,2	12761474	0,0224
74,62	C41H84O	1-Hentetracontanol	572	14190057	0,0249
80,78	C41H84O	1-Hentetracontanol	572	8862611	0,0156
88,33	C41H84O	1-Hentetracontanol	572	11239293	0,0197
98,35	C41H84O	1-Hentetracontanol	572	20663663	0,0363
		Total Area		567886365	

Table C. 7 - Run 6 peak analysis

Time(min)	Formula	Name	Boiling point(˚C)	Peak Area	Mass fraction
4,758	C14H30O	2-Hexyl-1-octanol	195	38568434	0,0354
7,25	C25H52	2-methyltetracosane	381	36084558	0,0332
11,502	C25H52	2-methyltetracosane	381	21383709	0,0196
18,525	C16H34	hexadecane	286	16380955	0,0150
26,18	C14H30	Tetradecane	253	23841109	0,0219
30,78	C17H36	Heptadecane	302	27047831	0,0248
34,15	C29H60	2-methyloctacosane	413	31273752	0,0287
36,96	C19H33F5O2	Pentafluoropropionic acid, hexadecyl ester		11219976	0,0103
37,18	C20H42	Eicosane	342	30131305	0,0277
39,65	C19H33F5O2	Pentafluoropropionic acid		6501441	0,0059
39,84	C25H52	2-methyltetracosane	381	29614081	0,0272
44,505	C25H52	2-methyltetracosane	381	25198319	0,0231
45,73	C16H34O	3-Hexadecanol	304	14996262	0,0138
46,66	C27H56	2-methylhexacosane	381	25044558	0,0230
48,69	C27H56	2-methylhexacosane	381	21006295	0,0193
49,19	C34H58O4	Bis(tridecyl) phthalate	477	10540513	0,0097
50,65	C27H56	2-methylhexacosane	381	20830110	0,0191
52,51	C27H56	2-methylhexacosane	381	18320293	0,0168
54,32	C36H74	Hexatriacontane	497	53913300	0,0496
56,06	C27H56	2-methylhexacosane	381	21685963	0,0199
57,89	C60H122	Hexacontane	620	29781061	0,0274
59,14	C24H72O12Si12	Tetracosamethyl-cyclododecasiloxane	518	65120334	0,0599
60,07	C60H122	Hexacontane	620	23558659	0,0216
62,71	C60H122	Hexacontane	620	27327720	0,0251
69,99	C60H122	Hexacontane	620	22131097	0,0203
81,19	C60H122	Hexacontane	620	15357381	0,0141
		Total Area		1086588000	

Table C. 8 - Run 7 380 peak analysis

Time(min)	Formula	Name	Boiling point(˚C)	Peak Area	Mass fraction
4,71	C16H34	Hexadecane	286	3493919	0,0165
7,06	C14H30	Tetradecane	253	4618288	0,0218
11,08	C14H30	Tetradecane	253	3881440	0,0184
12,44	C14H14	Bibenzyl $$ Benzene	284	6204727	0,0294
17,94	C16H34	Hexadecane	286	4614551	0,0218
25,62	C16H34	Hexadecane	286	3507203	0,0166
30,27	C16H34	Hexadecane	286	4687665	0,0222
33,85	C20H42	Eicosane	342	4535985	0,0215
36,85	C21H44	Pentadecane	270	4456374	0,0211
39,51	C27H56	2-methylhexacosane	381	3864233	0,0183
41,94	C27H56	2-methylhexacosane	381	3939249	0,0186
44,19	C27H56	2-methylhexacosane	381	3389490	0,0160
46,315	C27H56	2-methylhexacosane	381	3673835	0,0174
48,35	C44H90	Tetratetracontane	547	3413347	0,0161
50,29	C27H56	2-methylhexacosane	381	3862499	0,0183
52,15	C27H56	2-methylhexacosane	381	5039996	0,0238
53,95	C44H90	Tetratetracontane	547	5619864	0,0266
55,68	C27H56	2-methylhexacosane	381	6543198	0,0310
57,35	C27H56	2-methylhexacosane	381	6560631	0,0311
58,39	C28H48	17.alfa.,21.beta.-28,30-Bisnorhopane	447	10525980	0,0499
59,5	C27H56	2-methylhexacosane	381	11711936	0,0555
60,2	C16H30O2	1R,2R,8S,8Ar)-8-hydroxy-1-(2-hydroxyethyl)-1,2,5,5-tetramethyl-cis-decalin	353	9024847	0,0427
62	C60H122	Hexacontane	620	14380776	0,0681
62,72	C20H38O2	1-Naphthalenepropanol	398	8981162	0,0425
65,08	C27H56	2-methylhexacosane	381	17506098	0,0829
68,89	C60H122	Hexacontane	620	12976555	0,0615
73,64	C60H122	Hexacontane	620	14422455	0,0683
79,55	C60H122	Hexacontane	620	10283917	0,0487
86,95	C41H84O	1-Hentetracontanol	572	15206742	0,0720
		Total Area		210926962	

Table C. 9 - Run 8 peak analysis

Time(min)	Formula	Name	Boiling point(˚C)	Mass fraction	Peak Area
31	C16H17ClN2O3	4(4-Chlorphenyl)-3-morpholinopyrrol-2-carboxylic acid, methyl ester $$ Methyl 4-(4-chlorophenyl)-3-(4-morpholinyl)-1H-pyrrole-2-carboxylate # $$	467,4	377355	0,0168
34,75	C16H17ClN2O3	4(4-Chlorphenyl)-3-morpholinopyrrol-2-carboxylic acid, methyl ester $$ Methyl 4-(4-chlorophenyl)-3-(4-morpholinyl)-1H-pyrrole-2-carboxylate # $$	467,4	232789	0,0104
36,65	C16H17ClN2O3	4(4-Chlorphenyl)-3-morpholinopyrrol-2-carboxylic acid, methyl ester	467,4	252036	0,0112
37,75	C16H17ClN2O3	4(4-Chlorphenyl)-3-morpholinopyrrol-2-carboxylic acid, methyl ester	467,4	258861	0,0115
40,4	C16H17ClN2O3	4(4-Chlorphenyl)-3-morpholinopyrrol-2-carboxylic acid, methyl ester	467,4	139243	0,0062
42,85	C16H17ClN2O3	4(4-Chlorphenyl)-3-morpholinopyrrol-2-carboxylic acid, methyl ester	467,4	165568	0,0074
49,8	C16H17ClN2O3	4(4-Chlorphenyl)-3-morpholinopyrrol-2-carboxylic acid, methyl ester	467,4	1902708	0,0850
50,4	C27H42O4	Propanoic acid, 2-(3-acetoxy-4,4,14-trimethylandrost-8-en-17-yl)- $$	565	1143243	0,0511
52,55	C41H84O	Propanoic acid, 2-(3-acetoxy-4,4,14-trimethylandrost-8-en-17-yl)- $$	565	1488490	0,0665
55	C41H84O	1-Hentetracontanol	572	2270411	0,1015
56,7	C41H84O	1-Hentetracontanol	572	541700	0,0242
57,2	C41H84O	1-Hentetracontanol	572	1534654	0,0686
58,7	C41H84O	1-Hentetracontanol	572	526034	0,0235
62,8	C41H84O	1-Hentetracontanol	572	1323412	0,0591
64,2	C41H84O	1-Hentetracontanol	572	946279	0,0423
67	C41H84O	1-Hentetracontanol	572	2171401	0,0970
67,7	C41H84O	1-Hentetracontanol	572	772736	0,0345
72,3	C41H84O	1-Hentetracontanol	572	4047508	0,1809
79,6	C41H84O	1-Hentetracontanol	572	2269804	0,1014
		Total Area		22364232	

Table C. 10 - No catalyst peak analysis

Fraction(Boiling point)	***Feed***	***Run 1***	***Run 2***	***Run 3***	***Run 4***	***Run 5***	***Run 6***	***Run 7***	***Run 8***	***No Catalyst***
Product Masses (g)	*6.467*	*7.783*	*7.788*	*7.789*	*8.121*	*7.791*	*8.314*	*7.741*	*7.684*	*7.014*
Vacuum Residue(>565˚C)	0,7993	*0,4554*	0,2992	0,0801	0,1021	0,2347	0,1951	0,1087	0,3189	0,3283
Vacuum gas oil (360-565˚C)	0,2007	0,3572	0,5305	0,7819	0,4322	0,5032	0,2608	0,6677	0,4487	0,2918
Gas Oil(265-360˚C)	-	0,1873	0,1160	0,1092	0,4657	0,2621	0,4929	0,1882	0,2324	0,3799
Kerosene(140-265˚C)	-	-	0,0542	0,0288	-	-	0,0511	0,0354		-

Table C. 11 - Fractional yields of each fraction in each run (Feed basis)

Fixed Bed Reactor Data

Nickel Molybdenum

Time(min)	Formula	Name	Boiling point (˚C)	Area	Mass fraction
56,357	C9H18O	Cyclohexanol, 3,3,5-trimethyl-, cis-	198	22646	0,0110
58,255	C18H34O2	Palmitic acid vinyl ester, hexadecanoic acid	354,6	141171	0,0688
59,411	C19H38O3	Octadecanoic acid, 4-hydroxy-, methyl ester	380	46639	0,0227
60,505	C19H38O3	Octadecanoic acid, 4-hydroxy-, methyl ester	380	53543	0,0261
61,421	C22H42O2	Isophytol, acetate	313	42741	0,0208
63,295	C22H42O2	Isophytol, acetate	313	52520	0,0256
64,197	C41H84O	1-Hentetracontanol	572	35158	0,0171
66,713	C19H38O3	Octadecanoic acid, 4-hydroxy-, methyl ester	380	141923	0,0692
71,02	C69H138O2	Nonahexacontanoic acid	702	61747	0,0301
73,576	C69H138O2	Nonahexacontanoic acid	702	1450915	0,7081
		Total Area		2049003	

Table C. 12 - NiMo Peak Analysis at 360 ˚C

Time(min)	Formula	Name	Boiling Point (˚C)	Area	mass fractions
56,458	C9H18O	Cyclohexanol, 3,3,5-trimethyl-, cis-	161,8	20229	0,0432
58,369	C19H36O3	Tetradecanoic acid, 2-oxo-, methyl ester	250	26921	0,0576
59,541	C20H42O3	Hexadecanoic acid, 2-oxo-, methyl ester	351	60192	0,1288
60,664	C20H42O3	Hexadecanoic acid, 2-oxo-, methyl ester	351	30456	0,0651
63,501	C20H42O3	Hexadecanoic acid, 2-oxo-, methyl ester	351	43259	0,0925
64,357	C41H84O	1-Hentetracontanol	512,2	40168	0,0859
66,973	C50H102	Triacontane, 11,20-didecyl-	449,7	77354	0,1655
71,251	C69H138O2	Nonahexacontanoic acid	702	76113	0,1628
76,756	C69H138O2	Nonahexacontanoic acid	702	92596	0,1981
		Total Area		467288	

Table C. 13 - NiMo Peak analysis at 380 ˚C

Time(min)	Formula	Name	Boiling Points(˚C)	Area	mass fractions
26,06	$Ni(CO)_4$	Nickel tetracarbonyl	43	15170	0,0115
39,635	CH6N2O2	Carbamic acid, monoammonium salt	251	4542	0,0034
46,585	CH6N2O2	Carbamic acid, monoammonium salt	251	7541	0,0057
46,585	CH6N2O2	Carbamic acid, monoammonium salt	251	9028	0,0068
49,125	C3H9NO	(R) - (-)-2-amino-1-propanol	176	6889	0,0052
49,544	$Ni(CO)_4$	Nickel tetracarbonyl	43	11142	0,0084
51,02	$Ni(CO)_4$	Nickel tetracarbonyl	43	6070	0,0046
52,918	C10H18O4	Heptanoic acid, 2-(acetyloxy)-, methyl ester	223	20535	0,0156
54,735	C10H18O4	Heptanoic acid, 2-(acetyloxy)-, methyl ester	223	22900	0,0174
56,498	C18H38N2O	Stearic acid hydrazide	442,92	35766	0,0271
58,429	C18H38N2O	Stearic acid hydrazide	442,92	65529	0,0498
59,607	C24H32N2O3	Cyclohexanecarboxylic acid, 4-pentyl-, 2,3-dicyano-4-(pentyloxy)phenyl ester	233	75260	0,0572
60,737	C50H102	Triacontane, 11,20-Didecyl-	449,7	81288	0,0617
61,608	C34H58O4	Bis(tridecyl) phthalate	257	61748	0,0469
63,594	C50H102	Triacontane, 11,20-Didecyl-	449,7	108926	0,0828
64,456	C69H138O2	Nonahexacontanoic acid	702	99290	0,0754
64,834	C69H138O2	Nonahexacontanoic acid	702	81824	0,0622
67,07	C69H138O2	Nonahexacontanoic acid	702	165103	0,1255
71,427	C69H138O2	Nonahexacontanoic acid	702	103225	0,0784
76,891	C69H138O2	Nonahexacontanoic acid	702	150281	0,1142
83,755	C69H138O2	Nonahexacontanoic acid	702	183384	0,1394
		Total Area		1315441	

Table C. 14 - NiMo Peak analysis at 400 ˚C

Cobalt Molybdenum

Time(min)	Formula	Name	Boiling points (°C)	Area	Mass fraction
49,404	$Ni(CO)_4$	Nickel tetracarbonyl	43	11717	0,0056
50,88	$Ni(CO)_4$	Nickel tetracarbonyl	43	9344	0,0044
52,77	CH3N5	1H-Tetrazol-5-amine	387	17234	0,0082
54,588	CH3N5	1H-Tetrazol-5-amine	387	30795	0,0146
55,894	C18H38N2O	Stearic acid hydrazide	442,92	35378	0,0168
56,071	C18H38N2O	Stearic acid hydrazide	442,92	46573	0,0221
56,348	C18H38N2O	Stearic acid hydrazide	442,92	37358	0,0177
58,229	C18H38N2O	Stearic acid hydrazide	442,92	88963	0,0423
59,399	C18H38N2O	Stearic acid hydrazide	442,92	132328	0,0630
60,509	C18H38N2O	Stearic acid hydrazide	442,92	92956	0,0442
61,411	C41H84O	1-Hentetracontanol	572	76151	0,0362
63,278	C41H84O	1-Hentetracontanol	572	162804	0,0775
64,195	C41H84O	1-Hentetracontanol	572	116648	0,0555
64,539	C41H84O	1-Hentetracontanol	572	85865	0,0408
66,744	C69H138O2	Nonahexacontanoic acid	702	460136	0,2191
70,992	C69H138O2	Nonahexacontanoic acid	702	121697	0,0579
76,325	C69H138O2	Nonahexacontanoic acid	702	157337	0,0749
80,176	C69H138O2	Nonahexacontanoic acid	702	363771	0,1732
82,946	C69H138O2	Nonahexacontanoic acid	702	53017	0,0252
		Total Area		2100072	

Table C. 15 - CoMo Peak analysis at 360 °C

Time(min)	Formula	Name	Boiling point (℃)	Area	mass fractions
56,518	C6H11N3O4	Glycyl-D-asparagine	628,2	91146	0,0389
58,457	C6H11N3O4	Glycyl-D-asparagine	628,2	136713	0,0584
59,629	C10H18O4	Heptanoic acid, 2-(acetyloxy)-, methyl ester	223	167990	0,0718
60,761	C69H138O2	Nonahexacontanoic acid	702	173496	0,0742
61,657	C10H18O4	Heptanoic acid, 2-(acetyloxy)-, methyl ester	223	167901	0,0718
63,605	C27H56	2-methylhexacosane	416	225348	0,0964
64,498	C27H56	2-methylhexacosane	419	191046	0,0817
64,88	C27H56	2-methylhexacosane	416	119557	0,0511
67,123	C69H138O2	Nonahexacontanoic acid	702	364105	0,1557
71,53	C69H138O2	Nonahexacontanoic acid	702	200137	0,0856
77,02	C69H138O2	Nonahexacontanoic acid	702	274922	0,1176
83,848	C69H138O2	Nonahexacontanoic acid	702	224748	0,0961
		Total Area		2337109	

Table C. 16 - CoMo Peak analysis at 380 ˚C

Time(min)	Formula	Name	Boiling points (℃)	Area	Mass Fractions
52,84		4(4-Chlorphenyl)-3-morpholinopymol-2-carboxylic	380,8	14531	0,0140
54,667		4(4-Chlorphenyl)-3-morpholinopymol-2-carboxylic	380,8	22580	0,0218
56,428	C6H11N3O4	Glycyl-D-asparagine	628,2	37890	0,0367
58,326	C6H11N3O4	Glycyl-D-asparagine	628,2	80593	0,0781
59,478	C9H18O	Cyclohexanol, 3,3,5-trimethyl-, cis-	161,8	55454	0,0537
60,629	C9H18O	Cyclohexanol, 3,3,5-trimethyl-, cis-	161,8	76790	0,0744
61,471	C16H34	Hexadecane	286,8	43179	0,0418
63,433	C16H34	Hexadecane	286,8	106267	0,1029
64,295	C18H38N2O	Stearic acid hydrazide	442,92	81347	0,0788
66,89	C18H38N2O	Stearic acid hydrazide	442,92	142472	0,1380
71,252	C18H38N2O	Stearic acid hydrazide	442,92	159305	0,1543
76,644	C50H102	Triacontane, 11,20-didecyl-	449,7	88467	0,0857
83,395	C69H138O2	Nonahexacontanoic acid	702	100463	0,0973
84,845	C69H138O2	Nonahexacontanoic acid	702	22554	0,0218
		Total Area		1031892	

Table C. 17 - CoMo Peak analysis at 400 ˚C

Supported Magnetite Nanocatalyst

Time(min)	Formula	Name	Boiling Point(℃)	Area	Mass fraction
46,254	C5H10O2	1-Hydroxy-2-pentanone	152	23654	0,0033
48,287	C5H10O3	1-Hydroxy-2-pentanone	152	29465	0,0041
48,812	C24H38O4	Diisooctyl phthalate	384	1516790	0,2131
50,237	C5H10O3	1-Hydroxy-2-pentanone	152	50756	0,0071
52,113	C69H138O2	Nonahexacontanoic acid	702	71755	0,0100
53,902	C69H138O3	Nonahexacontanoic acid	702	126583	0,0177
55,636	C41H84O	1-Hentetracontanol	572	161055	0,0226
57,394	C69H138O3	Nonahexacontanoic acid	702	216683	0,0304
58,334	C16H26O3	2-Dodecen-1-yl(-)succinic anhydride	348	503112	0,0707
59,439	C25H55	2-methyltetracosane	390	374631	0,0526
60,127	C28H48O	Cholest-7-en-3-ol, 14-methyl-, (3.beta.)-	487	390303	0,0548
61,93	C41H84O	1-Hentetracontanol	572	478531	0,0672
62,634	C28H48O	Cholest-7-en-3-ol, 14-methyl-, (3.beta.)-	487	321894	0,0452
62,962	C22H42O2	Isophytol, acetate	498	154836	0,0217
64,981	C41H84O	1-Hentetracontanol	572	609337	0,0856
68,753	C41H84O	1-Hentetracontanol	572	532552	0,0748
73,44	C25H55	2-methyltetracosane	390	523713	0,0735
76,911	C41H84O	1-Hentetracontanol	572	627774	0,0882
79,287	C25H56	2-methyltetracosane	390	402450	0,0565
		Total Area		7115874	

Table C. 18 - Supported Magnetite Peak analysis at 360 ˚C

Time(min)	Formula	Name	Boiling Point (˚C)	Area	Mass Fraction
10,789	C11H24	2,2,6,6-Tetramethylheptane	163	72887	0,0074
17,453	C5H10O2	1-Hydroxy-2-pentanone	152	49134	0,0050
25,339	C5H18O3	2,2-Dimethylpropanoic anhydride	193	53109	0,0054
30,072	C5H18O3	2,2-Dimethylpropanoic anhydride	193	54106	0,0055
33,675	C5H18O4	2,2-Dimethylpropanoic anhydride	193	52299	0,0053
35,587	C9H20O	3-Heptanol, 3,5-dimethyl-	176	102194	0,0104
36,702	C11H24	Undecane	196	55254	0,0056
39,372	C5H18O4	2,2-Dimethylpropanoic anhydride	193	52785	0,0053
40,906	C10H22O	3-Octanol, 3,6-dimethyl-	230	68977	0,0070
41,807	C5H18O4	2,2-Dimethylpropanoic anhydride	193	57033	0,0058
44,083	C11H24	Undecane	199	50681	0,0051
46,218	C16H34	Hexadecane	287	67978	0,0069
48,26	C16H35	Hexadecane	287	59079	0,0060
48,787	C24H38O4	Diisooctyl phthalate	384	2215198	0,2260
50,2	C69H138O2	Nonahexacontanoic acid	702	79922	0,0081
52,067	C25H52	2-methyltetracosane	390	121502	0,0124
53,872	C25H53	2-methyltetracosane	390	178733	0,0182
55,609	C25H54	2-methyltetracosane	390	265738	0,0271
57,351	C25H55	2-methyltetracosane	390	310807	0,0317
58,28	C32H52O	17-(1,5-Dimethyl-hexyl)-4,4,9,13,14-pentamethylhexadecahydrocyclopenta[a]phenanthren-3-one	513	644141	0,0657
59,398	C25H55	2-methyltetracosane	390	438715	0,0447
60,062	C37H76O	1-Heptatriacotanol	490	522083	0,0532
61,872	C25H55	2-methyltetracosane	390	531831	0,0542
62,574	C16H23O3	2-Dodecen-1-yl(-)succinic anhydride	181	347393	0,0354
62,889	C16H23O4	2-Dodecen-1-yl(-)succinic anhydride	181	157429	0,0160
64,918	C25H55	2-methyltetracosane	390	891401	0,0909
68,674	C18H38O	1-Decanol, 2-octyl-	331	627185	0,0640
73,37	C25H55	2-methyltetracosane	390	617934	0,0630
76,512	C19H38	Tridecane, 7-cyclohexyl-	343	169734	0,0173
79,271	C19H39	Tridecane, 7-cyclohexyl-	343	882991	0,0901
		Total Area		9798253	

Table C. 19 - Supported Magnetite Peak analysis at 400 ˚C

Time(min)	Formula	Name	Boiling Point (˚C)	Area	Mass Fraction
6,92	C11H24	2,2,6,6-Tetramethylheptane	163	23376	0,0019
44,103	C5H10O2	1-Hydroxy-2-pentanone	152	53255	0,0044
41,838	C10H18O4	1-Hydroxy-2-pentanone	152	32504	0,0027
46,245	C10H18O4	Heptanoic acid, 2-(acetyloxy)-, methyl ester	223	67189	0,0056
48,282	C11H24	2,2,6,6-Tetramethylheptane	163	93354	0,0078
48,797	C28H46O4	Phthalic acid, 4,4-dimethylpent-2-yl tridecyl ester	402	41459	0,0034
50,231	C16H34	Hexadecane	286,8	148237	0,0124
52,099	C50H102	Triacontane, 11,20-didecyl-	449,7	205713	0,0172
53,908	C25H52	2-methyltetracosane	390	344805	0,0288
55,651	C25H52	2-methyltetracosane	390	451504	0,0377
57,402	C25H52	2-methyltetracosane	390	626644	0,0524
58,344	C17H30O2	4a,7,7,10a-Tetramethyldodecahydrobenzo[f]chromen-3-ol	329	998008	0,0835
59,469	C25H52	2-methyltetracosane	390	901989	0,0754
60,147	C32H54O4	7,8-Epoxylanostan-11-ol, 3-acetoxy-	601	822963	0,0688
61,968	C25H52	2-methyltetracosane	390	1107364	0,0926
62,685	C32H54O4	7,8-Epoxylanostan-11-ol, 3-acetoxy-	601	865694	0,0724
62,989	C32H54O4	7,8-Epoxylanostan-11-ol, 3-acetoxy-	601	420722	0,0352
65,039	C25H52	2-methyltetracosane	390	1390825	0,1164
68,845	C25H52	2-methyltetracosane	390	966550	0,0808
73,564	C25H52	2-methyltetracosane	390	1183208	0,0990
79,482	C25H52	2-methyltetracosane	390	1203167	0,1006
		Total Area		11948530	

Table C. 20 - Supported Magnetite Peak Analysis at 380 ˚C

Inert Glass Beads Run

Time(min)	Formula	Name	Boiling Point (˚C)	Area	Mass Fraction
4,581	C15H24O	Benzene, [(octyloxy)methyl]-	324	7633	0,0057
4,721	C21H26O6	Methyl 2,3-di-O-benzyl-beta-d-glucofuranoside	324	44212	0,0334
6,512	C21H26O6	Methyl 2,3-di-O-benzyl-beta-d-glucofuranoside	324	29561	0,0223
7,186	C21H26O6	Methyl 2,3-di-O-benzyl-beta-d-glucofuranoside	324	30130	0,0227
11,425	C21H26O6	Methyl 2,3-di-O-benzyl-beta-d-glucofuranoside	324	13009	0,0098
12,892	C10H18O4	Heptanoic acid, 2-(acetyloxy)-, methyl ester	223	25671	0,01935
30,808	C10H18O4	Heptanoic acid, 2-(acetyloxy)-, methyl ester	223	4665	0,0035
34,361	C10H18O4	Heptanoic acid, 2-(acetyloxy)-, methyl ester	223	6040	0,0045
37,377	C10H18O4	Heptanoic acid, 2-(acetyloxy)-, methyl ester	223	5531	0,0041
40,059	C10H18O4	Heptanoic acid, 2-(acetyloxy)-, methyl ester	223	5303	0,0040
42,515	C10H18O4	Heptanoic acid, 2-(acetyloxy)-, methyl ester	223	5546	0,0041
44,807	C10H18O4	Heptanoic acid, 2-(acetyloxy)-, methyl ester	223	5879	0,0044
46,974	C10H18O4	Heptanoic acid, 2-(acetyloxy)-, methyl ester	223	9507	0,0071
49,535	C10H18O4	Heptanoic acid, 2-(acetyloxy)-, methyl ester	223	11725	0,0088
50,999	C10H18O4	Heptanoic acid, 2-(acetyloxy)-, methyl ester	223	26816	0,0202
52,897	C18H38N2O	Stearic acid hydrazide	442,92	26285	0,0198
54,711	C18H38N2O	Stearic acid hydrazide	442,92	39773	0,0300
56,477	C18H38N2O	Stearic acid hydrazide	442,92	61783	0,0466
58,403	C69H138O2	Nonahexacontanoic acid	702	79197	0,0598
59,554	C69H138O2	Nonahexacontanoic acid	702	65618	0,0495
60,706	C69H138O2	Nonahexacontanoic acid	702	76851	0,0580
61,559	C69H138O2	Nonahexacontanoic acid	702	64819	0,0489
63,53	C69H138O2	Nonahexacontanoic acid	702	98732	0,0746
64,42	C69H138O2	Nonahexacontanoic acid	702	113881	0,0860
67,027	C69H138O2	Nonahexacontanoic acid	702	114467	0,0864
71,351	C69H138O2	Nonahexacontanoic acid	702	103932	0,0785
76,8	C69H138O2	Nonahexacontanoic acid	702	171096	0,1292
83,62	C69H138O2	Nonahexacontanoic acid	702	75814	0,0572
		Total Area		1323476	

Table C. 21 - Peak analysis of inert run at 400 ˚C

Fraction(Boiling point)	***Feed***	***360 ˚C***	***380 ˚C***	***400 ˚C***	***No Catalyst***
Cobalt Molybdenum					
Product masses (g)	10.401	5.740	9.071	5.981	4.975
Vacuum Residue(>565˚C)	0,7993	0,7607	0,6269	0,2340	0,3283
Vacuum gas oil (360-565˚C)	0,2007	0,2293	0,2293	0,4930	0,2918
Gas Oil(265-360˚C)	-	0	0	0,1449	0,3798
Kerosene(140-265˚C)	-	0,0100	0,1437	0,1282	-
Nickel Molybdenum					
Product masses (g)		*9.901*	*4.582*	*5.724*	
Vacuum Residue(>565˚C)		0,7554	0,3610	0,5953	
Vacuum gas oil (360-565˚C)		0,2335	0,2515	0,2216	
Gas Oil(265-360˚C)		0	0,2865	0,0469	
Kerosene(140-265˚C)		0,0111	0,1009	0,1361	
Supported Magnetite Nanocatalyst					
Product masses (g)		*5.311*	*7.305*	*2.501*	
Vacuum Residue(>565˚C)		0,3968	0,1938	0,0081	
Vacuum gas oil (360-565˚C)		0,5178	0,6877	0,6876	
Gas Oil(265-360˚C)		0,0707	0,0959	0,1844	
Kerosene(140-265˚C)		0,0145	0,0226	0,1197	

Table C. 22 - Fractional Yields of fixed bed reactor set up

Appendix D: Sample Calculation

The following sample calculation is based on run 6 of the batch reactor results:

Run Specifications: Temperature 400℃

Pressure = 48 bar (approximately)

Catalyst mass = 2 grams

Product mass: 8.314 grams

Feed mass = 10.4 g

The purpose of the sample calculation is to calculate the fractional yield of each fraction of the short residue by using their boiling points. These being vacuum residue, gas oil, vacuum gas oil kerosene and naphtha. The following table shows the boiling point range of each fraction.

VR	**>565 degrees**
VGO	360 to 565
GO	265 to 360
Ke	140 to 265
Naphtha	40 to 140

The following table below groups all the components into their boiling point ranges for ease of calculations:

Time	Formula	Name	Boiling Points	
4.82	C14H30O	2-Hexyl-1-octanol	195.00	**Kerosene**
7.37	C16H34	Hexadecane	286.00	
11.55	C16H34	Hexadecane	286.00	
18.71	C16H34	Hexadecane	286.00	
26.05	C17H36	Heptadecane	302.00	
30.65	C21H44	Heneicosane	305.00	**Gas Oil**
34.18	C29H60	2-methyloctacosane	413.00	
37.18	C20H42	Eicosane	343.00	
39.825	C20H42	Eicosane	343.00	
44.51	C34H70	Tetratriacontane	285.00	
46.65	C27H56	2-methylhexacosane	416.85	
48.68	C27H56	2-methylhexacosane	416.85	
50.62	C27H56	2-methylhexacosane	416.85	

52.48	C27H56	2-methylhexacosane	416.85	**Vacuum Gas Oil**
54.29	C27H56	2-methylhexacosane	416.85	
56.02	C27H56	2-methylhexacosane	416.85	
57.83	C27H56	2-methylhexacosane	416.85	
59.97	C60H122	Hexacontane	620.20	
62.58	C60H122	Hexacontane	620.20	
65.75	C60H122	Hexacontane	620.20	
69.72	C60H122	Hexacontane	620.20	**Vacuum Residue**
74.62	C41H84O	1-Hentetracontanol	572.00	
80.78	C41H84O	1-Hentetracontanol	572.00	
88.33	C41H84O	1-Hentetracontanol	572.00	
98.35	C41H84O	1-Hentetracontanol	572.00	

Table D. 1 - Boiling points of each fraction for run 3

From the raw data tables in Table C.7, the total peak area and mass fraction of each components is stated. Using the data from table C.7, the mass fraction is calculated as follows:

Component: 2-Hexyl-1-Octanol

Peak Area: 29015510

Total peak area for run 6 = 567886365

$$mass\ fraction = \frac{29015510}{567886365} = 0.051094$$

The boiling point of this component is 195℃. This is the only component falling in the Kerosene group, hence the kerosene mass fraction is *0.051094*.

The same step is done for each component and then each group is summed up to get an overall mass fraction of each group.

VR	0.195135344
VGO	0.260781658
GO	0.492989132
Ke	0.051093866

Lastly the yield must be calculated. **Note that yield is based on the feed mass.**

$$yield = \frac{mass\ fraction\ x\ feed\ mass}{feed\ mass}$$

Therefore, from the above equation the yield is the calculated mass fraction for each species. The mass lost to gaseous products was calculated to be extremely, hence it was assumed negligible. Therefore, the yield for the kerosene group is simply 0.05109. These calculations were done for all the runs and feed analysis.

Appendix E: MATLAB Code

```
close all
clear all
clc

Ea=1000*[152 180 188 167 101 245 150];      % activation energies kJ/mol

A=[2.315e+09 1.454e+11 2.934e+11 0*1.835e+10 0.4*3.050e+06 4.118e+14 6.284e+08];   % pre-exponential factors 1/min

%  Integration for Heat-up period

W0=[0.25 0.75 0 0 0 298];

%options=odeset('BDF','off','NonNegative',[1 2 3 4 5 6 7],'AbsTol',1e-8,'RelTol',1e-8);

options=odeset('BDF','off','NonNegative',[1 2 3 4 5 6]);
% Call the ode solver

[t,W]=ode15s(@(t,W) Slave(t,W,A,Ea),[0 150],W0,options);



counter1=size(W);
counter2=counter1(1,1);

W0s=W(counter2,1:5);
Temperature=W(counter2,6);

options=odeset('BDF','off','NonNegative',[1 2 3 4 5]);

[ts,Ws]=ode15s(@(ts,Ws) Slave1(ts,Ws,A,Ea,Temperature),[0 60],W0s,options);

ts=150+ts;

Time=[t' ts'];

% plotting for component 1, VR
figure(1)

Wh1=W(:,1)';
Wss1=Ws(:,1)';

W1=[Wh1 Wss1];

plot(Time,W1,'LineStyle','-','Color','b','LineWidth',2)
axis square
xlim([0 210]);

hold on
```

```
% plotting for component 2, VGO


Wh2=W(:,2)';
Wss2=Ws(:,2)';

W2=[Wh2 Wss2];

plot(Time,W2,'LineStyle','-','Color','r','LineWidth',2)
axis square


% plotting for component 3, GO

Wh3=W(:,3)';
Wss3=Ws(:,3)';

W3=[Wh3 Wss3];

plot(Time,W3,'LineStyle','-','Color','g','LineWidth',2)



% plotting for component 4, Ke+Naphtha

Wh4=W(:,4)';
Wss4=Ws(:,4)';

W4=[Wh4 Wss4];

plot(Time,W4,'LineStyle','-','Color','k','LineWidth',2)




% % plotting for component 5, Gas
%
% Wh5=W(:,5)';
% Wss5=Ws(:,5)';
%
% W5=[Wh5 Wss5];
%
% plot(Time,W5,'LineStyle','-','Color',[0.600000023841858 0 0.600000023841858],'LineWidth',2)



ylabel('Mass fractions','FontName','Calibri','FontSize',12,'FontWeight','normal','Color','k')
xlabel('time [min]','FontName','Calibri','FontSize',12,'FontWeight','normal','Color','k')

legend('VR','VGO','GO','Ke+Naphtha')

hold off
```

The additional files needed to complete the code is shown below:

```
function dW = Slave(t,W,A,Ea)

dW=zeros(6,1);

Temp=W(6);

k1=A(1)*exp(-Ea(1)/(8.314*Temp));

k2=A(2)*exp(-Ea(2)/(8.314*Temp));

k3=A(3)*exp(-Ea(3)/(8.314*Temp));

k4=A(4)*exp(-Ea(4)/(8.314*Temp));

k5=A(5)*exp(-Ea(5)/(8.314*Temp));

k6=A(6)*exp(-Ea(6)/(8.314*Temp));

k7=A(7)*exp(-Ea(7)/(8.314*Temp));


dW(1)=-(k1+k2+k3+k4)*W(1);

dW(2)=k4*W(1)-(k5+k6)*W(2);

dW(3)=k2*W(1)+k5*W(2)-k7*W(3);

dW(4)=k3*W(1)+k6*W(2);

dW(5)=k4*W(1);

dW(6)=2.1667;
```

```
function dWs =
Slave1(ts,Ws,A,Ea,Temperature)


dWs=zeros(5,1);


k1=A(1)*exp(-
Ea(1)/(8.314*Temperature));

k2=A(2)*exp(-
Ea(2)/(8.314*Temperature));

k3=A(3)*exp(-
Ea(3)/(8.314*Temperature));

k4=A(4)*exp(-
Ea(4)/(8.314*Temperature));

k5=A(5)*exp(-
Ea(5)/(8.314*Temperature));

k6=A(6)*exp(-
Ea(6)/(8.314*Temperature));

k7=A(7)*exp(-
Ea(7)/(8.314*Temperature));


dWs(1)=-(k1+k2+k3+k4)*Ws(1);

dWs(2)=k4*Ws(1)-(k5+k6)*Ws(2);

dWs(3)=k2*Ws(1)+k5*Ws(2)-
k7*Ws(3);

dWs(4)=k3*Ws(1)+k6*Ws(2);

dWs(5)=k4*Ws(1);
```

	K1	K2	K3	K4	K5	K6	K7
Activation Energy (kJ/mol)	152	180	188	167	101	245	150
A (1/min)	$2.315x10^{9}$	$1.454x10^{11}$	$2.934x10^{10}$	0	$1.22x10^{6}$	$4.118x10^{14}$	$6.284x10^{8}$

Table E. 1 - Kinetic constants

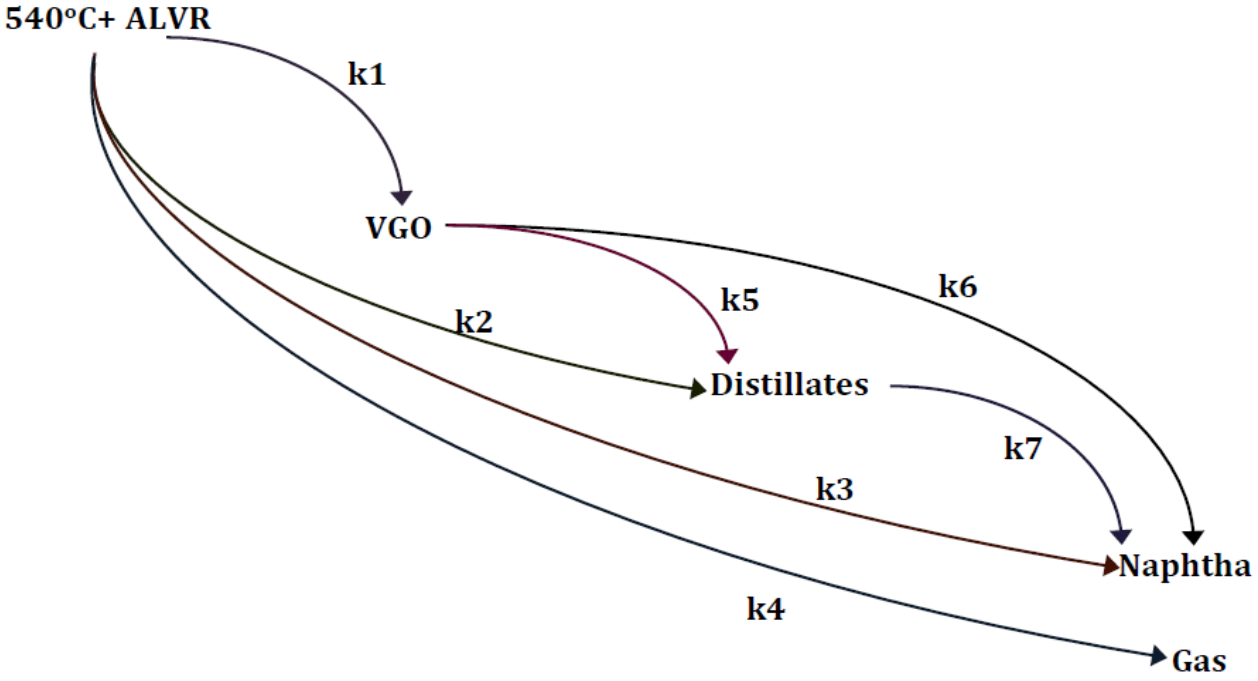

Figure E. 1 - Kinetic Model (Fathi.M., 2013)

Appendix F: Batch Simulations

The following mass composition profiles were generated using the kinetics reported by Fathi et al. (2013)

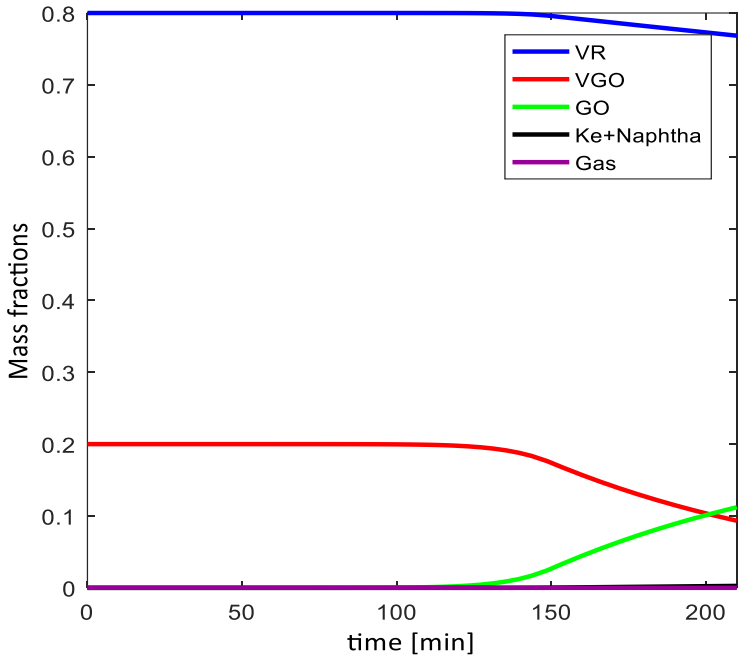

Figure F. 1 - Composition profile at 350˚C

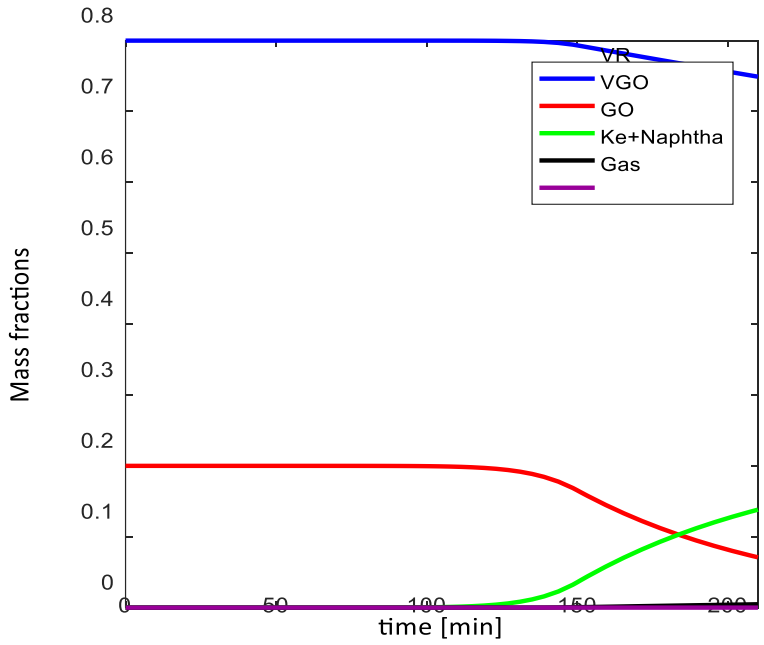

Figure F. 2 - Composition profile at 360˚C

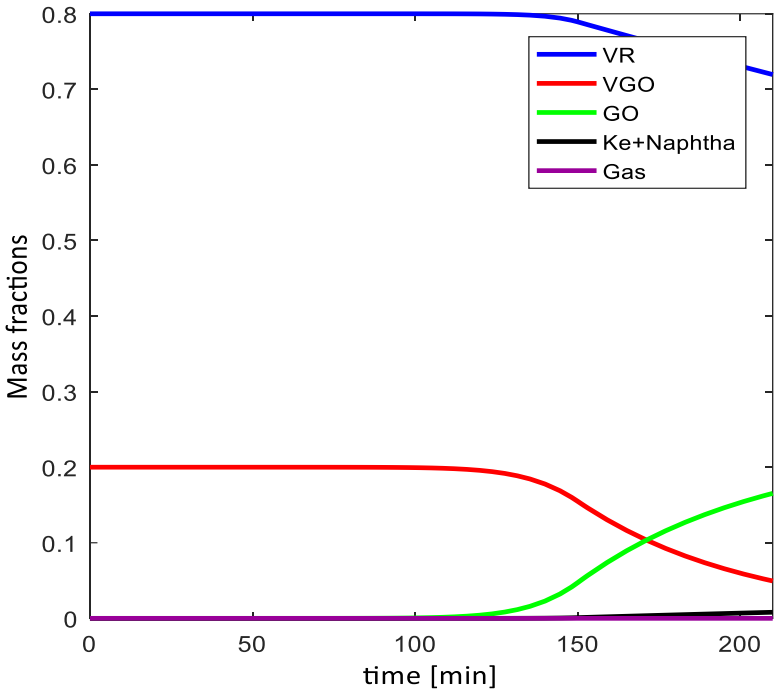

Figure F. 3 - Composition profile at 370˚C

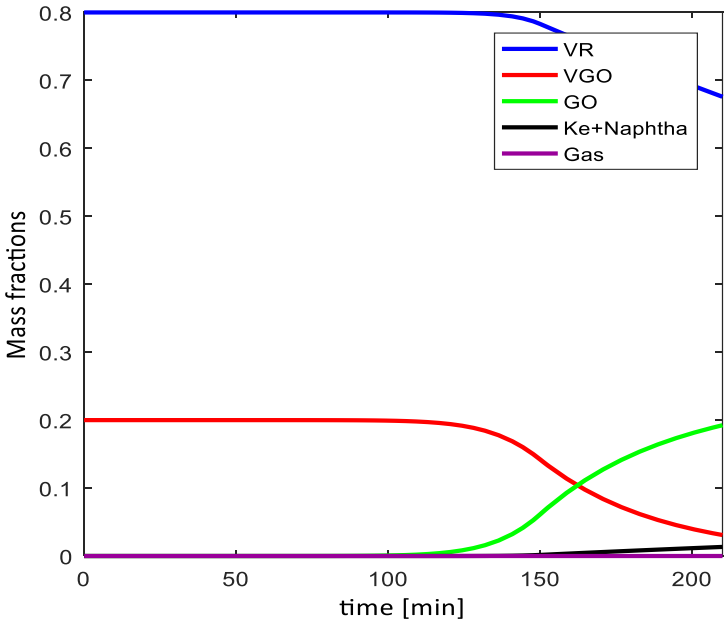

Figure F. 4 - Composition profile at 380˚C

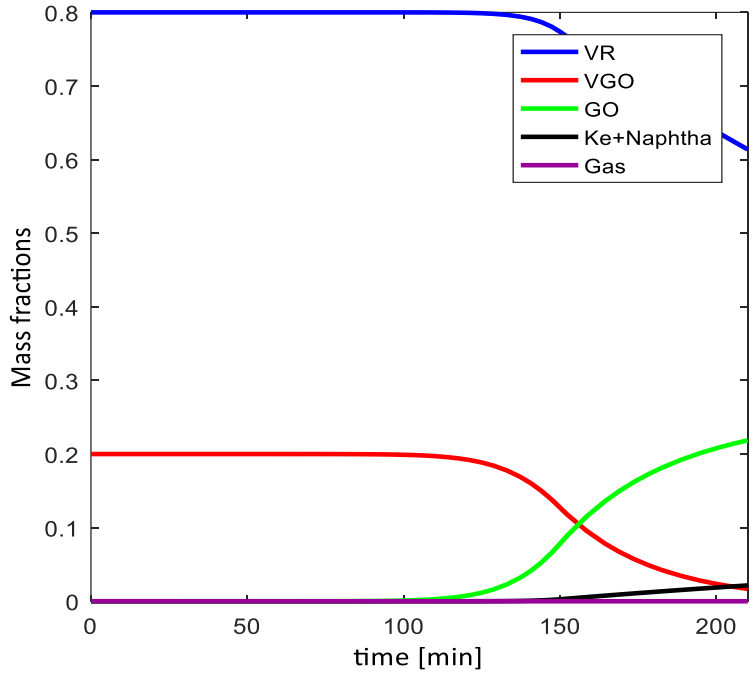

Figure F. 5 - Composition profile at 390˚C

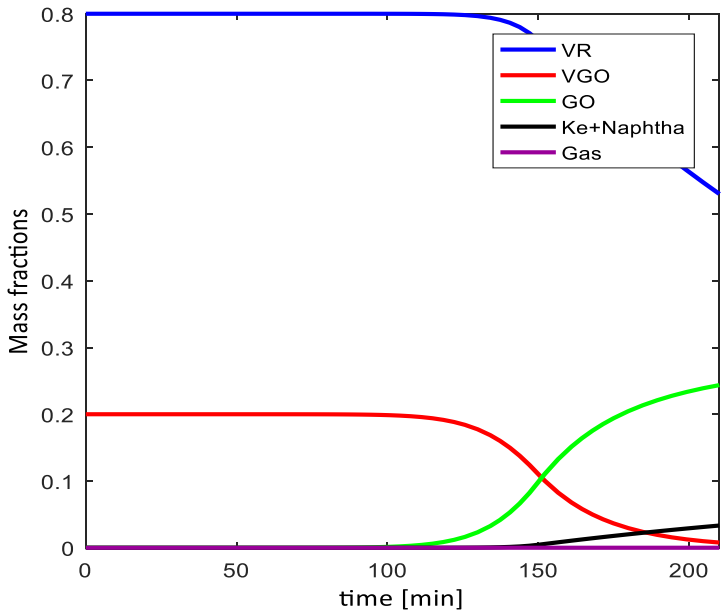

Figure F. 6 - Composition profile at 400˚C

Appendix G: Experimental Set up

Batch Set Up

Figure G. 1 - Batch Reactor set up

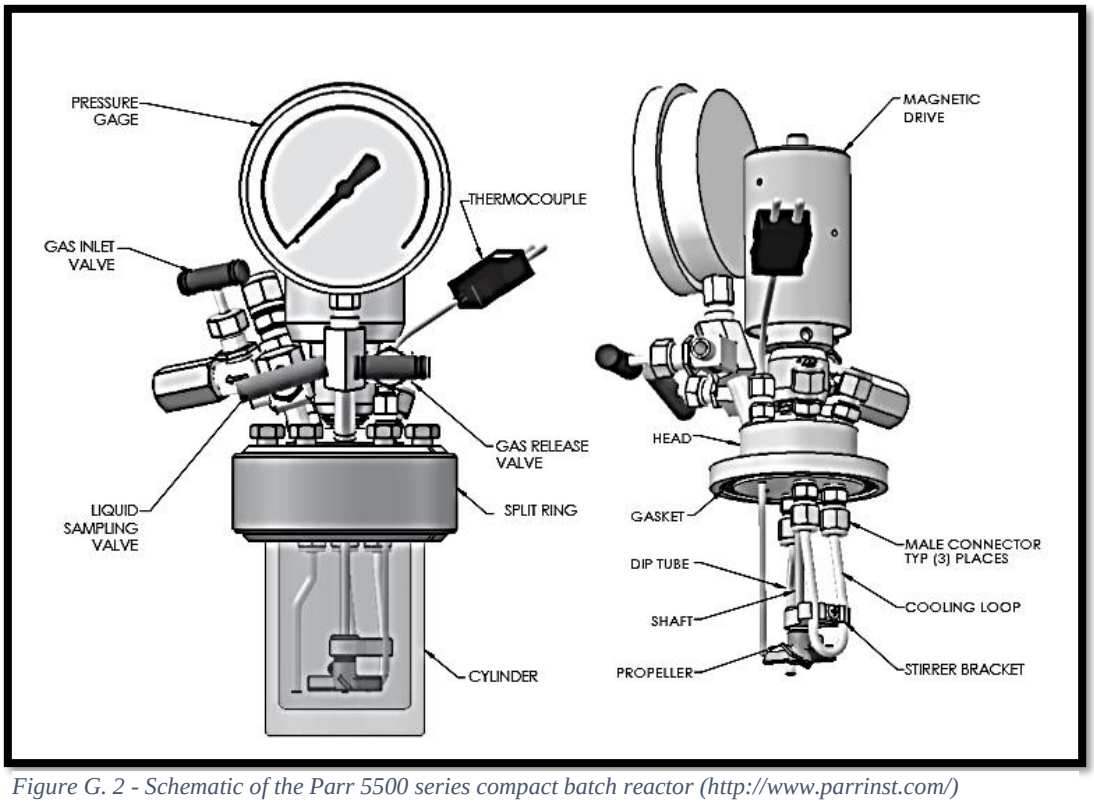

Figure G. 2 - Schematic of the Parr 5500 series compact batch reactor (http://www.parrinst.com/)

Specification	**Maximum Value**
Pressure	200 bar
Temperature:	
FKM o-ring	225 °C
FFKM o-ring	275 °C
PTFE flat gasket	350 °C
Volume	300 ml

Table G. 1 - Batch Reactor Specifications

Fixed Bed Reactor Set up

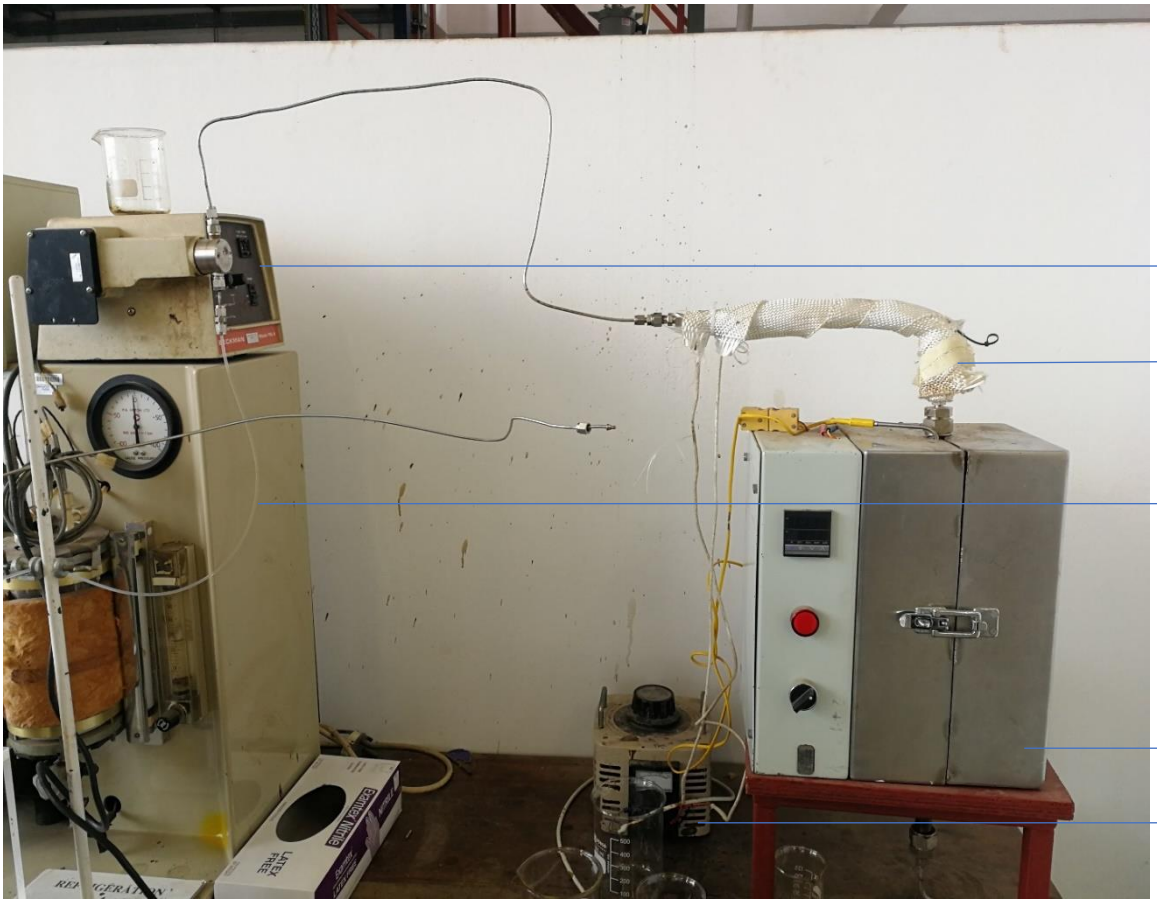

Figure G. 3 - Fixed bed reactor set up

Figure G. 4 - Fixed bed set up (extended)

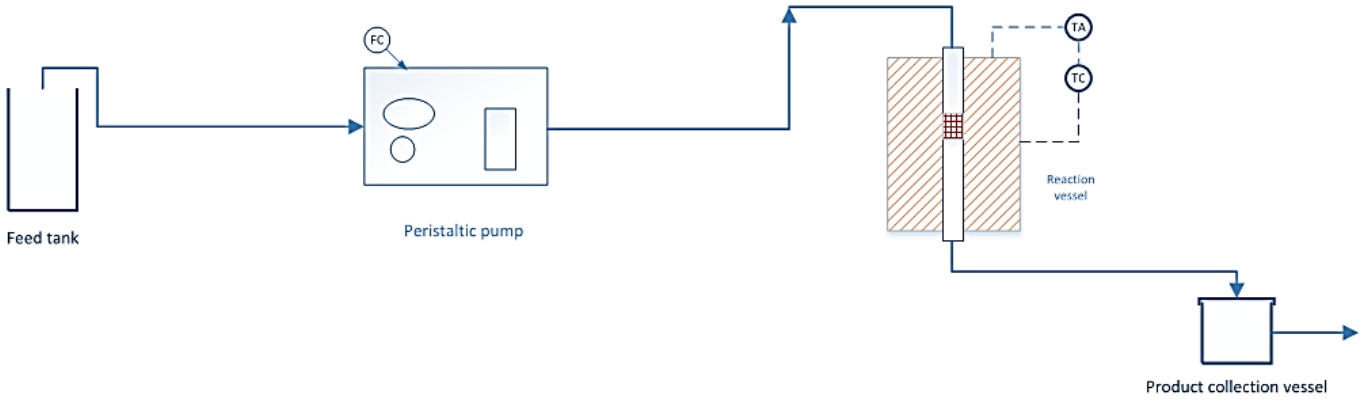

Figure G. 5 - Flow diagram of fixed bed reactor scheme

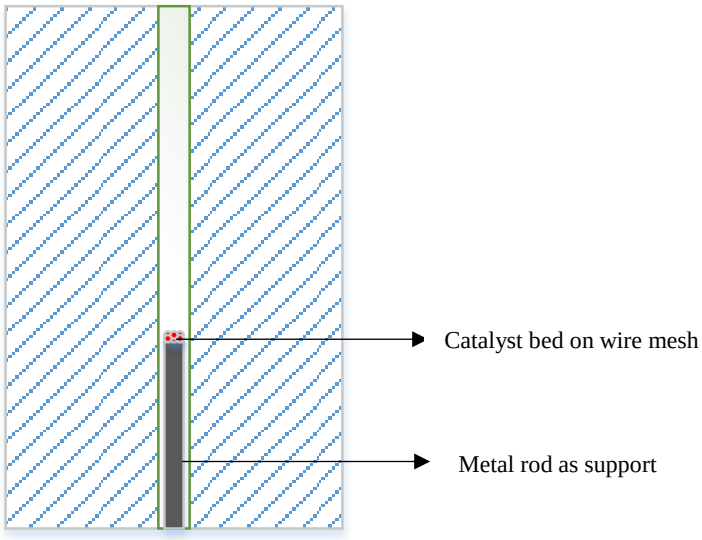

Figure G. 6 - Cross section of reaction vessel

Appendix H: Safety

SAFETY REQUIREMENTS

Heat resistant	Lab. coat	Closed Shoes	Hard Hat	Nitrile Gloves	Ear Muffs
X	X	X		X	

SAFETY EQUIPMENT

Use Fume-hood	Know location and use of Fire Extinguishes	Know location and use of Eye-wash Station
X		X

SPECIFIC CHEMICAL HAZARDS

Flammable	Carcinogenic	Toxic	Hazardous fumes	Oxidizing agent
X		X	X	

OTHER POSSIBLE HAZARDS

Electrical Hazards	Mechanical Hazards	Other Hazards
	X	

Safety Data Sheets

Short Residue

Physical and Chemical properties.

Appearance	Brown to black. Liquid at high temperatures.
Boiling Point	> 320 °C @ 1 atm
Flash Point	> 230 °C

Exposure:

Eye	May cause eye to burn.
Skin	Causes moderate skin irritation. May be absorbed through the skin.
Ingestion	Under normal conditions of use, this isn't expected to be a primary route of exposure
Inhalation	Causes irritation to nose and throat.
Chronic	May cause liver and kidney damage.

First Aid Measures:

Eye	Immediately flush eyes with plenty of water for at least 15 minutes
Skin	Immediately flush skin with plenty of water for at least 15 minutes while removing contaminated clothing and shoes. Apply burn ointments.
Ingestion	If conscious and alert, rinse mouth and drink 2-4 cupfuls of milk or water.
Inhalation	Remove from exposure and move to fresh air immediately. If not breathing, give artificial respiration

Stability and Reactivity:

Chemical Stability	No hazardous reaction is expected when handled and stored according to provisions.
Conditions to Avoid	Heating above the maximum recommended storage and handling temperature, will cause degradation and evolution of flammable vapours
Incompatibilities with Other Materials	Do not allow molten material to contact water or liquids as this can cause violent eruptions, splatter hot material, or ignite flammable material
Hazardous Decomposition Products	Hydrogen sulphide.

Toxicology Information:

Acute Dermal Toxicity	2800 mg/kg
Oral, mouse: LD50	2900 mg/kg
Oral, rat: LD50	3700 mg/kg

Oral, rat: LD50	5290 mg/kg
Carcinogenicity	None reported
Mutagenicity	DNA inhibition: Human lymphocyte = 25 µmol/L.

(Fisher Scientific, 2006)

Toluene:

Physical and Chemical properties:

Appearance	Colorless.
Boiling Point	110.6°C@ 760.00mm Hg
Flash Point	4.44°C

Exposure:

Eye	May cause eye irritation.
Skin	Causes moderate skin irritation. May be absorbed through the skin.
Ingestion	May cause central nervous system depression, characterized by excitement, followed by headache, dizziness, drowsiness, and nausea
Inhalation	May cause respiratory tract irritation. Central nervous system effects characterized by nausea, headache and dizziness.
Chronic	Prolonged or repeated skin contact may cause dermatitis. May cause kidney injury.

First Aid Measures:

Eye	Immediately flush eyes with plenty of water for at least 15 minutes
Skin	Immediately flush skin with plenty of water for at least 15 minutes while removing contaminated clothing and shoes
Ingestion	If conscious and alert, rinse mouth and drink 2-4 cupfuls of milk or water.
Inhalation	Remove from exposure and move to fresh air immediately. If not breathing, give artificial respiration

Stability and Reactivity:

Chemical Stability	Stable under normal temperatures and pressures.
Conditions to avoid	Heat, ignition sources, incompatible materials
Incompatibilities with Other Materials	Reactive with oxidizing agents.
Polymerization	Will not occur

Toxicology Information:

Oral, mouse: LD50	28 mg/kg;
Oral, rat: LD50	1300 mg/kg
Carcinogenicity	None reported
Mutagenicity	Mutation,mammalian somatic cells =400mg/L

(Fisher Scientific UK, 2000)

Hazard and Operability Study

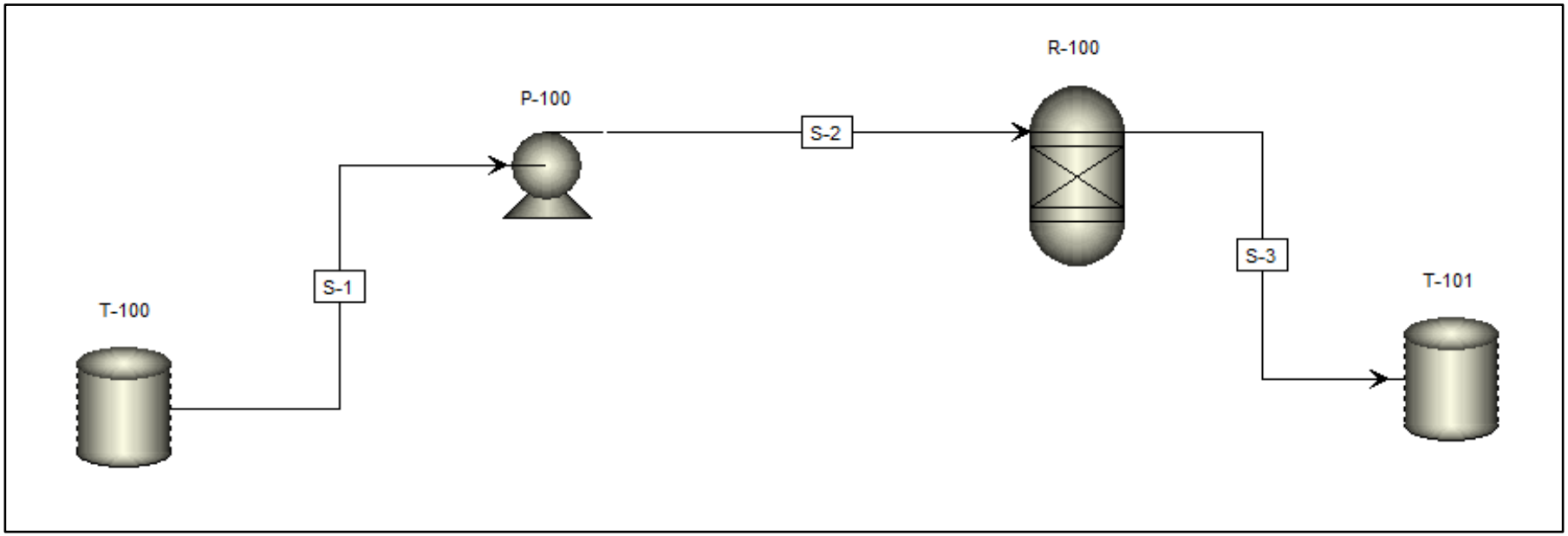

Figure H. 1 - Process flow diagram of Fixed bed reactor set up

T-100	Feed Tank
P-100	Pump
R-100	Reactor
T-101	Product Tank

Table H. 1 - Equipment list for process flow diagram

NODE 1: FEED TANK (T-100)				
DEVIATION		CAUSE	CONSEQUENCE	RECOMMENDATIONS
LEVEL	HIGH	• Blockage at exit point • Pipeline blockage. • Low pump flow rate.	• Less feed is pumped to the reactor. • Accumulation of vacuum residue mixture in the feed tank. • Reaction rate and conversion decrease.	• Regular inspection and maintenance of feed tank. • Install level indicator. • Install high level alarm.
	LOW	• Feed tank leakage. • High pump flow rate.	• More feed is pumped to reactor. • Reaction rate and conversion increase. • Reactor could overflow. • Could introduce air bubbles into pipeline.	• Regular inspection and maintenance of feed tank. • Install level indicator. • Install low level alarm.
NODE 2: FEED TANK TO REACTOR PIPELINE (S-1, S-2)				
DEVIATION		CAUSE	CONSEQUENCE	RECOMMENDATIONS
FLOW	NO	• Blockage in pipeline. • Pipeline leak. • Flow control failure. • Pump failure. • No feed in the tank. • Wrong routing. • Gas locking. • Cavitation.	• No feed is pumped to the reactor. • Accumulation of vacuum residue mixture in the feed tank. • Reaction rate and conversion decrease.	• Regular inspection and maintenance of pipeline. • Install flow indicator. • Install no flow alarm. • Switch off the pump. Disconnect the pipeline to the reactor. Using a syringe, create suction in pipeline from the feed until it reaches the pump. Reconnect the pipeline and restart the pump.

FLOW	LESS	• Leak in pipeline. • Partial pipeline blockage. • Pipe restrictions. • Wrong routing. • Cavitation. • Valve not fully open. • Faulty pump.	• Insufficient flow of vacuum residue into reactor thus loss of production. • Reaction rate and conversion decrease. • Accumulation of vacuum residue in feed tank.	• Regular inspection and maintenance of pipeline. • Install flow indicator. • Install control valve. • Install low flow alarm. • Switch off the pump. Disconnect the pipeline to the reactor. Using a syringe, create suction in pipeline from the feed until it reaches the pump. Reconnect the pipeline and restart the pump.
	MORE	• High pump speed. • High feed tank pressure.	• Poor product quality. • Reactor overflows.	• Install flow indicator. • Install control valve. • Install high flow alarm.
	REVERSE	• Pump malfunction. • Pump operation reversed. • Incorrect pressure differential.	• No feed to the reactor and no product forms. • Feed is drawn out of reactor. • Feed in tank is contaminated.	• Switch off the pump. Disconnect the pipeline to the reactor. Using a syringe, create suction in pipeline from the feed until it reaches the pump. Reconnect the pipeline and restart the pump.
	AS WELL AS	• Feed stream impurities. • Rupture in pipeline.	• Less product. • Lower product purity. • Poisoning of catalyst.	• Operator should check feed composition before starting operation. • Regular inspection and maintenance of pipeline.
	OTHER THAN	• Incorrect specification of feedstock. • Incorrect operation.	• Corrosion or malfunctioning of reactor. • Lower product purity.	• Operator should check feed before start of operation.
MAINTENANCE	OTHER	• General equipment failure or catalyst changeover in the reactor.	• Process stops.	• Good practices in construction operation. • Ensure shutdown and start up procedures are well understood.

NODE 3: REACTOR (R-100)				
DEVIATION		CAUSE	CONSEQUENCE	RECOMMENDATIONS
LEVEL	HIGH	• Blockage at exit point. • Residue entrained in catalyst bed. • Low pump flow rate.	• Accumulation of vacuum residue mixture in the reactor. • Less product exits reactor.	• Regular inspection and maintenance of reactor. • Install level indicator. • Install high level alarm.
	LOW	• Reactor leakage. • High pump flow rate.	• Poor quality product. • More product exits reactor.	• Regular inspection and maintenance of reactor. • Install level indicator. • Install low level alarm.
PRESSURE	HIGH	• High temperature in reactor. • Blockage at exit point. • Accumulation of vapour in reactor.	• Reactor could rupture/explode. • Possibility of runaway reaction. • Poor product quality.	• Regular inspection and maintenance of reactor. • Install pressure indicator. • Install high pressure alarm. • Vent vapours to atmosphere.
	LOW	• Low temperature in reactor.	• Poor product quality. • Product remains in reactor due to insufficient pressure differential.	• Install pressure indicator. • Install high pressure alarm
TEMPERATURE	HIGH	• Heating jacket set too high. • High pressure in reactor.	• Poor product quality. • Reaction rate increases. • Damage to equipment. • Sintering of catalyst. • Possibility of runaway reaction.	• Install temperature indicator. • Install high temperature alarm. • Ensure emergency cooling quench is available.

TEMPERATURE	LOW	• Heating jacket set too low. • Endothermic reaction lowers temperature. • Low pressure in reactor.	• Poor quality product. • Reaction rate decreases.	• Install temperature indicator. • Install low temperature alarm.
NODE 4: REACTOR TO PRODUCT TANK PIPELINE (S-3)				
DEVIATION		CAUSE	CONSEQUENCE	RECOMMENDATIONS
FLOW	NO	• Pipeline blockage. • Pipeline burst. • Flow control failure. • Cavitation.	• No products. • Accumulation of vacuum residue mixture in the reactor. • Pressure increase in reactor.	• Regular inspection and maintenance of pipeline. • Install flow indicator. • Install flow alarm. • Switch off the pump. Disconnect the pipeline to the reactor. Using a syringe, create suction in pipeline from the feed until it reaches the pump. Reconnect the pipeline and restart the pump.
	LESS	• Pipeline leakage. • Partial pipeline blockage. • Pipeline restrictions.	• Insufficient flow of vacuum residue from reactor thus loss of production. • Pressure increase in reactor. • Accumulation of residue in reactor.	• Install flow indicator. • Install control valve. • Install low flow alarm. • Switch off the pump. Disconnect the pipeline to the reactor. Using a syringe, create suction in pipeline from the feed until it reaches the pump. Reconnect the pipeline and restart the pump.

FLOW	MORE	• Operator sets a higher than required flow rate of the fluid from the storage tank. • Increased pressure in reactor.	• Poor product quality. • Reactor dries up. • Damage to pipeline.	• Install flow indicator. • Install control valve. • Install high flow alarm.
	REVERSE	• Pump malfunction.	• No product exits the reactor. • Feed in feed tank contaminated.	• Switch off the pump. Disconnect the pipeline to the reactor. Using a syringe, create suction in pipeline from the feed until it reaches the pump. Reconnect the pipeline and restart the pump.
TEMPERATURE	HIGH	• Heating jacket set too high. • Increase in reactor temperature.	• Could cause damage to pipeline. • Safety hazard to workers in the vicinity of the pipeline.	• Install temperature indicator. • Install high temperature alarm. • Ensure emergency cooling quench is available after product exits reactor.
	LOW	• Heating jacket set too low. • Decrease in reactor temperature. • Rapid heat loss to surroundings.	• Increase in viscosity of product. • Could lead to flow problems and accumulation in pipeline.	• Install temperature indicator. • Install low temperature alarm. • Regular inspection and maintenance of pipeline.
MAINTENANCE	OTHER	• General equipment failure or catalyst changeover in the reactor.	• Process stops.	• Good practices in construction operation. • Ensure shutdown and start up procedures are well understood.

Table H. 2 - HAZOP Table analysis for fixed bed reactor set up